CZECH TECHNICAL UNIVERSITY IN PRAGUE

FACULTY OF MECHANICAL ENGINEERING

DOCTORAL THESIS

AERODYNAMIC PARAMETERS FOR DESCRIPTION OF FLIGHT OF ROTATING VOLLEYBALL

DOCTORAL STUDY PROGRAM: Mechanical Engineering

STUDY FIELD: Thermomechanics and fluid mechanics

Ing. Jan Dumek

SUPERVISOR

Prof. Ing. Pavel Šafařík, CSc.

PRAGUE 2018

ACKNOWLEDGEMENT

My profound gratitude to my supervisor, Prof. Ing. Pavel Šafařík, CSc. for leading me with great patience in many years of studies of fluid mechanics and also for showing me the real values of life.

I want to thank to my fiancée Tanja for patience and for supporting me in composing this Doctoral thesis. Further I want to thank to my parents for support and my brother Libor for opinions "out of the box". Officially I want to thank to VZLÚ Czech Aerospace Research Center for support of my measurements, CVF for test objects and my friend Ing. M. Váňa for engineer opinions on the construction of experimental stand solutions. I also want to thank to Buddy for sharing the pure happiness with me in the times I need it.

DECLARATION OF AUTHORSHIP

I, Jan Dumek, declare that this thesis entitled "Aerodynamic parameters for description of flight of rotating volleyball" and the work presented in it are my own and has been generated by me as the results of my own original research.

I also declare that I have worked under the supervision of Prof. Ing. Pavel Šafařík, CSc and where I have consulted the published work of others, this is always clearly attributed in references.

Signed: _____

Date: _____

ANOTACE

Práce se zabývá popisem vlivu rotace na let volejbalového míče v proudu vzduchu při definovaném bočním úhlu náběhu. Popis je založen na výsledcích měření v aerodynamickém tunelu. Let je popsán pomocí bezrozměrných aerodynamických charakteristik, jako jsou koeficienty odporu, vztlaku a boční síly a koeficienty momentů – klonivého momentu, klopivého momentu a zatáčivého momentu – s parametry: Reynoldsovo číslo, spin a boční úhel náběhu. Při realizaci experimentu byly simulovány reálné podmínky letu volejbalového míče, které jsou definovány Reynoldsovým číslem (*Re = 150 000 – 420 000*), tento interval obsahuje i oblast kritického Reynoldsova čísla. Všechny získané výsledky jsou připraveny k použití v systému rovnic prostorové balistiky. Rovnice prostorové balistiky jsou také navrženy v disertační práci. Systém prostorových balistických rovnic a dat z experimentu může řešit všechny typy letů volejbalového míče včetně zvláštních případů jako je let míče s vlivem bočního větru a let míče bez rotace. Příklad výpočtu letu je uveden v disertační práci.

Experiment byl navržen za účelem měření všech sil a momentů působících na volejbalový míč v aerodynamickém tunelu. Dosažené výsledky jsou v práci prezentovány. Důležitou částí práce je diskuse o pozorovaných jevech a analýza vlivu rotačního působení na koeficient vztlaku. Závislost koeficientu vztlaku na rotaci je po statistickém zpracování vyjádřena rovnicí polynomu třetího stupně. Efekt ukazuje pokles růstu gradientu při rostoucím spinu.
Speciální režim letu volejbalového míče – let bez rotace (plachtící let) – je v práci analyzován. Vliv drsnosti povrchu je v disertační práci popsán na základě praktických testů a porovnán s údaji z literatury. V závěrečné části diskuze je proveden výpočet CFD za definovaných podmínek (Reynoldsovo číslo, otáčky, boční úhel náběhu).

ABSTRACT

This thesis deals with description of effect of revolutions on the flight of a rotating volleyball with airstream in defined side angle of attack. The description is based on results of measurements in an aerodynamic tunnel. The flight is described by using dimensionless aerodynamical characteristics such as coefficients of Drag, of Lift and of Side force and coefficients of moments – Roll, Pitch, Yaw with parameters of Reynolds number, spin and side angle of attack. It is important to state, that real conditions of flight of a volleyball, which were simulated (*Re = 150 000 – 420 000*) all fall within the region of critical Reynolds number. All collected results are prepared to be used in the system of 3D ballistic equations, which are also proposed in this thesis. The system of ballistics and data from the experiment can solve all types of flights of a volleyball including the special cases: influence of side wind, flight of ball without rotation. An example of the calculation of flight is presented in thesis.

The experimental set up was developed for the purpose of measuring all forces and moments acting on a volleyball in a wind tunnel. Achieved results are presented in the thesis and observed effects are discussed. The important part of the thesis is discussion and analysis of the effect of spin acting on coefficient of Lift. The dependence of coefficient of Lift on spin, is after statistical treatment, expressed by equation of polynomial of third grade. The effect shows a decrease in the gradient of growth for higher spin.

The special mode of flight of a volleyball, ball without rotation – knuckle ball – is described. Influence of surface roughness is discussed in the thesis based on practical tests and comparison with data from references. The CFD calculation of one defined conditions (Reynolds number, revolutions, side angle of attack) is performed.

CONTENTS

NOMENCLATURE

A	[m^2]	area
a	[m]	distance of F_1 to axis z
b	[m]	distance of F_3 to axis y
c	[m]	distance of F_5 to axis y
f	[m]	distance of F_4 to axis z
C_D	[1]	coefficient of Drag
C_L	[1]	coefficient of Lift
C_P	[1]	coefficient of pressure
C_S	[1]	coefficient of Side force
C_{Mx}	[1]	coefficient of Roll - moment about axis x
C_{My}	[1]	coefficient of Pitch - moment about axis y
C_{Mz}	[1]	coefficient of Yaw - moment about axis z
d	[m]	diameter
F_D	[N]	Drag
F_L	[N]	Lift
F_S	[N]	Side force
k	[mm]	absolute roughness of surface
m	[1]	amount of results – in Student's distribution
M_X	[Nm]	Roll
M_Y	[Nm]	Pitch
M_Z	[Nm]	Yaw
n	[rps]	revolutions
n_l	[rps]	limit value of revolutions n
o	[m]	circumference
p	[Pa]	pressure
P	[1]	probability
R^2	[1]	reliability
$t_{m,P}$	[1]	constant from Student's distribution
v_∞	[m/s]	air stream velocity or velocity of volleyball
$v_{x'}$	[m/s]	component of vector of velocity, perpendicular to axis of

		revolutions of the volleyball
$v_{y'}$	[m/s]	component of vector of velocity, parallel to axis of revolutions of the volleyball
s	[1]	spin
U	[V]	voltage
α	[°]	angle of attack
β	[°]	side angle of attack
ρ	[kg/m^3]	density
τ	[N/m^2]	shear stress
μ	[Pa·s]	dynamic viscosity
σ	[1]	standard deviation
δ	[1]	uncertainty
ω	[rad/s]	angular velocity
φ	[°]	angle on the surface of sphere
Φ	[m^2/s]	full potential – potential flow
Ψ	[m^2/s]	stream function – potential flow
Γ	[m^2/s]	circulation

INDEXES

∞	infinity – used in designation of velocity of airstream
C	transformed direction– used in designation of velocity of airstream
D	quantities of Drag
L	quantities of Lift
P	quantities of pressure
S	quantities of Side force
W	quantities of side wind
X	quantities related to axis x
Y	quantities related to axis y
Z	quantities related to axis z

x'	quantities related to transformed axis x
y'	quantities related to transformed axis y
l	limit value
MIN	minimal value
MAX	maximal value

ABBREVIATIONS

CFD	Computational Fluid Dynamics
CTU	Czech Technical University in Prague
CVF	Czech Volleyball Federation
Eq.	Equation
FIVB	"Fédération Internationale De Volleyball" - International Volleyball Federation
NACA	Nation Advisory Committee for Aeronautics
VZLU	Czech Aerospace Research Center
2D	two-dimensional character
3D	three-dimensional character

LIST OF FIGURES

1 INTRODUCTION

Sport nowadays in modern society is more than just free time amusement. It is said, that sport is the ideal training field for life. Many social studies, describe the role of sport in today's society, moreover social relations in team sports are studied and described. According to some of the studies sport is also considered as a commodity for consumption, which promises a new identity for a customer. This maybe sad, but real reason, why sport is growing into all kind of fields of human interest, where it is not "just" about amusement. Science is more and more present in the development of different kinds of sports in recent decades. It is caused firstly by pressure to enhance performance in all sports and science has proved successful in achieving enhancement. Secondly presence of the sport in science or the science in sport is because the science can see physically interesting behaviours and effects in sport. The role of science in sport is 1st to improve and 2nd to describe and explain special effects. Science is practically using gained knowledge from sport.

The fluid dynamics in sports development is next to the car and plane sports used in cycling, skiing, rowing, swimming, yachting and many others. Mostly to improve device or tools, which are used in the sport. Games, where the ball is flying in the air, are dependent on laws and rules of aerodynamics as well. Some basic effects can be explained by similarities to the smooth sphere, but there are cases, where sport ball's behaviour is different from the smooth sphere. That is the reason, why even in the case of basic geometry, has been published numbers of studies in last years in regards to sphere.

This Doctoral thesis is focused to investigate and describe aerodynamic characteristics acting on rotating volleyball and the study of the influence of the rotation in the flight is based on experiment. The tests were set up in the laboratory of VZLU Czech Aerospace Research Centre. The experimental setting used in the second part of investigation allows turning of the axis of rotation in the horizontal plane, influence of the side angle of attack on the Drag, Lift and Side force are observed.

All knowledge gained in the experimental part of the work shall be further used in 3D ballistic equations. The ballistic equations with reliable foundation of aerodynamic characteristics are able to provide true description of the flight of the volleyball including special cases.

1.1 STATE OF THE ART

The sphere aerodynamics was thoroughly studied in the third decade of the 20th century, many tests of the sphere Drag in aerodynamic tunnels were made as described in [1] and [2]: Göttingen 1926, NACA 1923, NACA 1929 and others. Weiselsberger, Eiffel and others measured Drag of the sphere.

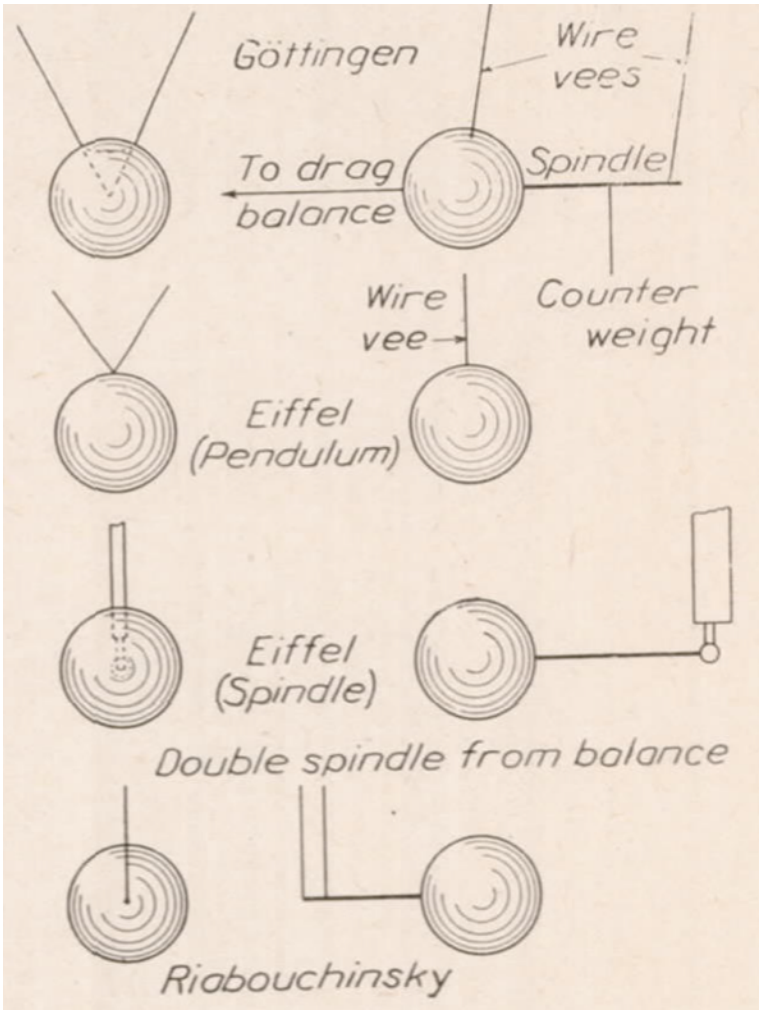

Figure 1-1: Examples of measurements settings – source [2]

The different set ups were measured and compared in [2], examples are described in Figure 1-1. As is visible in Göttingen was measured sphere on the back spindle supported by two wires. Eiffel measured Drag on the sphere at 1st "pendulum" setting and 2nd spindle. Riabouchinsky's setting is composed of double spindle from balance. Besides the mentioned scientists other

were also observing Drag at the sphere and all resulted by the unification of results, which are depicted in the Figure 1-2.

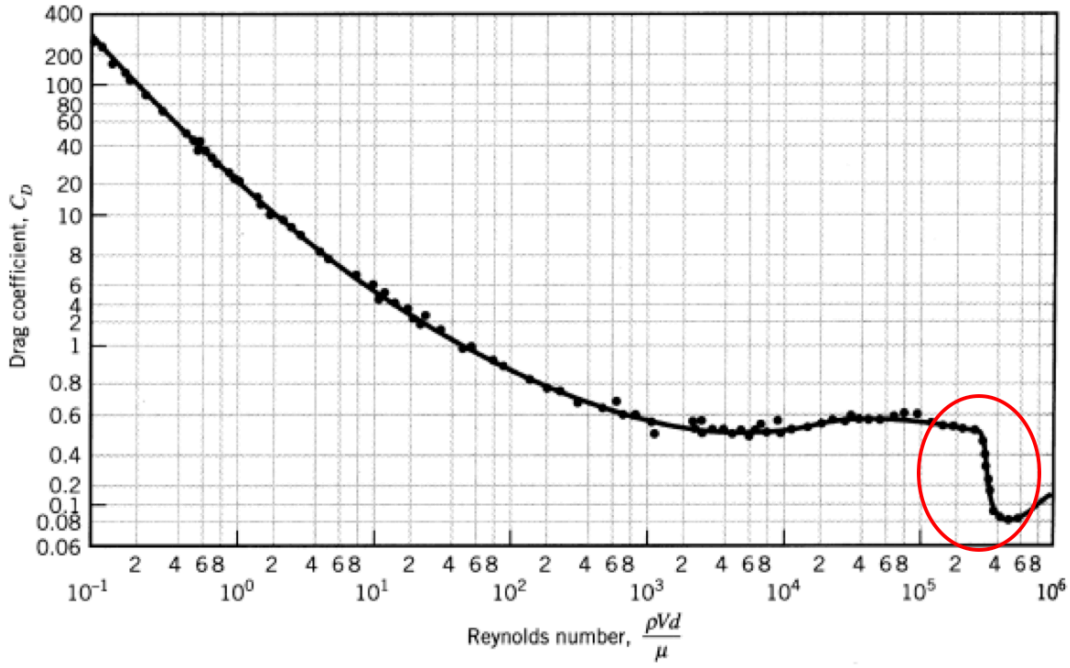

Figure 1-2: The effect of Reynolds number on the Drag coefficient C_D of a smooth sphere, source [3]

In the Figure 1-2 it is shown that the coefficient of Drag decreases with increasing Reynolds number, for Re < 6000. For higher Reynolds number the dependence is nearly constant until the area of critical Reynolds number (critical Reynolds number defines transition from laminar to turbulent flow). The area of critical Reynolds number is highlighted by red colour in the Figure 1-2 – this is interval of Reynolds numbers corresponding to real flight of a volleyball (definition of Reynolds number is in Section 2.2 and definition of concrete values of Reynolds numbers of the experiment are calculated in Section 3.2.3). Later it was Hörner 1935 [4], who studied the influence of roughness on the Drag of sphere.

Main conclusions, which were made already in the first half of 20th century follows, source [2]: 1. method of support of sphere, in sphere testing, is very important, 2. increase of turbulence is causing transition in lower Reynolds numbers.
In the second half of the 20th century another methods were used in observing of the Drag of sphere: instructive flow visualizations, 1982 by van Dyke [5]. Last year study published in the topic of Drag of sphere, Terra [6], is using large-scale tomographic-PIV. In Figure 1-3 influence of the support of the sphere is depicted, velocity contours (in the right part of Figure 1-3) show

how much field of wake behind the sphere is influenced by supportive spindle, this corresponds to the first conclusion of Bacon and Ried, 1924 [2].

According to Hoerner, [4]: critical Reynolds number is in the case of smooth sphere defined by $C_D = 0.3$, $Re_{CRIT.} = 300\,000$.

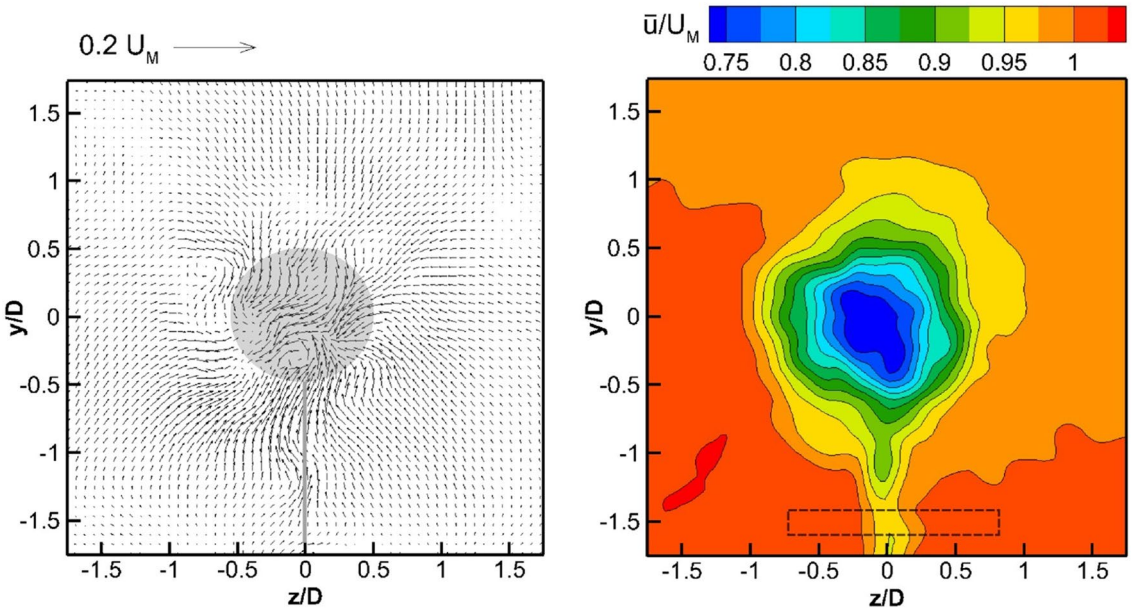

Figure 1-3: Example of the influence of sphere support - velocity vectors (left) in particular place behind the sphere and streamwise velocity contours (right), where u/U_M is velocity ratio, source [6]

The flight of a sports ball in the air has been an interesting topic for scientists for a long time. Based on references, firstly it was Newton [7], who mentioned the flight of a tennis ball already in 1672 (according to Mehta [8] Newton wrote it 1666 and published 1672) in the study of a ray of light. Theory of flight of a rotating sphere was written in 1852 by German physicist H.G. Magnus [9]. Description was made on the flight of a cannon-ball. Today, it is known as the Magnus effect.

The second interesting effect of the flight of a sports ball is, the ball's deviation from its initial straight path, resulting in a curved, unpredictable, flight path on the so called knuckle ball.

Nowadays, most of the studies on the topic of aerodynamics of sports balls are focused on descriptions of football flight, but also other sports balls were observed, e.g. R. D. Mehta [10], [11] studies cricket ball, baseball, golf ball and also volleyball.

The studies of flight of a volleyball are focused on investigating the flight in real conditions, analysed from video, as in [11]. Another way of investigating properties of the flight of a volleyball is to set up an experiment in an aerodynamic wind tunnel and measure the forces acting on the volleyball. Many experiments are dealing with a fixed ball, for example [12] and [13], in the same way as Eiffel tested a smooth sphere on the spindle, visible on the Figure 1-1. Studies [12] and [13], where a ball is supported by a spindle are describing the effect of the so called knuckle ball, but it is impossible to observe Magnus effect or even the combination of those two effects.
Description of complete forces acting on a rotating sphere requires a more sophisticated device, which allows the ball to rotate and at the same time measure forces.

Ball surface material is very important for aerodynamics property. In the historical development of the volleyball, the first ball was produced in 1895 [14], many materials were used on the surface for production of balls. In the last century the surface of the ball was mostly leather, which was substituted in the 21st century by synthetic materials. Volleyballs were originally composed of 18 panels. FIVB ("Fédération Internationale De Volleyball") is regularly creating (mostly in one or two Olympic Games period) new balls for the purpose of making the sport more interesting. The latest official FIVB ball was introduced in the year 2008, when a new volleyball, respectively in 2009 a new beach volleyball, was introduced by FIVB. A description of the volleyball is established in FIVB rules of technical parameters is described in following statement:

[*"The ball shall be spherical…Its circumference is 65-67 cm and its weight is 260-280 g. Its inside pressure shall be 29.43 to 31.882 kPa."*]

Full description of volleyball is in source [15].

It is important to define in which conditions a volleyball can be evaluated as a smooth sphere and in which conditions (Reynolds number) it is important to define a volleyball's surface roughness.

1.2 AIMS OF THE DOCTORAL THESIS

Based on the summary of contemporary knowledge in the topic of the flow around a volleyball, which is briefly summarized in the Introduction, the goals of the Doctoral thesis are defined.

The main objective of the thesis is:

- based on measured forces and moments acting on a volleyball to describe the influence of revolutions, further more the influence of side angle of attack. The aerodynamic characteristics should make the foundation for 3D ballistic equations and are used to describe the complete flight of the ball.

However, in order to accomplish this main goal, some specific aims must be achieved and they are presented as follows:

- To design wind tunnel experiment for the purpose of obtain results of all forces acting on a volleyball in flight. The volleyball must be able to rotate in the direction perpendicular to the direction of the airstream. In the second stage of tests the axis of rotation is changing the angle to airstream direction – side angle of attack.

- To gain new knowledge about all aerodynamic characteristics (C_D, C_L, C_S, C_{M_X}, C_{M_Y}, C_{M_Z}) for different side angles of attack.

- To study and discuss the special case of the flight of a ball without any rotations, which is often discussed because of unstable flight path, called knuckle ball.

- To consider the influence of the roughness of the surface of the volleyball on aerodynamic characteristics.

- To define uncertainties of all results obtained in the experiment.

2 FUNDAMENTALS

To fulfil the objectives of the Doctoral thesis, which were formulated in Section 1.2, it is necessary to retrace some of the terms of aerodynamics. Not only theory, but also accepted experiment results, are presented in the Chapter of Fundamentals.

2.1 AERODYNAMIC FORCES

Based on third Newton's law of motion it is clear, that generation of aerodynamic force on a body involves a complex interaction of the body and the air. The aerodynamic forces and moments on the body are due to only two basic sources [16]:

1. pressure distribution over the surface,
2. shear stress distribution over the body surface.

Pressure p *[Pa]* acts normal to body surface, while τ *[N/m²]* acts tangential, as it is visible in the Figure 2-1. The effect of pressure $p(s)$ and shear stress $\tau(s)$ distribution integrated over all surface A *[m²]* is a resultant aerodynamic force F *[N]* and moment M *[Nm],* defined by Eqs. (1) and (2), as visible in Figure 2-1 b), where v_∞ is free stream velocity.

$$F = \oiint (p\cos\alpha + \tau\sin\alpha)\, dS, \tag{1}$$

$$M = \oiint (\tau_s \times r)\ dS, \tag{2}$$

where M is taken about the centre of gravity and r *[m]* is distance of dS to the centre of gravity.

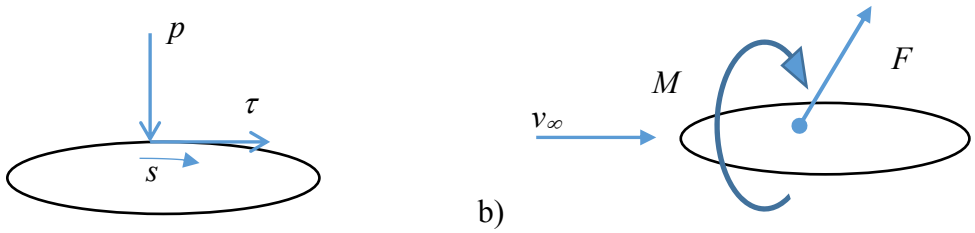

Figure 2-1: a) Pressure and shear stress acting on the surface, b) Resultant aerodynamic force and moment on the body

The resultant force F can be divided in three dimensions into components along the coordinate system, it is visible in the Figure 2-2:

F_D is component of F parallel to direction of v_∞, is called "Drag"

F_L is component of F in direction of axis "z" is called "Lift"

F_S is component of F in direction of axis "y" is called "Side force"

Similarly, moment M can be divided into 3 components according coordinate system, Figure 2-3:

M_X – Roll, positive direction from axis y to axis z,

M_Y – Pitch, positive direction from axis z to axis x,

M_Z – Yaw, positive direction from axis x to axis y.

Dynamic pressure is defined according Eq. (3):

$$q_\infty = \frac{1}{2}\rho_\infty v^2, \tag{3}$$

where ρ $[kg/m^3]$ is density of the fluid and v_∞ $[m/s]$ is the fluid stream velocity. Then dimensionless coefficients of forces and moments are defined by Eqs. (4) – (9):

$$C_D = \frac{2F_D}{\rho v_\infty^2 A}, \tag{4}$$

$$C_L = \frac{2F_L}{\rho v_\infty^2 A}, \tag{5}$$

$$C_S = \frac{2F_S}{\rho v_\infty^2 A}, \tag{6}$$

$$C_{Mx} = \frac{2M_X}{\rho v_\infty^2 A r_X}, \tag{7}$$

$$C_{My} = \frac{2M_Y}{\rho v_\infty^2 A r_Y}, \tag{8}$$

$$C_{Mz} = \frac{2M_Z}{\rho v_\infty^2 A r_Z}, \tag{9}$$

where $\frac{1}{2}\rho v_\infty^2$ is dynamic pressure, $A\ [m^2]$ is area of body in the plane (in the case of Figure 2-2 plane is defined by axes y and z) perpendicular to air stream direction and $r_{X,\ Y,\ Z}$ are reference lengths used to reduce moments to coefficient form.

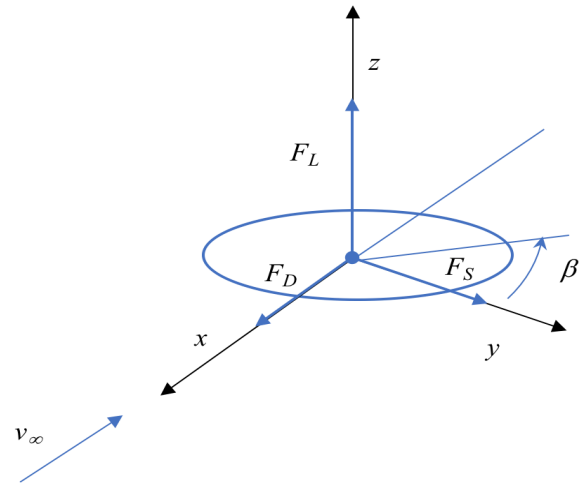

Figure 2-2: Definition of Drag, Lift and Side force.

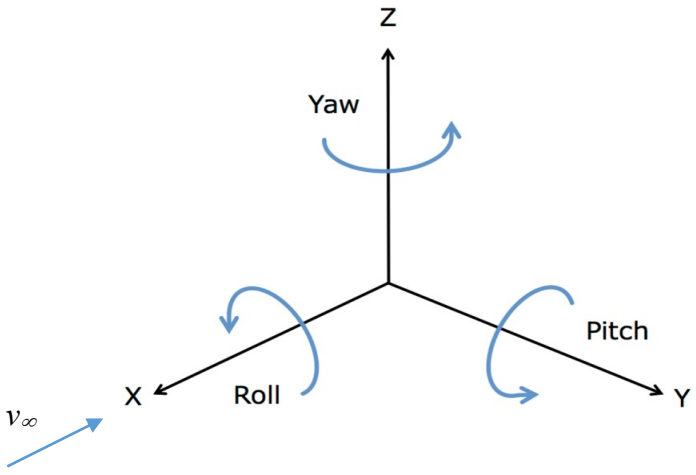

Figure 2-3: Coordinate system, definition of Roll, Pitch, Yaw, source [17]

2.2 REYNOLDS NUMBER

Reynolds number is a dimensionless number. According to [16]:

"The Reynolds number is physically a measure of the ratio of inertia forces to viscous forces in a flow and is one of the most powerful parameters in fluid dynamics."

For Reynolds number is usually used marking *Re [1]*, according to [18]. Reynolds number is defined by the Eq. (10):

$$Re = \frac{v_\infty d \rho}{\mu}, \tag{10}$$

where ρ *[kg/m³]* is density of fluid, μ *[Pa·s]* is dynamic viscosity of the fluid, and *d [m]* is characteristic dimension.

2.3 SPIN

The spin is dimensionless coefficient, which compares angular speed of rotating body and air stream velocity, defined by Eq. (11):

$$s = \frac{\omega d}{2 v_\infty}, \tag{11}$$

where ω *[rad/s]* is angular velocity, *d [m]* diameter and v_∞ *[m/s]* is velocity. The angular velocity can be described by Eq. (12):

$$\omega = 2\pi n, \tag{12}$$

where *n [rps]* are revolutions.
Spin is used to describe influence of Lift coefficient C_L on the rotating bodies in the airstream.

2.4 DRAG OF SPHERE

Drag of sphere, as mentioned already in Chapter 1 Introduction, has been studied since the beginning of 20th century. For practical use the results of experiments are depicted in diagram of coefficient of Drag C_D vs. Reynolds number *Re*, visible in the Figure 1-2.

The influence of roughness was studied in detail by Achenbach and published in 1974 [18]. The results of dependence of Drag coefficient C_D on the Reynolds number of sphere with diameter *d* and parameter of surface roughness *k/d* ratio is visible in Figure 2-4. The surface roughness is defined by dimensionless *k/d* ratio, where *k* is absolute roughness of surface (defined as a distance difference of the highest peak and lowest place of the surface) and *d* is a diameter.

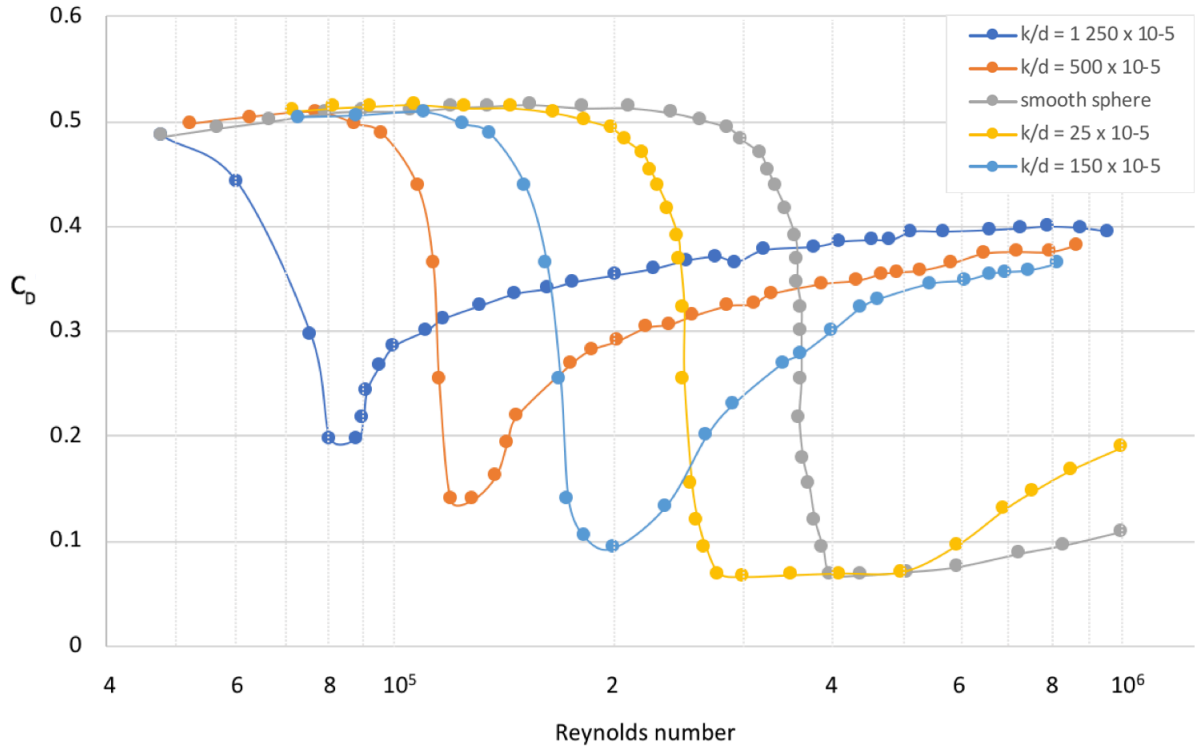

Figure 2-4: Coefficient of Drag C_D vs. Reynolds number Re, roughness of surface *k/d* is parameter, source [18]

2.5 PRESSURE DISTRIBUTION ON THE SURFACE, OVER THE SPHERE AND TRANSITION

The distribution of pressure defines Lift force according to Eq. (1). Different distribution of pressure on the surface of the sphere is for laminar flow and for turbulent flow. Particular dependences of coefficient of pressure C_P are depicted in the Figure 2-5. Coefficient of pressure is defined by Eq. (13):

$$C_P = \frac{p - p_\infty}{\frac{1}{2}\rho_\infty v_\infty^2}, \tag{13}$$

where p is static pressure, p_∞ is static pressure in the freestream, ρ_∞ is the freestream fluid density. Theoretical solution of potential flow is according to [16] defined by Eq. (14), in the Figure 2-5 by dot-and-dash code. Turbulent regimes are of similar trends as theoretical solution of potential flow. Laminar regime, in the Figure 2-5 *Re = 160 000*, is defined by a full line. It is also visible that in laminar flow surface pressure dependence deflects from the ideal case in the angle of $\varphi = 60°$, while turbulent cases deflect for much higher angles φ.

$$C_P = 1 - \frac{9}{4} sin^2\,(\alpha), \tag{14}$$

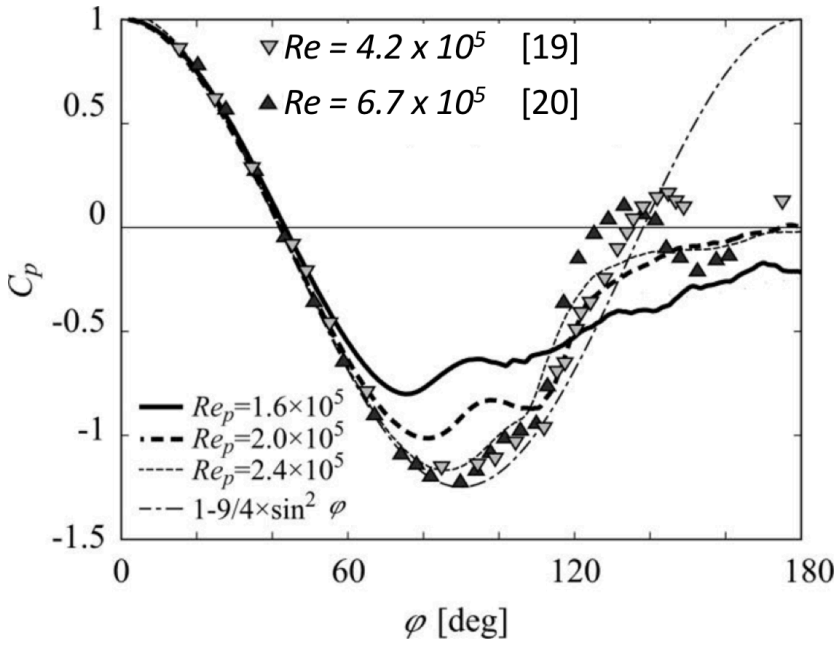

Figure 2-5: Distribution of pressure on the surface of a spheres, parameter is Reynolds number, source [21]

2.6 LIFT FORCE ON A SPHERE

Lift force on a smooth sphere is generated by different pressure distribution on the upper part and the lower part of a sphere. There are two ways to create pressure distribution imbalance:

1. rotation,
2. unsymmetrical transition from laminar to turbulent regime of flow.

2.6.1 Magnus Effect

The lift force is generated on a rotating sphere (as well as a rotating cylinder) in the flow as it is visible in Figure 2-6. Steady sphere in the stream of laminar flow (low Reynolds number) in accordance to principle of symmetry does not generate any Lift force. Lift force starts to appear if the sphere starts to rotate. Rotation of a sphere causes deformation of stream lines around sphere, as shown in Figure 2-6.

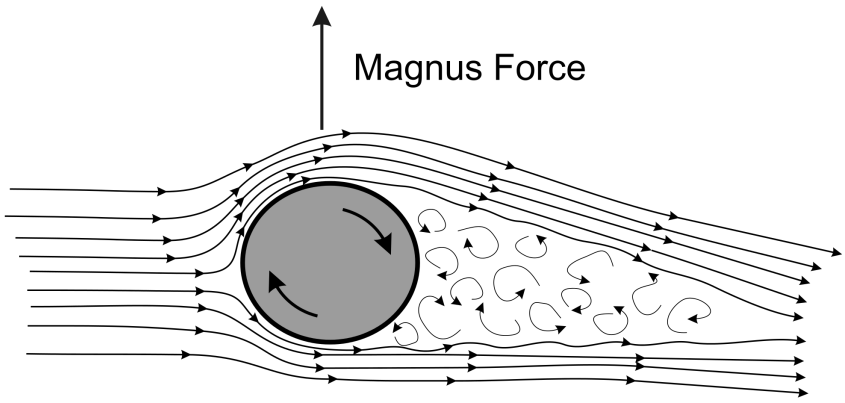

Figure 2-6: Magnus effect, source [21]

2.6.2 Knuckling Effect

Knuckling effect is denomination of the flight of a sphere (ball) which does not rotate in the expected values of Magnus force generation (revolutions $n = 0$ *rps* or very close to zero). In different sports (football, baseball, cricket, volleyball and others) athletes deal with this

phenomena when flight of the ball is unpredictable. In volleyball it is mostly during service, where the knuckling effect appears. In study [23] the conclusion is made, that knuckling effect is occurring only in the narrow range of Reynolds number, area of critical Re, together with the condition of revolutions $n = 0\ rps$.

2.7 UNCERTAINTIES

Physical experiments are fundamentally about measuring physical values of reality. Each measured value in an experiment is of certain value of uncertainty, error of the measurement. There are two basic types of errors: 1. systematic and 2. random. The results from measurement have defined value by accuracy and precision. Accuracy means how close the result is to the true value. Precision describes how repeat readings are close together. Accuracy is improved by reducing systematic errors. Precision is improved by reducing random errors.

If the error is **systematic**, the uncertainty can be defined by the smallest division on the instrument. Systematic error is defined by the instruments and devices used in the measurement.

If the error is **random**, the uncertainty is usually determined by the growth of the amount of readings.
Random errors are appointed by statistical mathematics: values such as *standard deviation* and *dispersion* describe error value. Calculation of uncertainties is important for expressing the real value of the measured results. Practical description of appointing of uncertainties is in [24] and [25].
The CEN standard ENV 13005:1999 [26] contains a complete description of assessing the uncertainties. ‘Standard deviation’ and ‘enlarged uncertainty’ are the main modes of expressing the uncertainty about a measurement. The use of the Taylor approximation for the uncertainty propagation and classification of uncertainties of **type A** and **type B** based on use or lack of use of a statistical approach of evaluating the standard deviation.

2.8 BALLISTIC EQUATIONS

The Ballistics is the part of physics, which deals with motion of bodies launched in to a medium, such as air, water or space. A typical body which is studied in ballistics is projectile. There are four cases of Ballistics: 1. Object dropped from a known altitude, 2. Object thrown upward, 3. Object thrown horizontally from a height above the ground, 4. Object launched from the ground at an angle.

Ballistic equations are based on Newtons second law of motion, as described in [D1]. Commonly used case of ballistic equations describes the case of motion in the plane with Drag and Lift – 2D ballistics.

In this case differential motion equations are described in Eqs. (15) and (16):

$$\ddot{x} = -\frac{\rho A}{2m}(\dot{x}^2 + \dot{y}^2)(C_D \cdot cos\alpha - C_L \cdot sin\alpha) \tag{15}$$

$$\ddot{y} = \frac{\rho A}{2m}(\dot{x}^2 + \dot{y}^2)(C_L \cdot cos\alpha - C_D \cdot sin\alpha) - g \tag{16}$$

for boundary and initial conditions in time *t = 0*:

$$x(0) = 0 \tag{17}$$

$$y(0) = y_0 \tag{18}$$

value of velocity:

$$v(0) = \sqrt{\dot{x}^2(0) + \dot{y}^2(0)} = v_0 \tag{19}$$

and the vector velocity argument:

$$\alpha(0) = arctg\frac{\dot{y}(0)}{\dot{x}(0)} = \alpha_0, \tag{20}$$

after converting Eqs. (15) and (16) to a system of ordinary differential equations of first order and conditions Eqs. (17 – 20) it is possible to solve the shape of the ballistic curve by numerical integration, for example Runge-Kutta method.

For the purpose of describing real motion in real space it is necessary to extend performed ballistic equations in two 3D and to integrate influence of Drag, Lift and Side forces. This adjustment of the equations is shown in more detail in Chapter 5 Discussion and analysis.

3 EXPERIMENT

Experiment was installed in the laboratories of the Department of Aerodynamics, VZLU Aerospace Research and Test Establishment in Prague. A low speed wind tunnel with open test section was used. In the development of the project two independent measurements were performed. Firstly the set up, which measured Drag and Lift acting on a volleyball with rotation in the airstream was published in [D2]. Secondly experiment setting was made to accomplish all aims of the doctoral thesis, specially to describe aerodynamic characteristics of a rotating volleyball, based on [D3]. Final experimental set up is briefly described in this Chapter.

Experimental setting accomplished requirements for the purpose to achieve all aims defined in Chapter 1.2:

1. to measure forces and moments acting on a volleyball in wind tunnel test section,
2. to create and control revolutions of a volleyball,
3. to allow all the setting to turn in defined angles in relation to airstream direction.

3.1 MEASUREMENT DESCRIPTION

Sketched scheme was proposed to fulfil set objectives above (1. – 3.), firstly presented in [D3]. The scheme which is depicted in the Figure 3-1, describes way how to measure all forces acting on rotating volleyball in a wind tunnel test section.

3.1.1 Measuring of forces and moments

Forces are measured in six independent positions: F_1, F_2, F_3, F_4, F_5, F_6 (as visible in Figure 3-1): there are three forces to define Drag F_D and moment of Pitch M_Y: F_3, F_4 and F_5, two forces to define Lift F_L and moment of Roll M_X: F_1 and F_2, one force to define Side force F_S: F_6. Moment of Yaw M_Z is defined by F_3 and F_4.

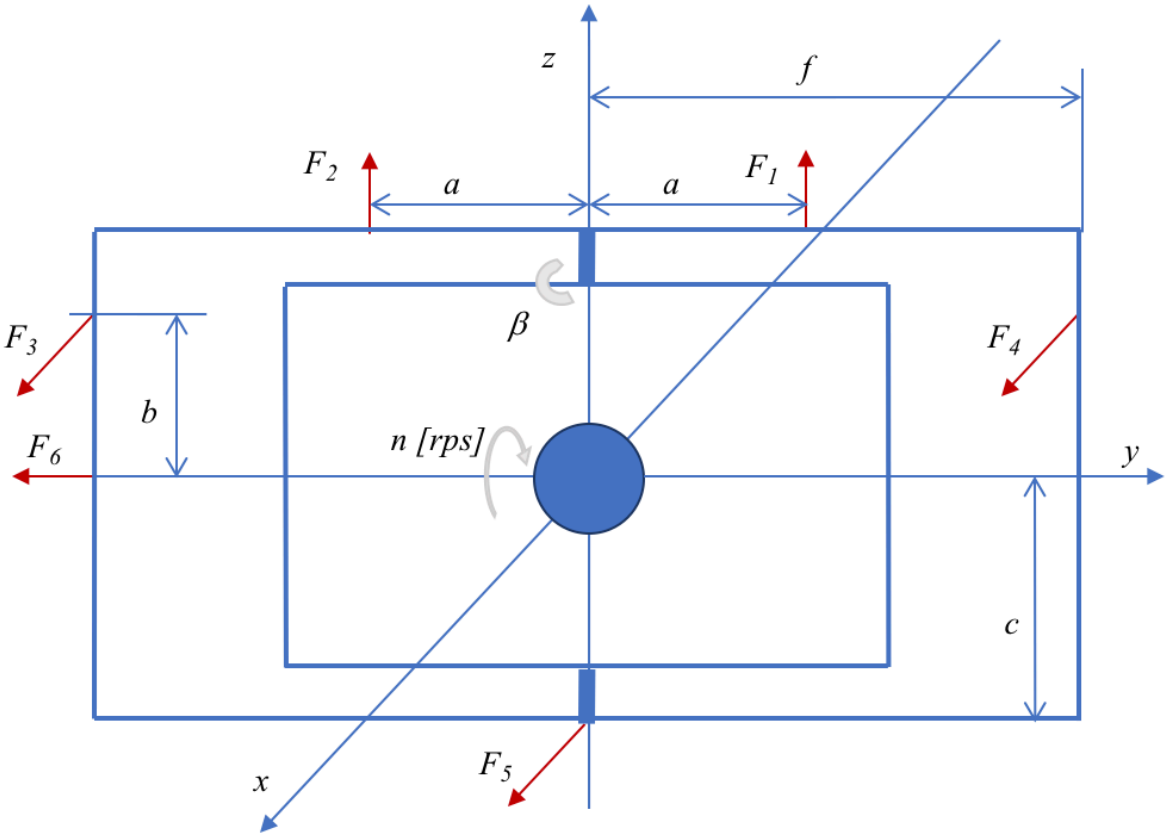

Figure 3-1: Scheme of experiment, source [D3]

Forces and moments are calculated according to Eqs. (21 – 26).

- Drag:

$$F_D = F_3 + F_4 + F_5 \tag{21}$$

- Lift:

$$F_L = F_1 + F_1 \tag{22}$$

- Side force:

$$F_S = F_6 \tag{23}$$

- Roll:

$$M_X = F_1 \cdot a - F_2 \cdot a \tag{24}$$

- Yaw:

$$M_Z = F_4 \cdot f - F_3 \cdot f \tag{25}$$

- Pitch:

$$M_Y = (F_3 + F_4) \cdot b - F_5 \cdot c \tag{26}$$

3.1.2 Revolutions of volleyball

Free for rotation shaft is proposed in the scheme, it is visible in Figure 3-1 along the y axis. Revolutions *n [rps]* are induced on the free rotation shaft by a stepping motor. The stepping motor is controlled by software.

3.1.3 Side angle of attack β

The side angle of attack is implemented by a special developed connection of two independent frames: 1. outer frame, on which are measured forces by strain gauges, 2. inner frame, which holds the volleyball and the stepping motor. The inner frame is depicted in Figure 3-2. Connection of the frames is made the way that the user is simply able to set and fix the exact angle (this is the β angle) in between inner and outer frame.

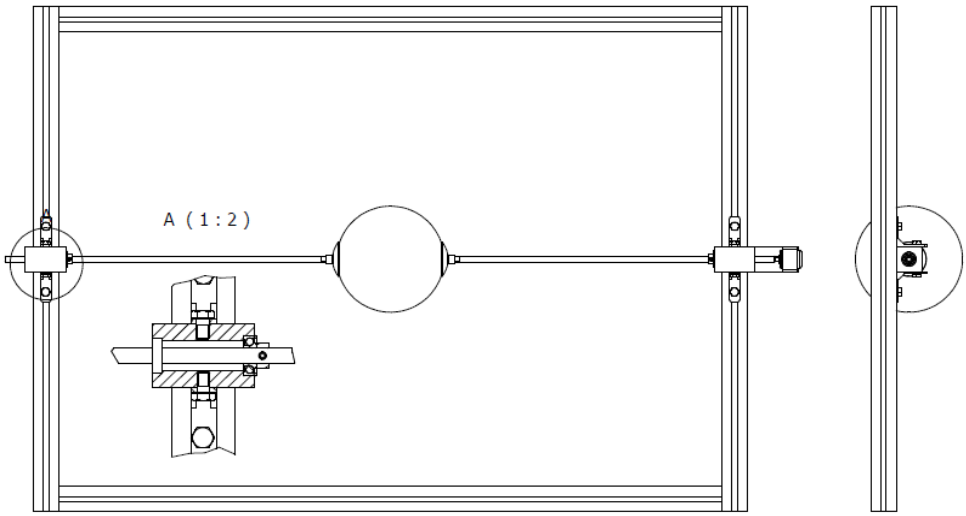

Figure 3-2: Construction draft of the inner frame, which holds the volleyball and the stepping motor

All details of the experiment description such as definition and description of the devices and instruments used for construction and installation of the measurement are summarized in [D4].

3.2 METHODOLOGY

Conditions of experiment (density, temperature, viscosity) including values of all used quantities such as velocity, revolutions and side angle of attack are defined in this Section.

3.2.1 Conditions of experiment

Air density: $\rho = 1.2135$ kg / m^3.

Average temperature: t = 9°C (T = 282,15 K),

Dynamic viscosity: $\mu = 17{,}8179 \times 10^{-6}$ N.s/m^2 was calculated according to Sutherland's formula, defined in Eq. (27):

$$\mu = \mu_0 \frac{T_0 + C}{T + C} \left(\frac{T}{T_0}\right)^{\frac{3}{2}}, \tag{27}$$

where reference temperature $T_0 = 291.15$ K, C is Sutherland's constant, for air C = 120 K, reference viscosity at reference temperature T_0 is $\mu_0 = 18.27 \times 10^{-6}$ N.s/m^2 and ρ is density [kg/m^3].

Measured values of quantities for experiment are defined:

measured air stream velocities: $v_\infty = 10; 15; 17; 19; 21; 25$ m / s,

controlled ball revolutions: n = 0; 5; 6.25; 7.5; 8.75; 10; 11.25; 12.5; rps,

set of side angles of attack: β = 0°; 9.92°; 20.56°; 30.70°; 41.15°; 47.08°.

3.2.2 Examined body

The aim of the doctoral thesis is to described forces and moments acting on the rotating volleyball. A volleyball ball is the examined body. There are many different volleyballs, which have different properties, such as weight, size etc. For the purpose of the observation the official volleyball, approved by FIVB[1] was chosen. The ball, which is FIVB approved is used in official competitions of volleyball worldwide.

Observed ball: Mikasa VLS 300, determined for beach volleyball.

Detailed properties of ball Mikasa VLS 300 are defined in [27]. For the experiment purposes, the most important quantity is the diameter of the ball. According to *FIVB rules* [15] and according to [27] the circumference of the ball for beach volleyball is $o = 0.67 \pm 0.01\ m$, which responds to diameter $d = 0.2164\ m$. The particular sample of the measured ball Mikasa VLS 300, which was examined in the wind tunnel experiment, diameter was measured and presented in [D5]:
diameter of the Mikasa VLS 300 according to measurement is: $d = 0.24\ m$.

In further computation $d = 0.24\ m$ is used.

3.2.3 Reynolds number

Based on velocity and ball dimensions, Reynolds number is calculated according to Eq. (10). According to Eq. (10) the values of quantities defined in this Section the range of Reynolds numbers is defined by Re_{MIN} and Re_{MAX}.

$$Re_{MIN} = \frac{v_{\infty MIN} \cdot d \cdot \rho}{\mu} = 164\,500$$

[1] FIVB: „Fédération Internationale de Volleyball“ is international volleyball federation. Ball, which is FIVB approved is tested according [27], after approval ball is used for official competitions.

$$Re_{MAX} = \frac{v_{\infty MAX} \cdot d \cdot \rho}{\mu} = 411\ 260$$

The range of Reynolds numbers is $Re = \langle 163\ 453 \div 411\ 260 \rangle$. As diameter d is constant and dynamic viscosity μ was also constant in the measurement the Reynolds number depends only on velocity v_∞. For each velocity exists one value of Reynolds number, exact values are summarized in Table 3-1.

Table 3-1: Table of Reynolds numbers *Re* observed in experiment

velocity v_∞ *[m/s]*	**10**	**15**	**17**	**19**	**21**	**25**
Reynolds number *Re [1]*	164 500	246 750	279 650	312 550	345 450	411 260

The investigated area of Reynolds numbers is around critical Reynolds number, as defined in Section 1.1: "critical Reynolds number is in the case of smooth sphere defined by $C_D = 0.3$, $Re_{CRIT.} = 300\ 000$". The effect of critical Reynolds number on the results of aerodynamic parameters is expected.

3.2.4 Spin

Spin is calculated according to Eq. (11). For quantification of the used spin in the experiment the revolutions *n [rps]* must be calculated into *ω [rad/s]*, as it is in Eq. (12).

Minimal spin is naturally $s = 0$ in the case of flight without rotation ($n = 0$ *rps*). Maximal spin is calculated as follows:

$$s_{max} = \frac{\omega_{max} d}{2 v_{\infty min}} = 0.94.$$

The range of spin is $s = \langle 0 \div 0.94 \rangle$.

It is visible in the Eq. (11), that spin depends on the velocity v_∞. Therefore the values of the spin can not be defined in the same simple way as for Reynolds number. The particular values of the spin, corresponding to measurer conditions, are summarized and presented in Table 3-2.

Table 3-2: The particular values of spin number observed in experiment

SPIN *s [1]*	velocity v_∞ *[m/s]*	10	15	17	19	21	25
revolutions *n [rps]*	Reynolds number *Re [1]*	164 500	246 750	279 650	312 550	345 450	411 260
5		0.3794	0.2529	0.2232	0.1997	0.1807	0.1518
6.25		0.4743	0.3162	0.279	0.2496	0.2258	0.1897
7.5		0.5691	0.3794	0.3348	0.2995	0.271	0.2276
8.75		0.664	0.4426	0.3906	0.3495	0.3162	0.2656
10		0.7588	0.5059	0.4464	0.3994	0.3613	0.3035
11.25		0.8537	0.5691	0.5022	0.4493	0.4065	0.3415
12.5		0.9485	0.6324	0.558	0.4992	0.4517	0.3794

For the cases of measurements with side angle of attack $\beta \neq 0$ the values of spin are different – this is thoroughly discussed and explained in Section 5.3.2.

3.2.5 Calibration

Independent calibration of each strain gauge was done. Six constants were resulting from the calibration, each for one strain gauge. Constants from calibrations are used to recalculate force *F [N]* from measured voltage *U [V]*.

3.2.6 Measurement procedure

Measurement of the forces acting on the volleyball in the airstream was performed according to economical planned procedure. All conditions of the flight of a ball (*Re, n,* β) defined in Section 3.2 were measured. The procedure is described and published in [D4].

Forces acting on the frames were measured firstly without the ball. Different side angles of attack β and velocities v_∞ were measured without installed volleyball – revolutions of empty axis were neglected. Secondly all procedures were done with the ball fixed in the frame.

3.2.7 Data processing

The experimental devices, such as wind tunnel and stepping motor were controlled by software Labview. The data from measurement were collected by software Labview. The data were further processed in MatLab software according to equations presented in the Doctoral thesis.

4 RESULTS OF EXPERIMENT

The purpose of the experimental investigation is to achieve reliable results of aerodynamic characteristics, which would be further used in 3D ballistic equations. The complete flight is described by using 3D ballistic equations.

The results of the experiment are presented in this Chapter. The results are further discussed in Chapter 5 in different topics according to aims, which were defined in the Introduction of this Doctoral thesis. Firstly, the results of coefficient of Drag C_D, Lift C_L and Side force C_S are introduced in condition of side angle of attack $\beta = 0°$, secondly coefficients of moments are presented. Uncertainties of all values of the measurement are in the last part of Chapter 4 Results of experiment.

4.1 COEFFICIENTS OF DRAG C_D, LIFT C_L AND SIDE FORCE C_S WITH SIDE ANGLE OF ATTACK $\beta = 0°$

4.1.1 Coefficient of Drag CD

The dependence of coefficient of Drag C_D on Reynolds number Re of a smooth sphere of diameter d was shown in Figure 1-2. The results of the experiment are compared to a smooth sphere at first, the effect of surface roughness is discussed later in Chapter 5.
The dependence of coefficient of Drag C_D versus Reynolds number Re and revolutions n is depicted in Figure 4-1. It is important to mention that all results are close to critical Reynolds number, as is visible in Figure 4-1. It is also visible, that in the case of $n = 0$ rps for lower Reynolds numbers the values of C_D are high – as expected according to Figure 1-2, there is coefficient of Drag ($C_D = 0.5$) acting on the smooth sphere in the case of laminar flow. With increasing Reynolds number the area of transition appears (C_D decreases). Afterwards with increasing Reynolds number the coefficient of Drag increases.

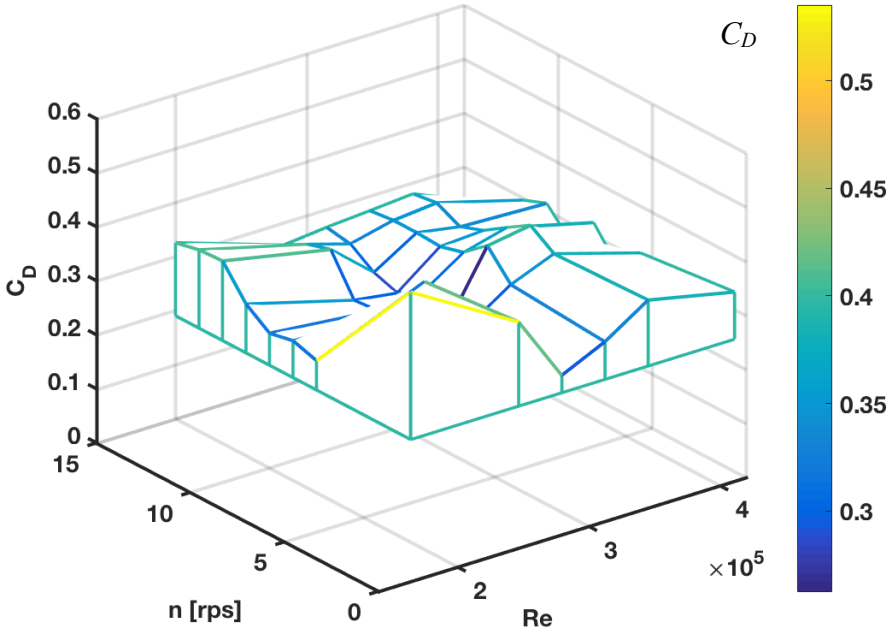

Figure 4-1: Coefficient of Drag C_D, $\beta = 0°$

4.1.2 Coefficient of Lift C_L

The dependence of coefficient of Lift on Reynolds number and on revolutions is depicted in the Figure 4-2. The basic trend is visible in the Figure 4-2: The higher revolutions n, the higher coefficient of Lift C_L – this is caused by Magnus effect as described in Section 2.6.1. Further analysis is discussed in Section 5.1.2.

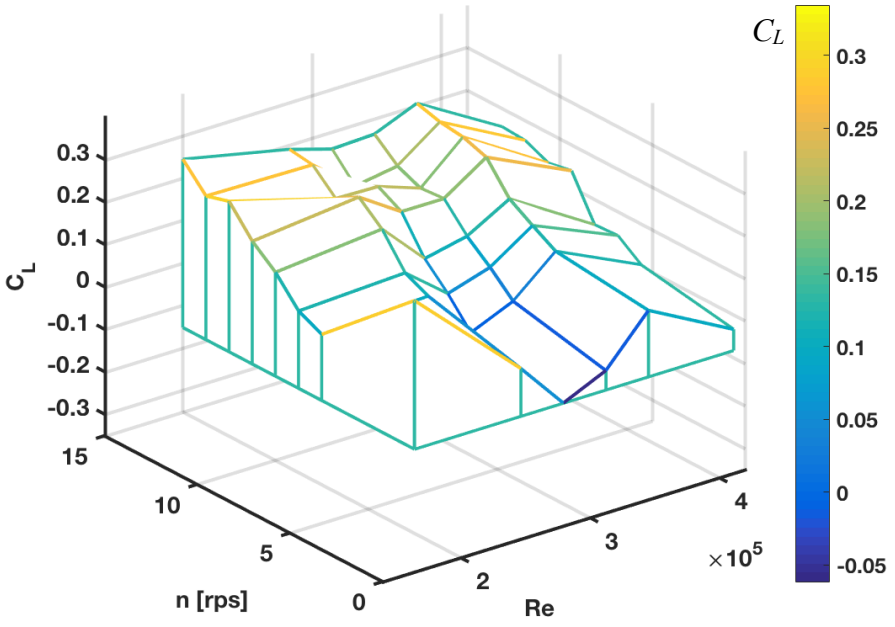

Figure 4-2: Coefficient of Lift C_L, $\beta = 0°$

4.1.3 Coefficient of Side force C_S

Side force F_S was measured in the experiment, according to Eq. (6) the coefficient of side force was calculated. The dependence of coefficient of Side force C_S on Reynolds number and revolutions is depicted in the Figure 4-3.
Minimum value of C_S is at maximum value of Reynolds number $Re = 410\ 000$.

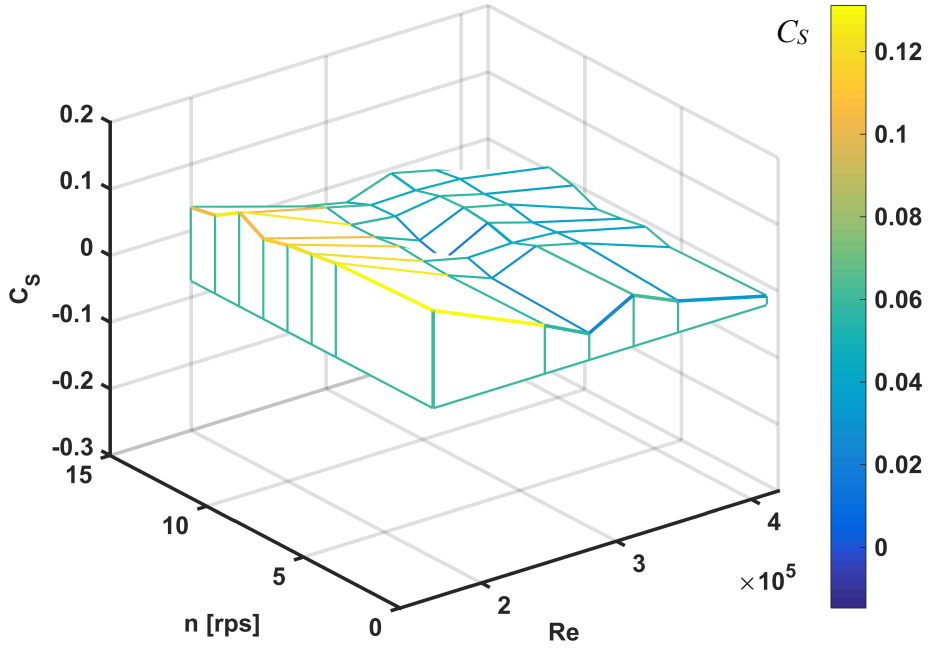

Figure 4-3: Coefficient of Side force C_S, $\beta = 0°$

4.2 COEFFICIENTS OF MOMENTS ACTING ON THE VOLLEYBALL

The results of the moments (Roll, Pitch and Yaw) were calculated according to Eqs. (23 – 25) and coefficients of moments further according to Eqs. (7 – 9). The final results of coefficients of moments in the case $\beta = 0°$ are depicted in the following figures: Figure 4-4, Figure 4-5 and Figure 4-6.

In the Figure 4-4 it is visible that the effect of the rotation (revolutions n) on the course of **coefficient of Roll** C_{Mx} is not intensive, specially not for $Re > 280\ 000$.

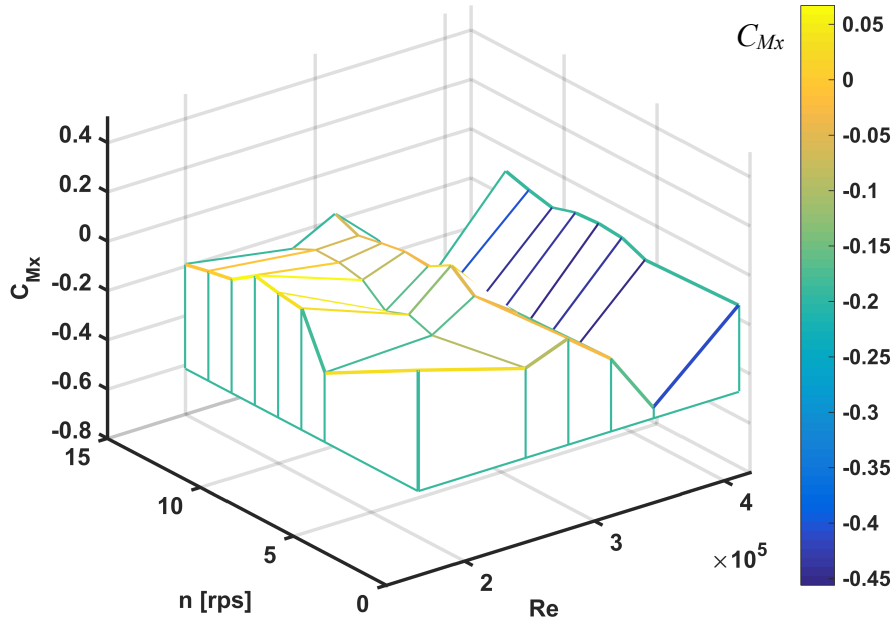

Figure 4-4: The effect of Reynolds number and revolutions on coefficient of Roll C_{Mx}, side angle of attack $\beta = 0°$

The coefficient of Pitch is depicted in the Figure 4-5. The effect of the rotation (revolutions n) is not very intensive.

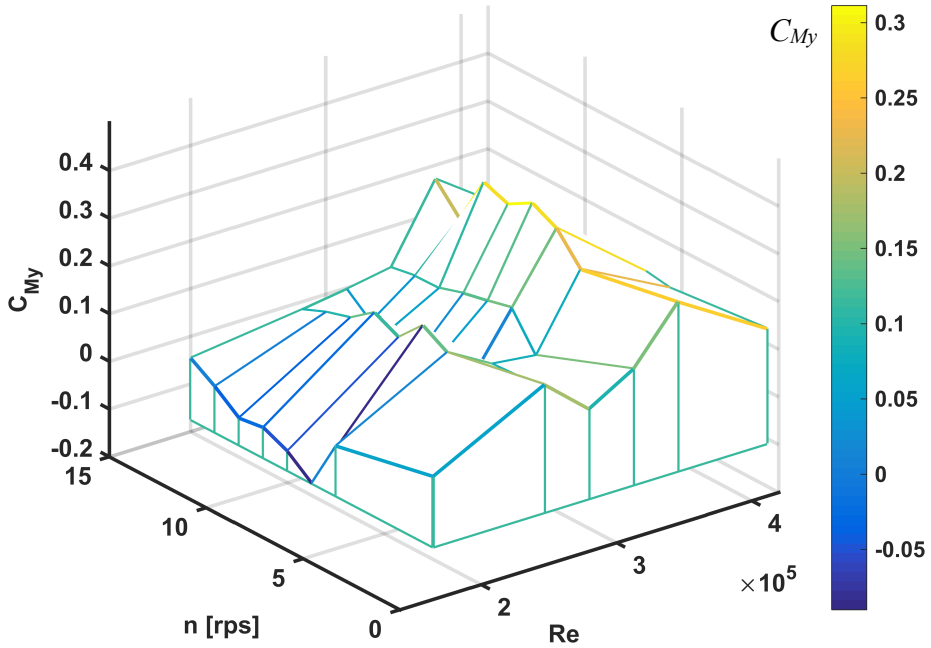

Figure 4-5: The effect of Reynolds number and revolutions on coefficient of Pitch C_{My}, side angle of attack $\beta = 0°$

The results of **coefficient of Yaw** are depicted in the Figure 4-6. "Side components" of the Drag, forces F_3 and F_4, are acting on the same distance f, see Figure 3-1.
The effect of revolutions on the course of C_{Mz} is recognizable in the area of critical Reynolds number, $Re_{C\,sphere} = 300\,000$, as visible in the Figure 4-6.

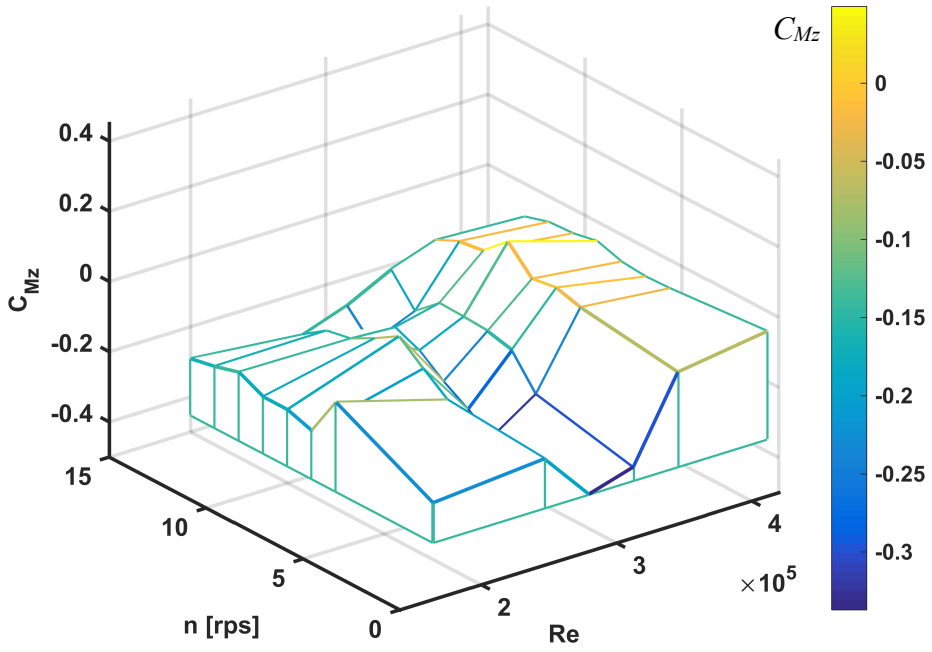

Figure 4-6: The effect of Reynolds number and revolutions on coefficient of Yaw C_{Mz}, side angle of attack $\beta = 0°$

4.3 RESULTS OF COEFFICIENTS OF FORCES FOR DIFFERENT SIDE ANGLE OF ATTACK β

To measure the influence of side angle of attack on the aerodynamic characteristics is one of the main topics of this Doctoral thesis. The motivation to study influence of side angle of attack on aerodynamic characteristics is to describe more complicated cases of a flight, which includes: 1. turn of the axis of rotation in the flight, 2. side wind acting on the volleyball in the flight. The results shall be used as definition of aerodynamic coefficients into the 3D ballistic equations. In this Section dependences are shown and described, the discussion over the results is in Section 5.3.

The new knowledge gained in the observation of the ball can be used in another areas of aerodynamics such as basic research of a smooth sphere.

For simplicity, the Section is divided according to aerodynamic characteristics into organized pieces: coefficient of Drag, coefficient of Lift, coefficient of Side force.

4.3.1 Coefficient of Drag C_D

With the aim to describe the effect of side angle of attack on coefficient of Drag, the dependences are shown in order of increasing side angle of attack β in the following figures. The dependence of C_D on Re and on n for $\beta = 9.92°$ is depicted in the Figure 4-7. The basic courses and trends are recorded:

1. The area of critical Reynolds number (according to previous investigation expected for $240\ 000 < Re < 340\ 000$) is noticeable as well, even for all values of revolutions.
2. Unexpected is, that highest values of coefficient of Drag C_D occur for high Reynolds numbers $Re = 410\ 000$ and $n = 5\ rps$. In average (across all the values of revolutions n) highest C_D occurs for $Re = 340\ 000$.
3. With increasing revolutions n the coefficient of Drag C_D decreases for all Reynolds numbers Re.

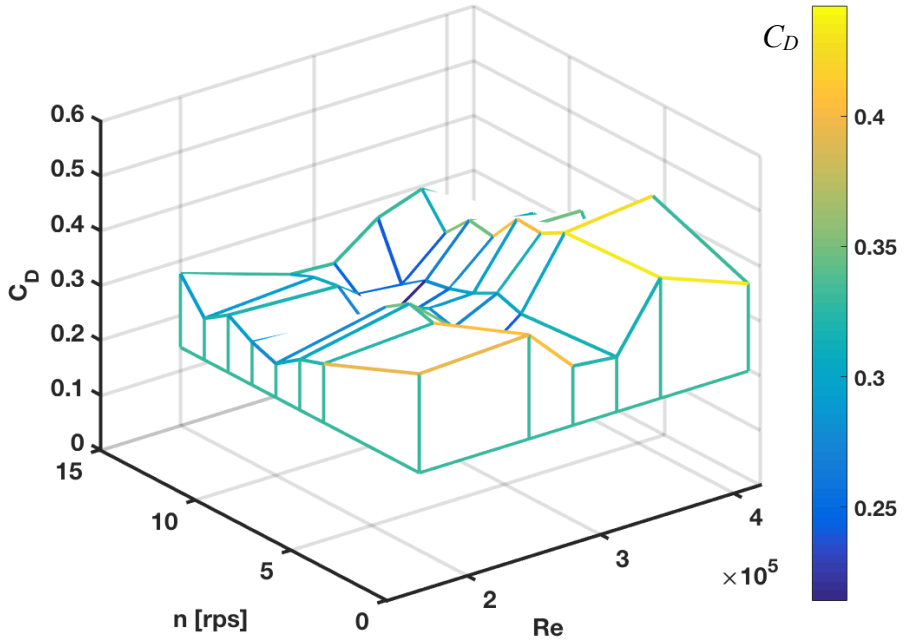

Figure 4-7: The dependence of the coefficient of Drag C_D on Reynolds number Re and on revolutions n – side angle of attack $\beta = 9.92°$

The dependence of C_D on Re and on n for $\beta = 20.56°$ is depicted in the Figure 4-8. The basic courses and trends are recorded:

1. The area of very low coefficient of Drag C_D is visible for $Re = 2.5 \times 10^5$ and $n = 6.25$ *rps*. Values of C_D are in this area very close to $C_D = 0.1$.
2. The high peak $C_{D\,max}$ is according to Table 5-1 at low Reynolds number $Re = 1.6 \times 10^5$ and $n = 0$ *rps* – this could be marked as a laminar flow.
3. The courses and trends for $\beta = 20.56°$ are similar to $\beta = 0°$.
4. For each $Re = const.$ values of C_D increases with revolution increase. This is the start of the effect of the increase of side angle of attack β.

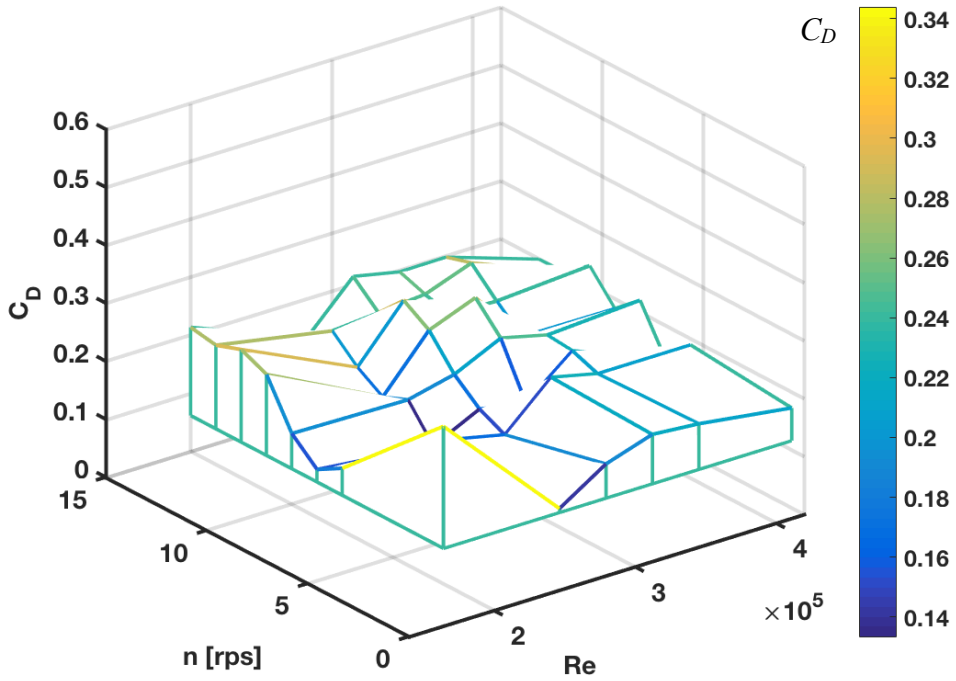

Figure 4-8: The dependence of the coefficient of Drag C_D on Reynolds number Re and on revolutions n – side angle of attack $\beta = 20.56°$

The dependence of C_D on Re and on n for $\beta = 30.7°$ is depicted in the Figure 4-9. The basic courses and trends are recorded:

1. Comparably as in the previous case the area of very low values of C_D appears in the conditions of $Re = 250\,000 – 310\,000$ and $n = 5 – 7.5$ *rps*.
2. The maximum value of coefficient of Drag $C_{D\,max}$ occurs at $Re = 160\,000$ and revolutions $n = 12.5$ *rps*.

3. The trend of increase of values of C_D (Re = const.) with increase of revolutions n is present. The phenomena is significant for lower Reynolds numbers, particularly: $Re < 250\ 000$, but also $Re = 410\ 000$.
4. The coefficient of Drag C_D in the case of revolutions $n = 0\ rps$ and $n = 5\ rps$ is low: $C_D < 0.2$.

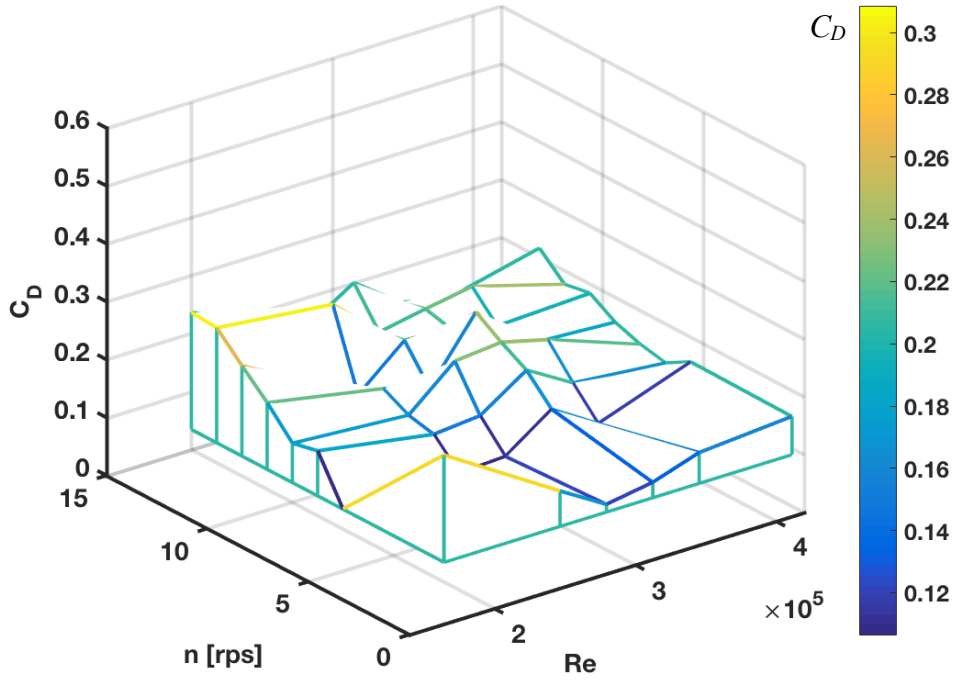

Figure 4-9: The dependence of the coefficient of Drag C_D on Reynolds number Re and on revolutions n – side angle of attack $\beta = 30.7°$

The dependence of C_D on Re and on n for $\beta = 41.15°$ is depicted in the Figure 4-10. The basic courses and trends are recorded:

1. The area of low values of C_D (which was reported in previous cases) is noticeable for $\beta = 41.15°$ as well, but it is visibly modified.
2. The maximum value of coefficient of Drag $C_{D\ max}$ occurs at $Re = 160\ 000$ and revolutions $n = 0\ rps$.
3. The trend of the increase of values of C_D (Re = const.) with the increase of revolutions n is again present. The phenomena is significant already for all Reynolds numbers.
4. The coefficient of Drag C_D in the case of $n = 0\ rps$ is very low: even $C_D < 0.1$, for $Re > 310\ 000$.

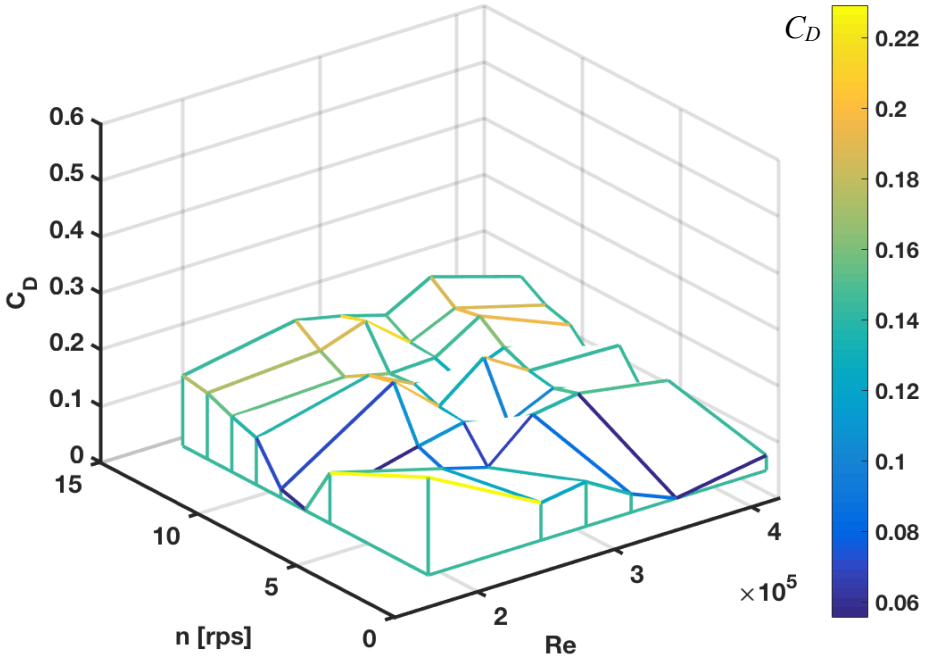

Figure 4-10: The dependence of the coefficient of Drag C_D on Reynolds number Re and on revolutions n – side angle of attack $\beta = 41.15°$

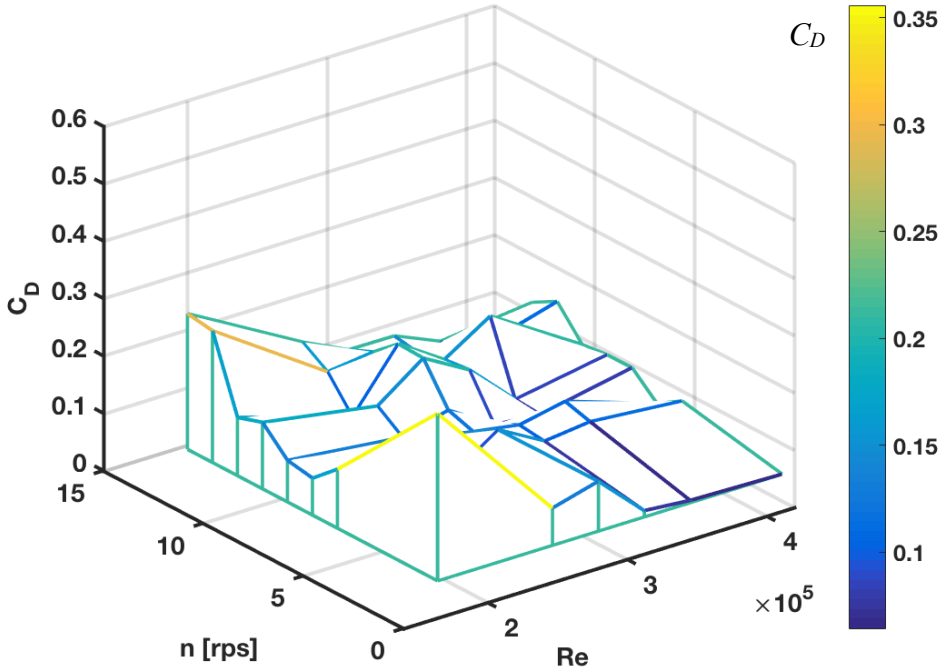

Figure 4-11: The dependence of the coefficient of Drag C_D on Reynolds number Re and on revolutions n – side angle of attack $\beta = 47.08°$

The dependence of C_D on *Re* and on *n* for $\beta = 47.08°$ is depicted in the Figure 4-11. The basic courses and trends are recorded:

1. The area of low values of C_D (which was reported in previous cases) is noticeable.
2. The maximum value of coefficient of Drag $C_{D\ max}$ occurs at $Re = 160\ 000$ and revolutions $n = 0\ rps$ – refers to laminar flow.
3. The trend of the increase of values of C_D (Re = const.) with the increase of revolutions *n* is again present. The phenomena is significant for all Reynolds numbers, but the effect is more intensive in the case of lower Reynolds numbers, as it is visible in the Figure 4-11 $Re < 280\ 000$.
4. The coefficient of Drag C_D in the case of $n = 0\ rps$ is very low: even $C_D < 0.1$, for $Re > 310\ 000$.

4.3.2 Coefficient of Lift C_L

The dependences of coefficient of Lift C_L on Reynolds number *Re* and revolutions *n* for different side angles of attack β are presented in this Section in figures: Figure 4-12 – side angle of attack $\beta = 9.92°$, Figure 4-13 – side angle of attack $\beta = 20.56°$, Figure 4-14 – side angle of attack $\beta = 30.7°$, Figure 4-15 – side angle of attack $\beta = 41.15°$, Figure 4-16 – side angle of attack $\beta = 47.02°$.

In the Table 4-1 and Table 4-2 it is visible, that minimal values of C_L respond to $n = 0\ rps$. The minimal values of C_L are in higher Reynolds numbers in the case of $\beta > 30°$. The minimum values are at the n = 0 rps and the values of C_L are randomly distributed. This effect is discussed in the Section 5.5, flight of ball without rotation.
On the other hand the maximum values of C_L are at high revolutions ($n = 11.25 – 12.5\ rps$), that confirms the predicted Magnus effect.

Table 4-1: The effect of side angle of attack on the maximal values of coefficient of Lift C_L

β [°]	**0**	**9.92**	**20.56**	**30.7**	**41.15**	**47.08**
C_L [1]	0.33	0.37	0.32	0.33	0.25	0.27
Re [1]	160 000	340 000	160 000	160 000	280 000	160 000
n [rps]	12.5	11.25	12.5	11.25	11.25	11.25

Table 4-2: The effect of side angle of attack on the minimal values of coefficient of Lift C_L

β [°]	0	9.92	20.56	30.7	41.15	47.08
C_L [1]	- 0.06	- 0.29	- 0.22	- 0.04	- 0.13	- 0.09
Re [1]	280 000	160 000	160 000	410 000	350 000	350 000
n [rps]	0	0	0	0	0	0

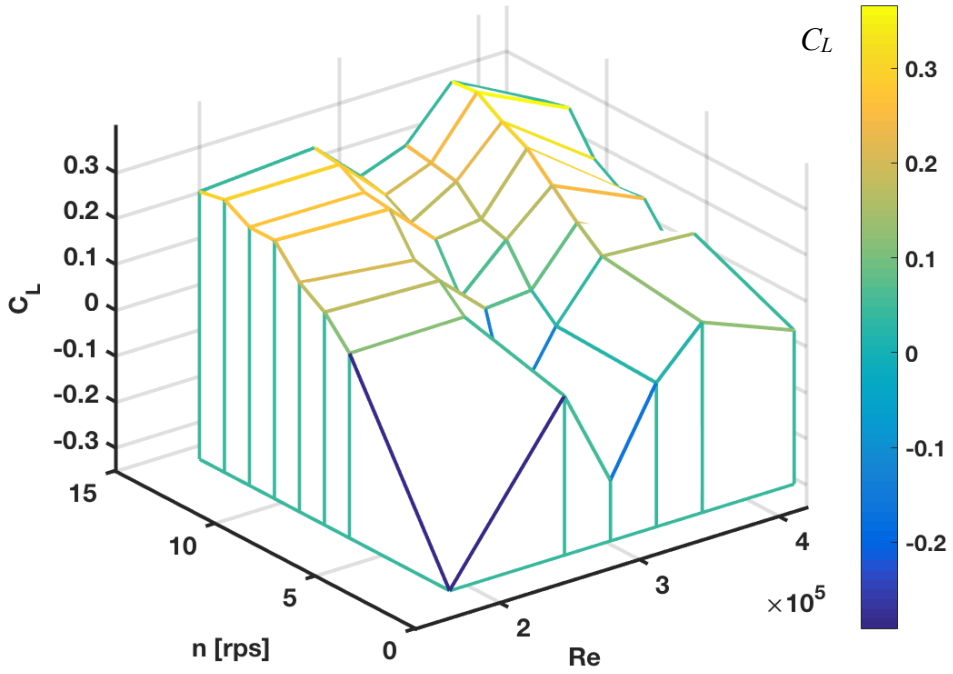

Figure 4-12: The dependence of coefficient of Lift C_L on Reynolds number Re and on revolutions n – side angle of attack $\beta = 9.92°$

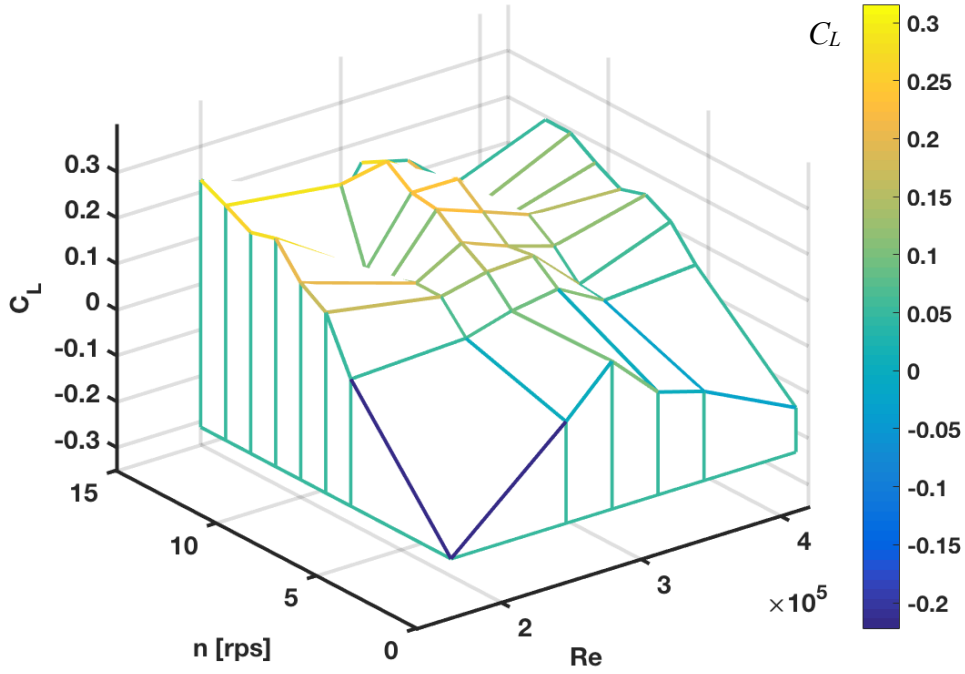

Figure 4-13: The dependence of coefficient of Lift C_L on Reynolds number *Re* and on revolutions *n* – side angle of attack $\beta = 20.56°$

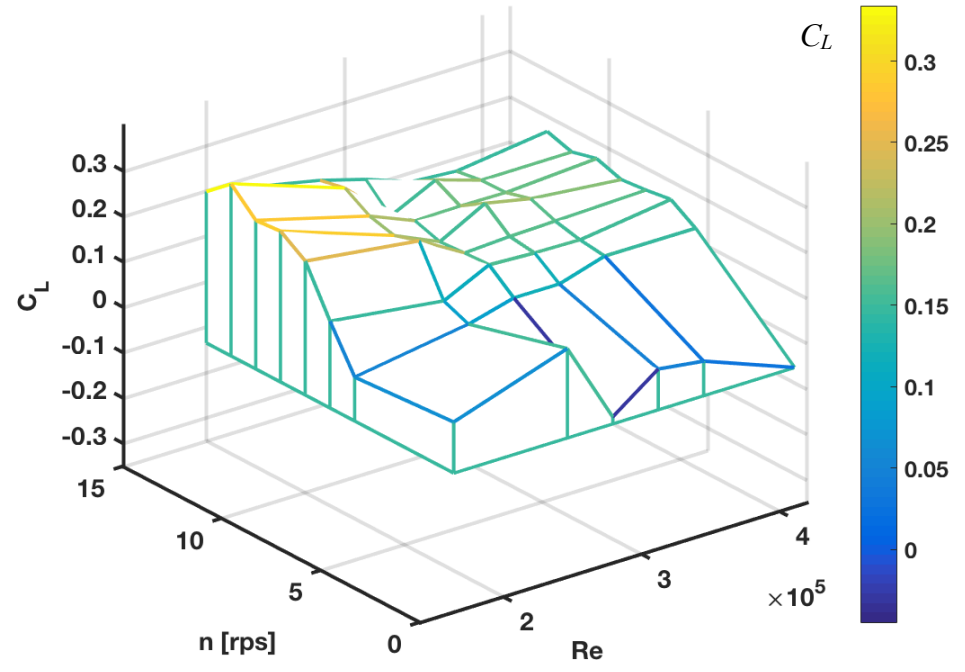

Figure 4-14: The dependence of coefficient of Lift C_L on Reynolds number *Re* and on revolutions *n* – side angle of attack $\beta = 30.7°$

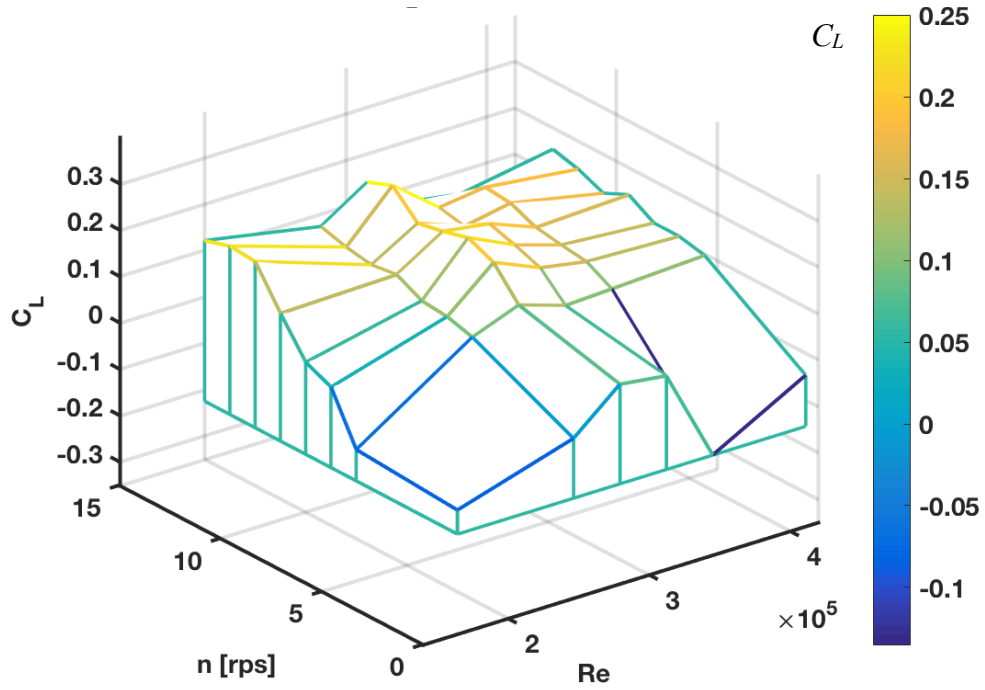

Figure 4-15: The dependence of coefficient of Lift C_L on Reynolds number *Re* and on revolutions *n* – side angle of attack $\beta = 41.15°$

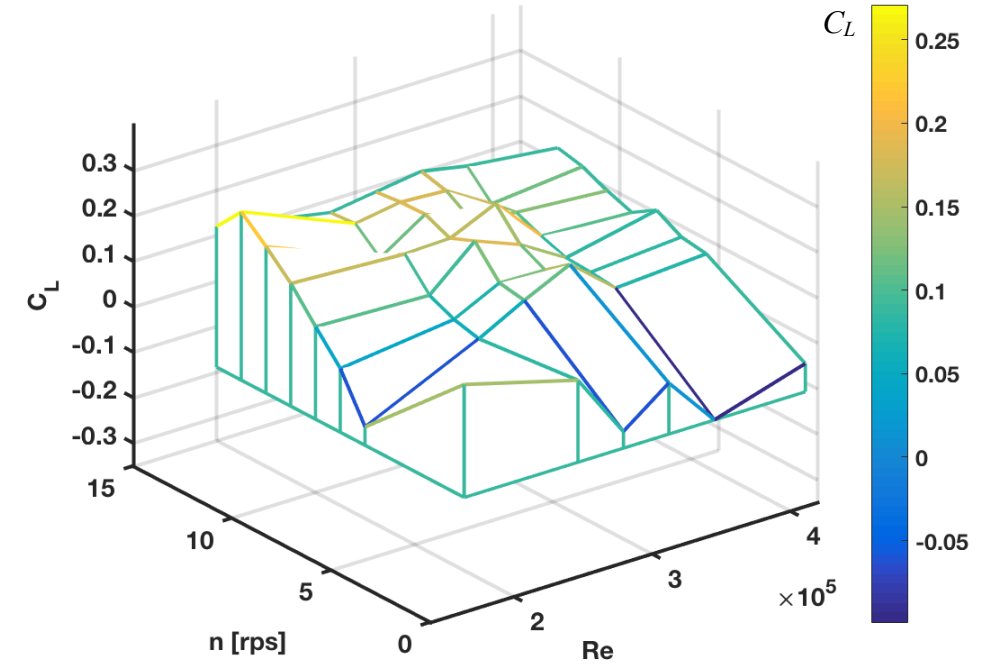

Figure 4-16: The dependence of coefficient of Lift C_L on Reynolds number *Re* and on revolutions *n* – side angle of attack $\beta = 47.08°$

The analysis of the effect of side angle of attack on the coefficient of Lift is in Section 5.3.2.

4.3.3 Coefficient of side force C_S

The results of coefficient of Side force C_S for increasing angle of attack β in accordance to Reynolds number Re and revolutions n are depicted in figures: Figure 4-17 – side angle of attack $\beta = 9.92°$, Figure 4-18 – side angle of attack $\beta = 20.56°$, Figure 4-19 – side angle of attack $\beta = 30.7°$, Figure 4-20 – side angle of attack $\beta = 41.15°$ and Figure 4-21 – side angle of attack $\beta = 47.02°$.

It is important to consider the values of C_S as an absolute value, where minus signs the direction of force action. According to the Figure 3-1 was set up positive direction of Side force.

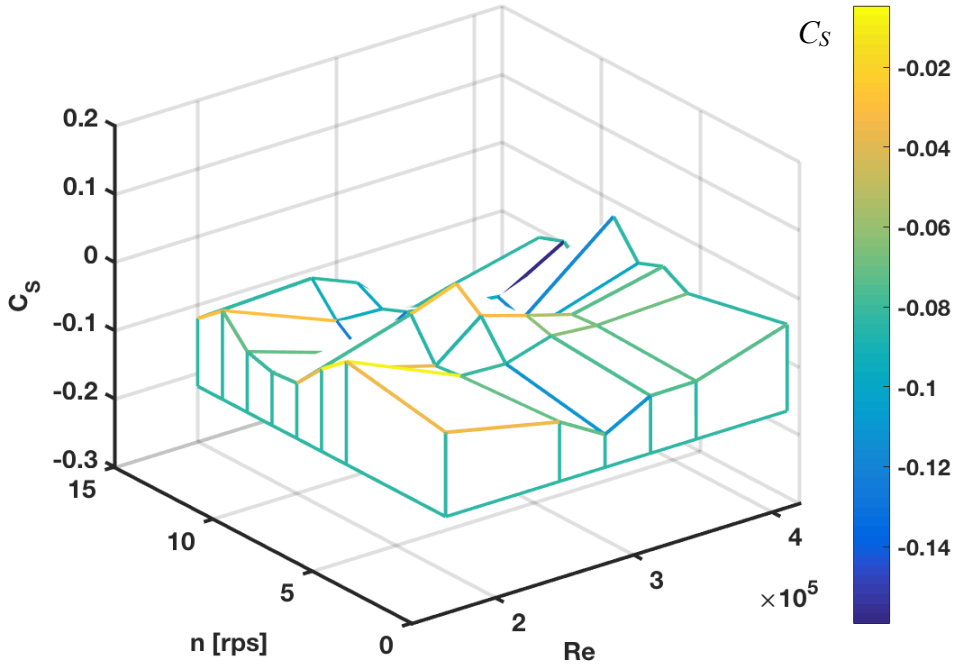

Figure 4-17: The dependence of coefficient of Side force C_S on Reynolds number Re and on revolutions n – side angle of attack $\beta = 9.92°$

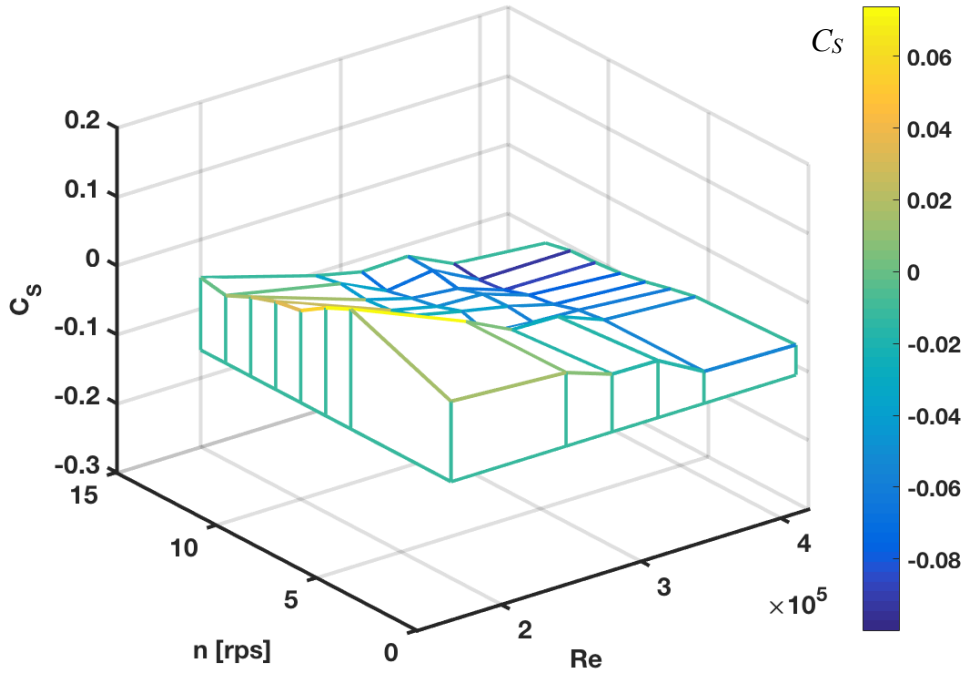

Figure 4-18: The dependence of coefficient of Side force C_S on Reynolds number Re and on revolutions n – side angle of attack $\beta = 20.56°$

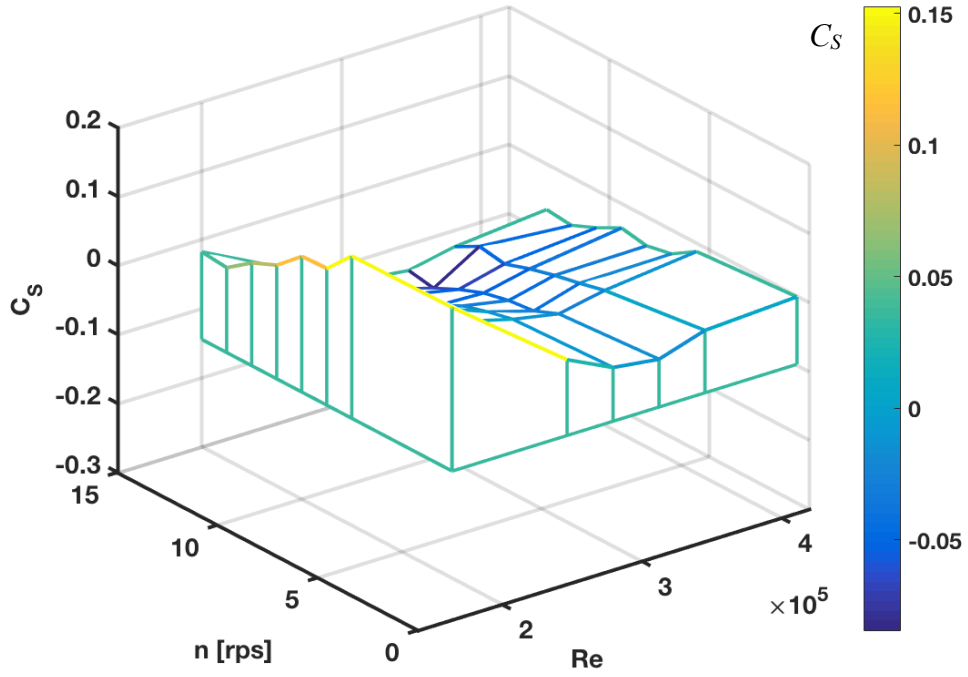

Figure 4-19: The dependence of coefficient of Side force C_S on Reynolds number Re and on revolutions n – side angle of attack $\beta = 30.7°$

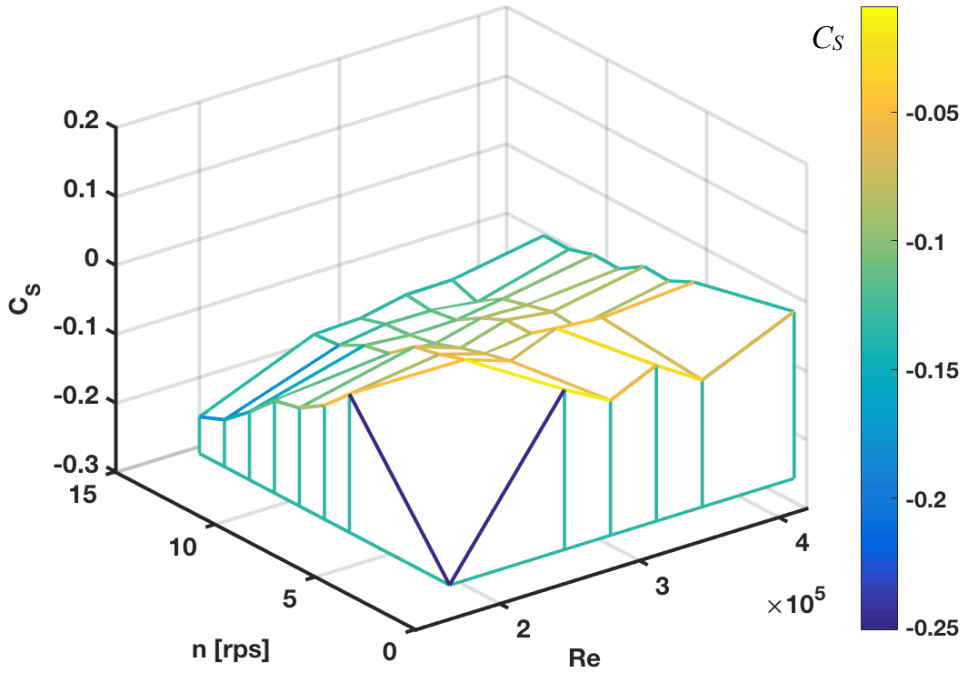

Figure 4-20: The dependence of coefficient of Side force C_S on Reynolds number Re and on revolutions n – side angle of attack $\beta = 41.15°$

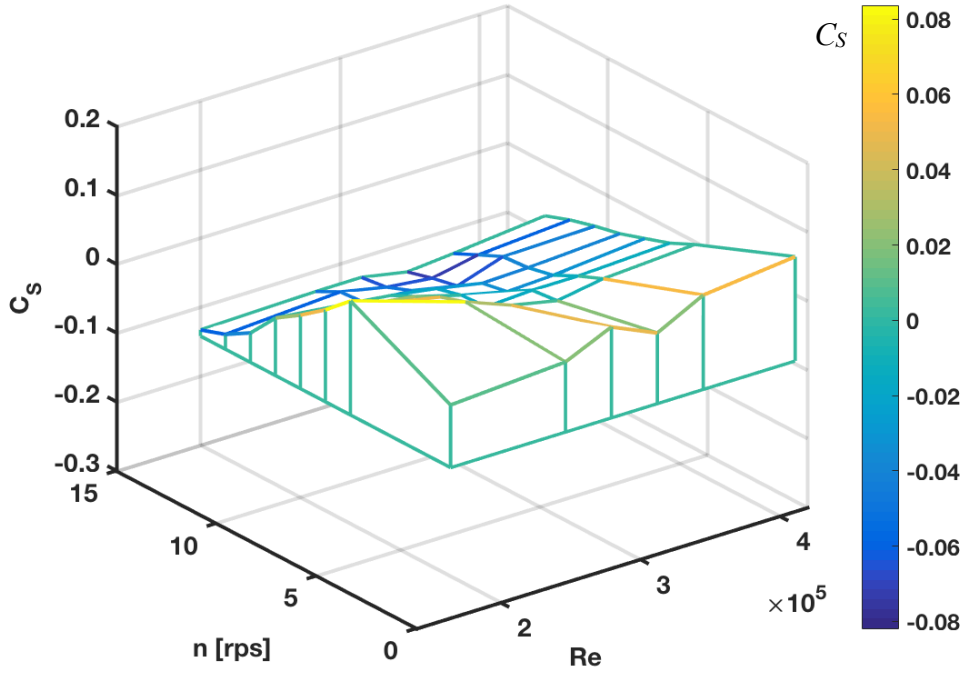

Figure 4-21: The dependence of coefficient of Side force C_S on Reynolds number Re and on revolutions n – side angle of attack $\beta = 47.08°$

4.4 UNCERTAINTIES

The uncertainties, as defined in Section 2.7, were evaluated according to [26] in the following steps:

1. Gross errors were detected by basic control of the data files. After gross errors were found, those were deleted and no longer considered in further evaluation.

2. Random uncertainties were evaluated by statistical methods.

The measured data from experiment were firstly noted three times per defined conditions (as stated in the Section 3.2.6) – three results: X1, X2, X3 – therefore statistical methods could be used.

Average of the values was calculated:

$$\bar{X} = \frac{1}{n}\sum X_i, \tag{28}$$

further the standard deviation was calculated:

$$\sigma = \sqrt{\frac{\sum(X_i - \bar{X})^2}{m-1}}. \tag{29}$$

From standard deviation was calculated the uncertainty:

$$\delta(X) = t_{m,P} \cdot \frac{\sigma}{\sqrt{m}}, \tag{30}$$

where $t_{m,P}$ is a constant from Student's distribution, defined by probability P and amount of results m.

The uncertainty calculation of coefficient of Lift C_L is performed here for defined conditions (the conditions were chosen randomly):

- Reynolds number *Re = 312 550,*
- side angle of attack: $\beta = 9.92°$,
- revolutions: *n = 0 – 12.5 rps*.

Calculation of average of one measured force, for example F_1 (*n = 6.25 rps*):

1. Average values of F_1 and F_2 were calculated:

$$\overline{F_1} = 1.8989N, \qquad \overline{F_2} = 1.5452N$$

2. Total Lift force:

$$\overline{F_L} = \overline{F_1} + \overline{F_2} = 3.4441N.$$

3. Standard deviations σ were calculated accordingly:

$$\sigma_{F1} = 0.02605N \qquad \sigma_{F2} = 0.06996N,$$

4. Further the uncertainties were calculated, for probability *P = 0.68* and *m = 3* the coefficient of Students distribution is *t = 1.321*:

$$\delta(F_1) = t_{m,P} \cdot \frac{\sigma_{F1}}{\sqrt{m}} = 1.321 \frac{0.02605}{\sqrt{3}} = 0.0198N,$$

$$\delta(F_2) = t_{m,P} \cdot \frac{\sigma_{F2}}{\sqrt{m}} = 1.321 \frac{0.06996}{\sqrt{3}} = 0.0531N.$$

5. Total uncertainty of the Lift is:

$$\delta(F_L) = \delta(F_1) + \delta(F_2) = 0.0729N.$$

6. The uncertainty of coefficient of Lift C_L can be calculated with application of Eq. (5):

$$\delta(C_L) = \frac{2\delta(F_L)}{\rho v^2 A} = \frac{2 \cdot 0.0729}{1.2135 \cdot 19^2 \cdot \pi \cdot 0.12^2} = 0.00736.$$

The zone of uncertainties, which means zone of existence of coefficient of Lift with probability 68 % is defined by interval:

$$C_L = \langle \overline{C_L} - \delta(C_L),\ \overline{C_L} + \delta(C_L) \rangle.$$

The zone is depicted in the Figure 4-22. It is visible, that uncertainties don't have an intensive impact on the trends of the coefficient of Lift.

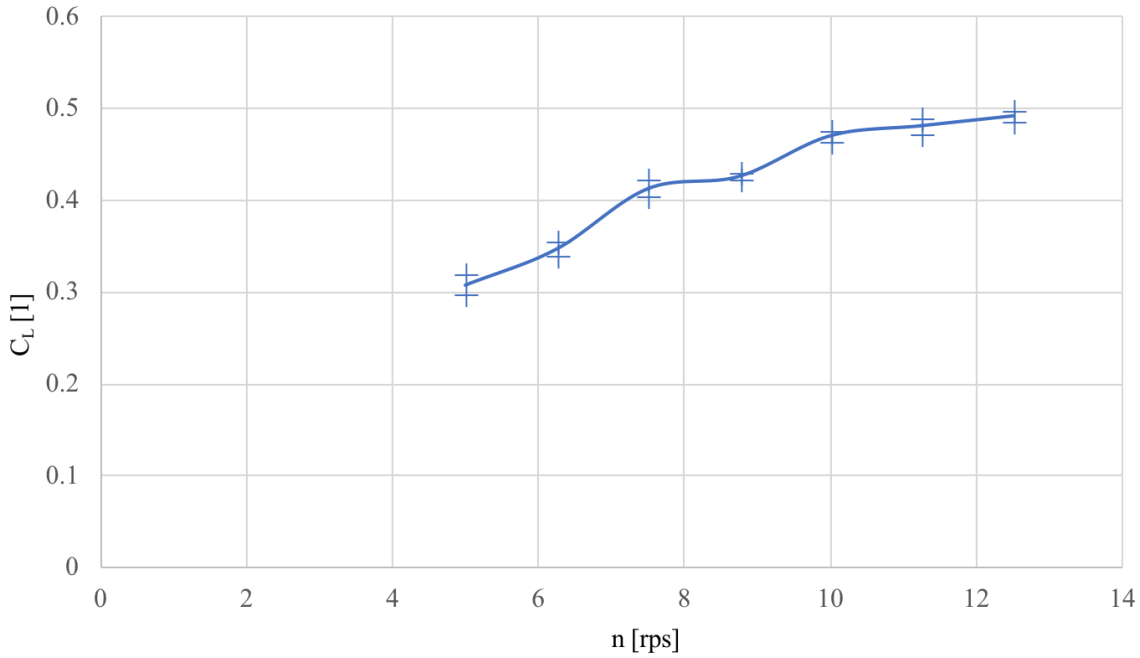

Figure 4-22: The effect of the coefficient of Lift C_L acting on revolutions n, including uncertainties.

The uncertainties of all the results were evaluated the same way, which was shown in the example. The conclusion is, that uncertainties don't have an intensive impact on the trends of the observed quantities, but it is important to be aware of the presence of the uncertainties.

5 DISCUSSION AND ANALYSIS

The achieved results are presented and briefly described in the previous Chapter 4 Results of experiment. The discussion of achieved results is divided into Sections according to conditions of results in this Chapter. Later also the ways of use of the results, are discussed and basic analyses including comparison with CFD calculation are performed in this Chapter. The description of the flight of the ball without rotations – knuckle ball – follows. Influence of surface roughness is presented in the Section 5.6 of this Chapter.

5.1 DISCUSSION OF THE RESULTS OF COEFFICIENTS OF DRAG C_D, LIFT C_L AND SIDE FORCE C_S WITH SIDE ANGLE OF ATTACK $\beta = 0°$

5.1.1 Coefficient of Drag

The dependence, Figure 4-1, looks very interesting with acting revolutions n on the ball. For lower Re (up to $Re = 250\ 000$) coefficient of Drag is firstly decreasing (from $n = 5$ *rps*) and at $n = 8.75$ *rps* C_D increases again. The significant effect of revolutions on lower Reynolds numbers is recorded.

On the other hand for $Re = 310\ 000 – 410\ 000$ course, with increasing revolutions n, is opposite: for $n = 5 – 7.5$ *rps* C_D is of higher values than in the case of $n = 0$ *rps*.

The influence of ball rotation looks to be very intensive in the case of lower Re ($Re < 250\ 000$), but for higher Reynolds numbers ($Re > 300\ 000$) influence of rotation is not so intensive.

The effect of Reynolds number and revolutions on coefficient of Drag C_D shows that revolutions cause reduction of C_D for lower Reynolds numbers (lower Re means here: lower half of the investigated interval of Reynolds number $Re < 280\ 000$). This phenomena can be explained by the different shape of wake behind the sphere, which is caused by rotation of the ball. For visualization of the effect, CFD was used. An example of visualization of flow (vectors of velocities – defined directions and magnitude) around a sphere is depicted in the Figure 5-1 for a sphere without rotation and in the Figure 5-2 for a sphere with rotation. The discussed

pictures are from CFD, because visualization of the flow around the ball was not performed in this particular experiment.

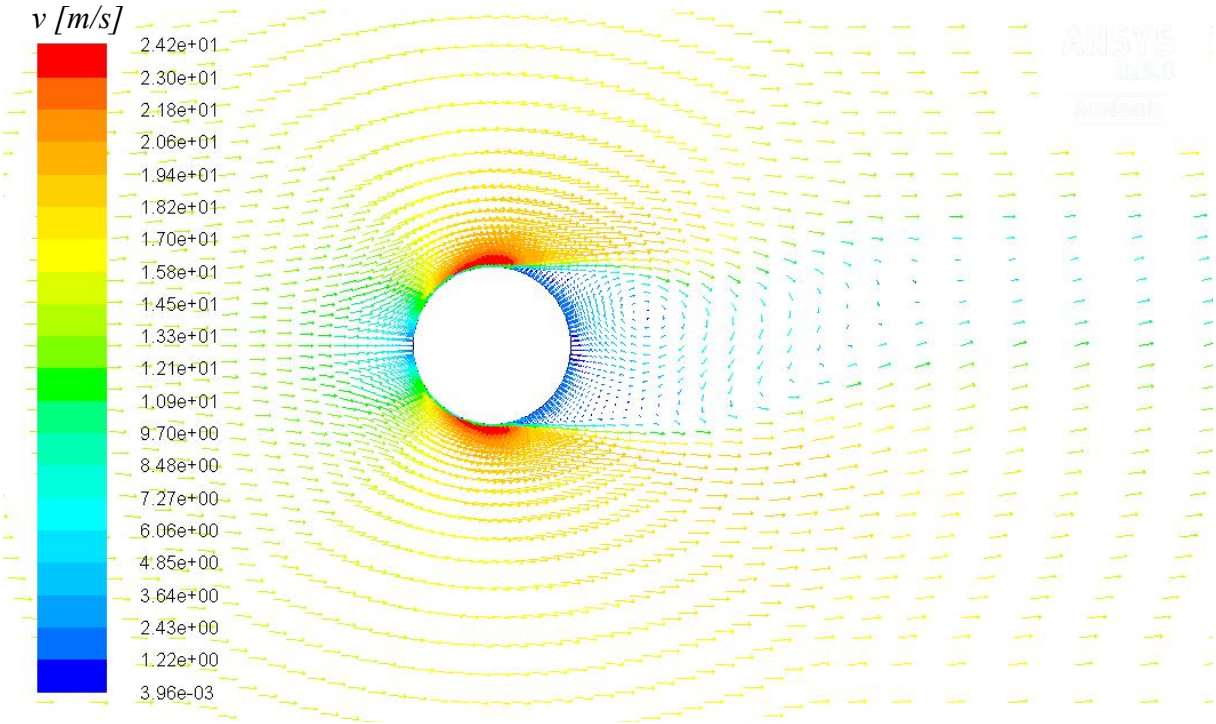

Figure 5-1: Vectors of velocity close to ball surface $v_\infty = 15\ m.s^{-1}$, $n = 0\ rps$

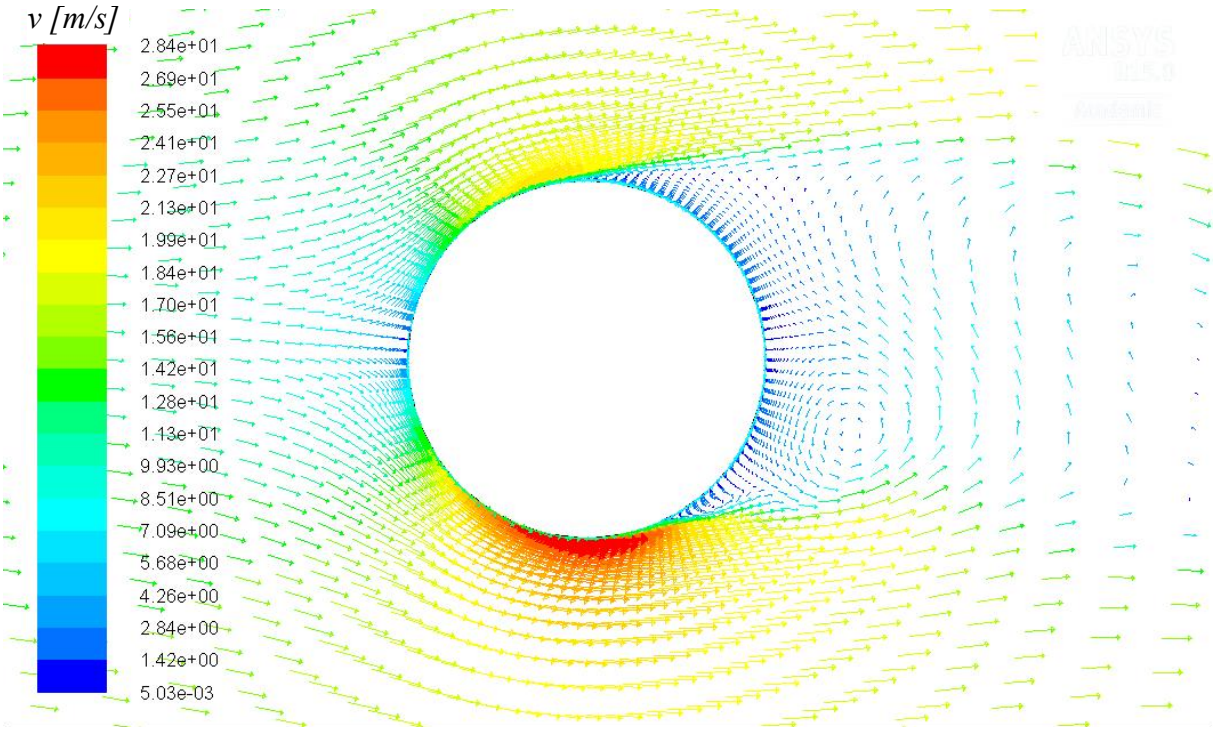

Figure 5-2: Vectors of velocity close to ball surface $v_\infty = 15\ m.s^{-1}$, $n = 10\ rps$, created in software ANSYS Fluent

5.1.2 Coefficient of Lift

Description of the situation around the rotating ball – 2D – is depicted in the Figure 5-2: The rotation of the ball causes, an increase of the dynamic pressure ($\frac{1}{2}\rho v^2$) on one side of the ball and decrease on the other side of the ball. The other way around it is for the static pressure.

The Lift force should be for symmetrical body equal to zero, $F_L = 0\ N$, therefore coefficient of Lift should be also $C_L = 0$. The dependence of coefficient of Lift C_L, which is in Figure 4-2 shows values unequal zero.
Furthermore the effect of Reynolds number on coefficient of Lift C_L for $n = 0\ rps$ looks to be affected by critical Reynolds number $Re_{CRIT.}$ – in area close to critical Reynolds number is very low the value of coefficient of Lift.
The flight of the ball without rotation, revolutions $n = 0$ rps is discussed in detail in Section 5.5.

In previous investigation, first experiment, published in [D2] and [D3] suspicion was stated in [D3]: "…the growth of C_L for constant velocity ($v_\infty = const.$, $Re = const.$) grows rapidly until $n = 8.75\ rps$, for higher revolutions ($n > 8.75\ rps$) the increase is very small. The explanation of this phenomenon is: there exists a border of rotation influence in growth of the lift force."

According to the description of dependences in Figure 4-2: limit value of revolutions n (is called n_l) is noticeable in each separate dependence for constant Reynolds number. Increasing revolutions above the limit $n > n_l$ doesn't cause increase of C_L, or the increase is very slow. Gradient of C_L for $n > n_l$ is close to zero or less than zero.
To investigate the previous statement in more detail, Figure 5-3 is depicted, where the effect of revolutions n on the coefficient of Lift C_L for different Reynolds number is visible.

All dependences in the Figure 5-3 show the discussed change in the course of coefficient of Lift at the revolutions $n = 8.75\ rps$. Even though this statement was confirmed by two independent experiments, it is still studied in more detail in Section 5.3, where spin number is calculated according to effective velocity for different side angles of attack β.

Second phenomena, which is obvious from the Figure 4-2 is **decrease of the value of C_L in the area of critical Reynolds number**. For all revolutions $n = const.$ decrease of coefficient of Lift C_L is noticeable.

Minimum value of coefficient of Lift $C_{L\ MIN} = 0.\ 005$ is for $Re = 280\ 000$.

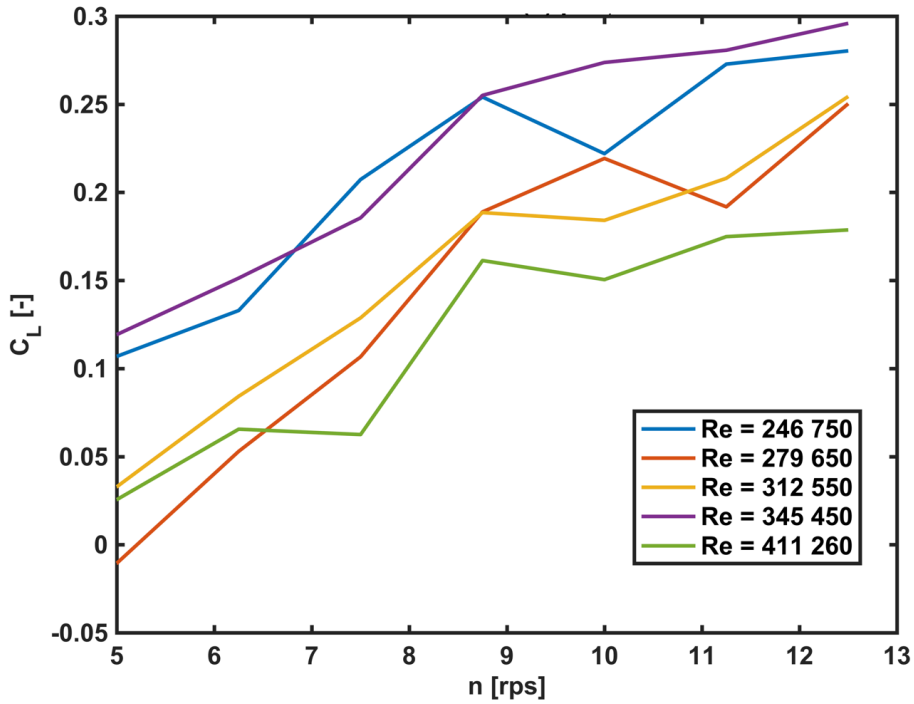

Figure 5-3: Comparison of the effect of revolutions n on Lift coefficient C_L, parameter is Reynolds number Re, $\beta = 0°$

The phenomena of limit of revolutions n_l can be explained by the example: the effect of separation of stagnation point in the case of 'flow past circular cylinder with circulation' in **potential flow**. The derivation of the case is not performed, because model of potential flow is too much simplified (basic assumptions of potential flow: 1. principal of superposition is used, 2. inviscid, 3. incompressible flow, 4. irrotational flow).

5.1.3 Coefficient of Side force

In the Figure 4-3 is visible, that the side force coefficient doesn't change rapidly for any $Re = const.$ Dependence of C_S for $n = const.$ decreases with increasing Reynolds number. In the case of $C_S\ (Re,\ n = 0rps)$ is visible the change of course at $Re = 280\ 000$ – increase, just until $Re = 310\ 000$ and further with increasing Reynolds number the C_S decreases again. It can be

explained as an influence of transition, but the effect is not as intensive as in the case of coefficient of lift C_L - Figure 4-2.

Summary:

All presented results in this Section 5.1 consider side angle of attack $\beta = 0°$. The effect of the side angle of attack β is discussed in the Section 5.3.

The critical Reynolds number has a significant influence on the coefficient of Drag C_D in the investigated area. The transition region is well identified for the flow $n = 0$ rps for $240\,000 < Re < 340\,000$. The region of low coefficient of Drag C_D appears for lower Reynolds number ($Re = 160\,000 – 280\,000$) in the area of revolutions n = (5 – 8.75) rps. This effect is evidence of the influence of revolutions acting on coefficient of Drag. It can be explained by the influence of rotation on the shape of the wake behind the volleyball, but the phenomena should be thoroughly studied further.

The coefficient of Lift was detected for case of n = 0 rps despite theoretical expectations (this phenomena is discussed thoroughly in 5.5). The basic trend was described in the course of coefficient of Lift C_L: increase of revolutions for $Re = const.$ results in the increase of the coefficient of Lift, that is confirmation of the "Magnus effect". Later the details of dependence coefficient of Lift were studied: two independent effects were observed and discussed: 1. Influence of critical Reynolds number on coefficient of Lift C_L, 2. The breaking point in course of all dependences of $C_L\,(Re = const.,\ n)$ – limit revolutions $n_l = 8.75$ rps.

The influence of critical Reynolds number on the course of coefficient of side force C_S was discussed. Minimal values of C_S were observed for $Re = 410\,000$. There is no effect of the revolutions n on the course of C_S. The basic trend in the course was found: the higher Reynolds number, the lower C_S.

All the results achieved in the observation and described in the Section are seen as a foundation for 3D ballistic equations. By the 3D ballistic equations the complete flight can be calculated. It is important to mention, that the results described in the Section 5.1 are not capable of describing special cases of flights: 1. The horizontal turn of the axis of rotation in flight, 2. The side wind influence.

5.2 DISCUSSION OF THE RESULTS OF COEFFICIENTS OF MOMENTS – ROLL, PITCH, YAW

From a closer look of Eqs. (23 – 25) is visible, that moments described, in this particular case, can be seen as a "ratio" of measured forces. In the case of M_X and M_Y (Roll and Yaw), forces are acting on the same distance *a* respectively *f*. In this case M_X and M_Y are a direct comparison of two forces F_1 and F_2, respectively F_4 and F_3. Let's see moment as a observation tool of balance in between forces acting on sphere. From the point of view of fluid dynamics, it is clear, that resulting forces acting on a body (sphere) in the airstream are caused by pressure distribution and shear stress on the surface of the body. It is not possible from the measured (integral) forces to reliably get exact pressure distribution and shear stress on the surface of a sphere, but **moments (coefficients of moments) give information on the pressure distribution**.

For example:
In the case of strict principle of symmetry (balanced pressure distribution on the surface) M_X would be equal to zero. From the Figure 4-4 it is visible, that there are conditions, where M_X is clearly not equal to zero. The following conclusion can be made: distribution of pressure and shear stress on the surface is unbalanced: asymmetric according to plane defined by axis "x" and "z".

The results of coefficients of moments are evaluated according to relation to symmetry (balance or unbalance, symmetry or asymmetry) in this Section 5.2.

5.2.1 Coefficient of moment Roll

In the Figure 4-4 it is visible, that symmetry of pressure distribution is very close to zero in area: $Re \in \langle 160\ 000 – 280\ 000 \rangle$ and $n \in \langle 0 – 12.5 \rangle$ *rps*. For higher Reynolds numbers $Re > 280\ 000$ relatively big difference occurs – technically, as visible from Eq. (23) F_2 is perceptibly higher than F_1, what means that Lift (F_1 and F_2 are according to Eq. 14 responsible for Lift)

generated on the right side of sphere is higher than on the left sphere side – according to Figure 3-1.

The most striking are in Figure 4-4 is for *Re = 340 000*. The minimum value of the coefficient of Roll is $C_{Mx\ min}$ = - *0.43*. Results can be calculated by the illustrative example:

If Eqs. (8) and (23) are considered, then value of $C_{Mx\ min}$ = - *0.43* means:

$$C_{Mx} = \frac{2M_X}{\rho v^2 A} = -0.43 = \frac{2a}{\rho A v^2} \cdot (F_1 - F_2).$$

With basic mathematical adjustments the following result is prepared:

$$F_2 = F_1 + \frac{0.43}{2a} \cdot \rho A v^2.$$

Presume F_1 = 1 N, and a,ρ, A, v_∞ are of the values used in measurement: density ρ = 1.2135 kg/m^3, distance a = 0.41 m, area A = 0.0458 m^2 and velocity v_∞ is according to Re = 340 000 calculated v_∞ = 20 m/s. Then following relation is:

$$F_2 = 1 + \frac{0.43}{2 \cdot 0.41} \cdot 1.2135 \cdot 0.00458 \cdot 20^2 = 2.16\ N.$$

The force on one side of the sphere is in the shown example significantly higher, than on the other side.

5.2.2 Coefficient of moment Pitch

From Eqs. (8) and (25) it is clear, that the coefficient of Pitch shows the Drag symmetry according to plane defined by axis "x" and "y". It is visible in the Figure 4-5, that for higher Reynolds number *Re > 280 000* are results of coefficient of Pitch $C_{My} > 0$. That is showing according to Eq. (25), that higher pressure is on the upper part of the sphere than on the bottom. Most intensive is the difference for *Re = 340 000*, where $C_{My} = 0.3$.

5.2.3 Coefficient of moment Yaw

The coefficient of Yaw is according to Eq. (24) a question of Drag symmetry according to plane defined by axis "x" and "z". Very close to symmetry is the case of coefficient of Yaw for higher Reynolds numbers $Re \geq 340\ 000$. In the case of lower Reynolds number, $Re < 340\ 000$ coefficient of Yaw is visibly lower than zero $C_{Mz} < 0$. For this area it can be stated, that $F_3 > F_4$, according to Figure 3-1 higher Drag is acting on the left side of the sphere.

The descriptions of the courses of coefficients of moments (Roll, Pitch, Yaw) were done. Based on Eqs. (7 – 9) and (23 – 25) the method of evaluation of symmetry of pressure distribution on the surface was created and used.

According to the evaluations, which were stated in this Section it is possible for each point, which is defined by conditions (Reynolds number *Re* and revolutions *n*) to create *primitive assumption of pressure distribution on the surface of the sphere* as in following example:

The conditions are: $Re = 340\ 000$, $n = 0$ rps.

The results of coefficient of Roll for defined conditions is: $C_{Mx} < 0$, therefore is clear: $F_2 > F_1$. The case is briefly shown in the Figure 5-4.

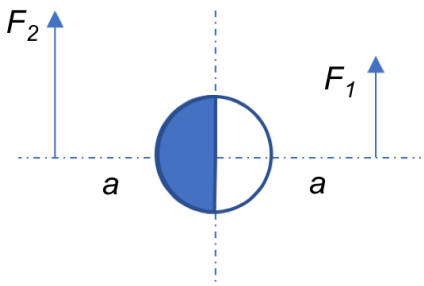

Figure 5-4: The sketch of the evaluation of C_{Mx}

The results of the coefficient of Yaw for defined conditions is: $C_{My} > 0$, by comparison of components from Eq. (25) is clear: $(F_3 + F_4) * b > F_5 * c$. The result is briefly sketched in Figure 5-5.

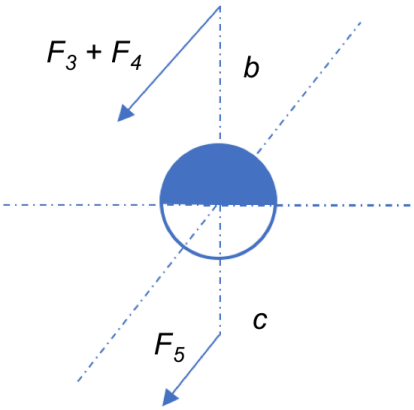

Figure 5-5: The sketch of the evaluation of C_{My}

The results of the coefficient of Pitch for defined conditions is: $C_{Mz} < 0$, from Eq. (24) is obvious: $F_3 > F_4$. The result of the evaluation is in the Figure 5-6.

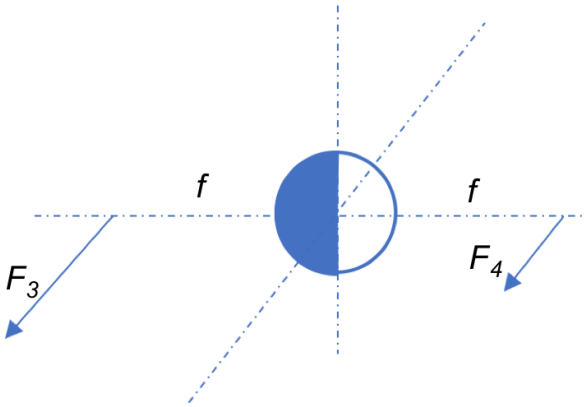

Figure 5-6: The sketch of the evaluation of C_{Mz}

5.3 DISCUSSION OVER THE EFFECT OF SIDE ANGLE OF ATTACK

The effect of side angle of attack on the aerodynamic characteristics of volleyball is studied based on dependences presented in the Section 4.3. The analysis of the effect of side angle of attack β is discussed in this Section, divided according to the aerodynamic characteristics.

5.3.1 Coefficient of Drag

In the previous Section 5.1, which dealt with coefficient of Drag for $\beta = 0°$, the area of critical Reynolds number $Re_{CRIT.}$ was found and the influence of revolutions n on the transition was discussed. Similar principals are studied in this Section and comparison of different side angles of attack is illustrated by definition of conditions (Re and n) under which coefficient of Drag C_D reaches maximum and minimum values.

The maximum and the minimum values of coefficient of Drag C_D are presented in Table 5-1 and in Table 5-2 respectively. From the Table 5-2 is visible, that in most cases $C_{D\,max}$ occurs for Reynolds number $Re = 160\,000$ and revolutions $n = 0$ *rps*. This fact confirms, that these conditions describe laminar flow. With the increase of Reynolds number, the transition occurs and the values of coefficient of Drag decrease. For higher Reynolds numbers the flow is turbulent and that is the reason, why fluctuations and unpredicted results of coefficient of Drag appear.

The effect of side angle of attack β is significant in the observation of minimum values of coefficient of Drag: in the cases, where $\beta > 30°$ the minimum value is clear in the case of highest Reynolds numbers.

The increase of side angle of attack effects results of coefficient of Drag C_D in this matter:

1. The C_D increases with increasing revolutions n, significantly more intensive for low Reynolds numbers.
2. With increase of side angle of attack β, the coefficient of Drag decreases for $Re > 340\,000$ and revolutions $n = 0$ *rps*. Extremely low is coefficient of Drag in the case of side angle of attack $\beta = 41.15°$ and $\beta = 47.08°$, the values of $C_D < 0.1$.

The development of two discussed trends is easily visible in Section 4.3.1 in the consequence of figures: Figure 4-7 – side angle of attack $\beta = 9.92°$, Figure 4-8 – side angle of attack $\beta = 20.56°$, Figure 4-9 – side angle of attack $\beta = 30.7°$, Figure 4-10 – side angle of attack $\beta = 41.15°$ and Figure 4-11 – side angle of attack $\beta = 47.02°$.

Table 5-1:The effect of side angle of attack on the maximal values of coefficient of Drag C_D

β [°]	0	9.92	20.56	30.7	41.15	47.08
C_D [1]	0.53	0.44	0.34	0.3	0.23	0.35
Re [1]	160 000	410 000	160 000	160 000	160 000	160 000
n [rps]	0	5	0	12.5	0	0

Table 5-2:The effect of side angle of attack on the minimal values of coefficient of Drag C_D

β [°]	0	9.92	20.56	30.7	41.15	47.08
C_D [1]	0.26	0.21	0.13	0.1	0.05	0.064
Re [1]	280 000	280 000	250 000	250 000	350 000	410 000
n [rps]	6.25	10	6.25	5	0	0

5.3.2 Coefficient of Lift

The coefficient of Lift C_L was studied in the case of $\beta = 0°$ in Section 5.1.2. Besides basic trends, such as Magnus effect, were observed two more effects:

1. Influence of critical Reynolds number on the coefficient of Lift C_L,
2. The breaking point in the course of all dependences of C_L ($Re = const.$, n), limit revolutions $n = 8.75$ *rps* was found.

In this Section the same effects are discussed and evaluated.

For the purpose of investigation of the breaking point in the course of C_L the perpendicular component vector of velocity to axis of rotation $v_{x\prime}$ is defined. The distribution of vector of velocity v_∞ after the rotation of coordinate system according to angle β is visible in Figure 5-7, components of velocity are then calculated according to Eqs. (31) and (32):

$$v_{x'} = v_{\infty} \cdot cos\beta, \tag{31}$$

$$v_{y'} = v_{\infty} \cdot sin\beta. \tag{32}$$

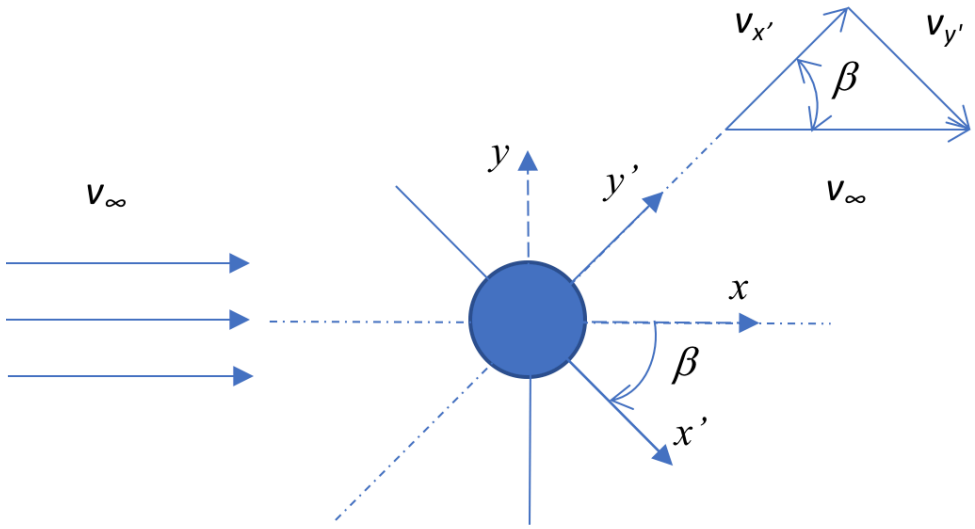

Figure 5-7: The distribution of vector of velocity according to rotated coordinate system x'y' – rotated according to angle β – effective velocity $v_{x'}$ and $v_{y'}$

The effective values are used because only the perpendicular component of velocity influences the increase of the Lift force, as defined in Eq. (33) – definition of Magnus Effect:

$$\vec{F}_L = \frac{1}{2}\rho v^2 C_L A(\vec{v} \times \vec{\omega}). \tag{33}$$

Based on the values of velocity $v_{x'}$ the spin number[2] was calculated according to Eq. (11) and **spin** ***s*** is further used for describing the effect of coefficient of Lift acting on a rotating volleyball.

[2] In the Section 3.2.4 is defined interval of spin $s = \langle 0 \div 0.94 \rangle$, which corresponds to revolutions n and Reynolds number Re respectively velocity v. As vector of velocity was divided, the same revolutions n are acting on lower velocity $v_{x'}$, which results to higher spin $s = \langle 0 \div 1.4 \rangle$.

The amount of results of coefficient of Lift C_L vs. spin s for velocity $v_{x'}$ is high, that is the reason, why a statistical approach was chosen. The population of the coefficient of Lift C_L is depicted in the Figure 5-8. In the distribution of the population basic statistical quantities were calculated:

- trend is described by equation of straight line – orange line in Figure 5-9:

$$C_L = 0.2316 \cdot s + 0.0517, \tag{34}$$

where reliability $R^2 = 0.3878$. The value of the reliability is low, that is the reason, why better approximation is searched.

Table 5-3: The values of components of vector of velocity $v_{x'}$ after the rotation of coordinate system according to angle β

	$\beta = 0°$	$\beta = 9.92°$	$\beta = 20.56°$	$\beta = 30.7°$	$\beta = 41.15°$	$\beta = 47.08°$
cos β	1	0.98504925	0.93630494	0.85985227	0.75298944	0.68097653
Velocity v_∞ [m/s]		Component of vector of velocity $v_{x'}$ [m/s]				
0	0	0	0	0	0	0
10	10	9.85	9.36	8.60	7.53	6.81
15	15	14.78	14.04	12.90	11.29	10.21
17	17	16.75	15.92	14.62	12.80	11.58
19	19	18.72	17.79	16.34	14.31	12.94
21	21	20.69	19.66	18.06	15.81	14.30
25	25	24.63	23.41	21.50	18.82	17.02

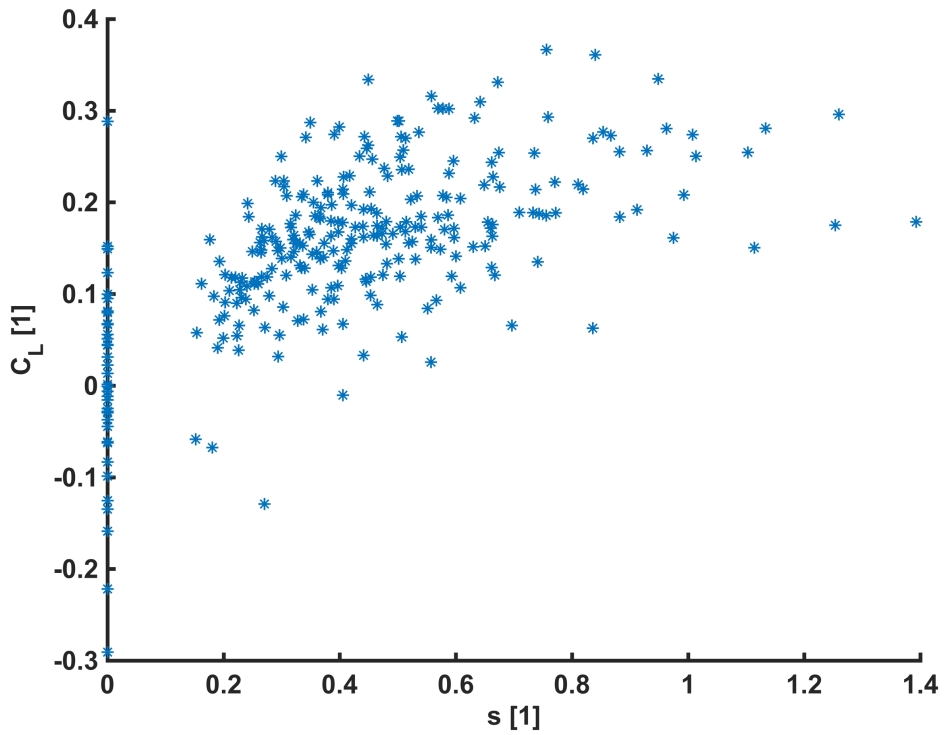

Figure 5-8: The dependence of coefficient of Lift on spin – calculated from $v_{x'}$.

Graphicly the results and trends are shown in Figure 5-9. In Figure 5-9 the trend is more accurately described by polynomial of third grade – dotted line – described by the Eq. (35):

$$C_L = 0.127 \cdot s^3 - 0.4824 \cdot s^2 + 0.585 \cdot \mathrm{s}, \qquad (35)$$

where the reliability $R^2 = 0.4799$.

- Dispersion of the population of C_L: $Var\ (C_L) = 0.\ 0094$,
- standard deviation of the population of C_L: $\sigma = 0.0967$.

In the trend of the population it is visible, that the interspersed polynomial corresponds with the distribution of the population better than the straight line (see for comparison the values of reliability R^2), especially for higher values of spin $s > 0.9$.
It is clear from Figure 5-9 that the trend of the population is rising in the interval of spin number $0 < s < 0.6$. For higher values of spin the trend stagnates. The effect of spin s on coefficient of Lift C_L is not linear.

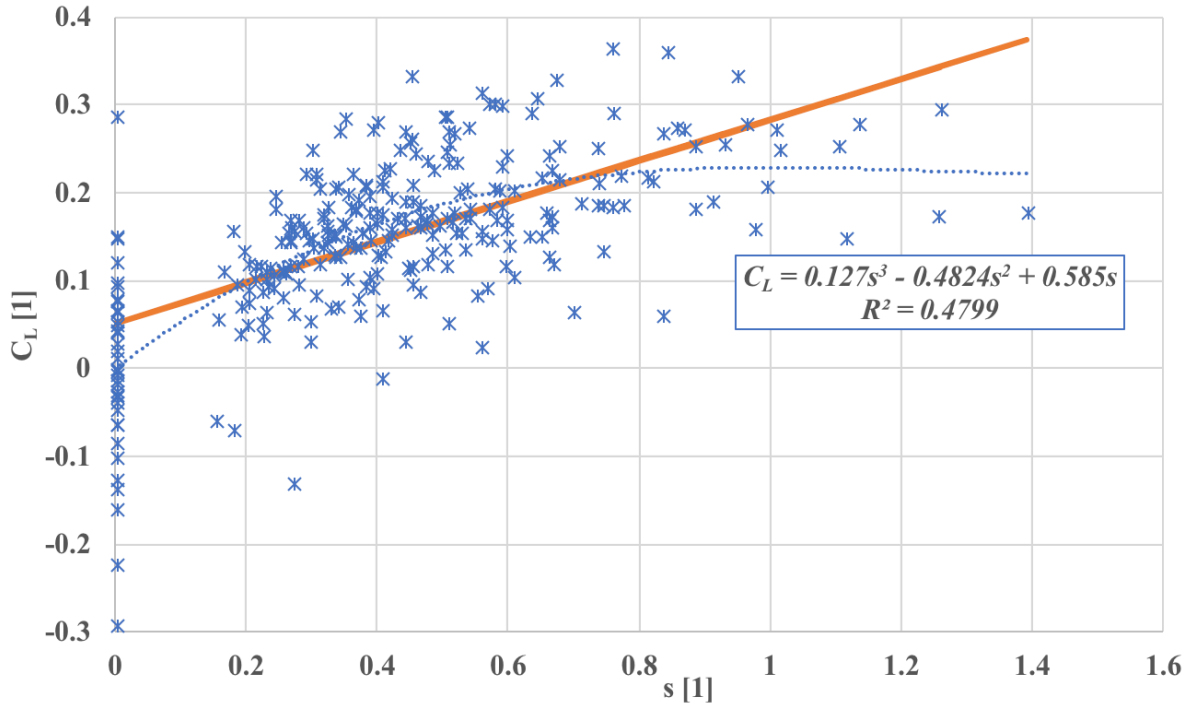

Figure 5-9: Trends in the effect of spin s on coefficient of Lift C_L

It is important to remind assumption which was made in the beginning of this consideration: vector of velocity was divided according to rotation of angle β - principal of superposition was used.

Note: *The effect of spin on coefficient of Lift, which was discussed in this Section is caused by v_x, component of vector of velocity v. According to rotated coordinate system x'y' there exists also v_y, component of velocity. The v_y, velocity is parallel to axis of rotation of volleyball. The effect v_y, can be also studied in following works.*

5.3.3 Coefficient of Side force

The dependences of coefficient of Side force on Reynolds number and revolutions for different side angle of attack are depicted in Section 4.3.3. The effect of side angle of attack β is discussed in this Section.

The dependences are smooth and trends much more direct than in cases of Drag or Lift coefficients. In Figure 4-18, where is $\beta = 20.56°$ and Figure 4-19, $\beta = 30.7°$ is a direct trend: the higher Reynolds number *Re* the lower coefficient of Side force C_S, independent of revolutions *n*.

In Figure 4-20, and Figure 4-21, $\beta = 41.15°$ and $\beta = 47.02°$ the change of trend is noticeable:

1. the higher *Re* the higher C_S and
2. the higher revolutions *n* the lower C_S.

The effect of revolutions (point 2) is more intensive in the conditions of lower Reynolds number.

Table 5-4: The effect of side angle of attack on the maximal values of coefficient of Side force C_S

β [°]	**0**	**9.92**	**20.56**	**30.7**	**41.15**	**47.08**
C_S [1]	0.13	- 0.005	0.07	0.15	- 0.01	0.08
Re [1]	1.6	2.8	1.6	1.6	4.1	1.6
n [rps]	0	7.5	5	0	0	5

Table 5-5: The effect of side angle of attack on the minimal values of coefficient of Side force C_S

β [°]	**0**	**9.92**	**20.56**	**30.7**	**41.15**	**47.08**
C_S [1]	- 0.01	- 0.16	- 0.1	- 0.08	- 0.25	- 0.08
Re [1]	4.1	3.5	4.1	3.1	1.6	3.1
n [rps]	12.5	11.25	12.5	11.25	0	12.5

The maximum and minimal values of C_S are concluded in Table 5-4 and Table 5-5, respectively. The values of coefficient of Side force are in general lower than values of C_D or C_L, but there are also conditions, where C_S is higher than C_L and C_D – as example for the conditions:

$$Re = 164\,500, \qquad \beta = 41.15°, \qquad n = 0 \text{ rps},$$

where absolute values of coefficient is:

$$C_S = 0{,}251 \quad > \quad C_D = 0.2291 \quad > \quad C_L = 0.0834.$$

It is visible, that in the described case and conditions the Side force is the most dominant force acting on the ball. This topic is discussed more in Section 5.5.

5.4 BALLISTIC EQUATIONS

The results, set of values of coefficients of Drag C_D, of Lift C_L and of Side force C_S, create the foundation of aerodynamic characteristics, which can be used for calculation of 3D ballistics. The 2D ballistic equations were introduced in Section 2.8 based on coefficients of Drag C_D and coefficient of Lift C_L, the derivation is presented in more detail in [D1]. In this Section is only a brief summary of result of derivation of the equations of real motion in three dimensions, it is called 3D ballistics (source [D1]):

$$\ddot{x} = -\frac{\rho A}{2m}(\dot{x}^2 + \dot{y}^2 + \dot{z}^2) \cdot (C_D \cdot cos\alpha + C_L sin\alpha) \cdot cos\gamma \tag{36}$$

$$\ddot{y} = \frac{\rho A}{2m}(\dot{x}^2 + \dot{y}^2 + \dot{z}^2) \cdot (C_L \cdot cos\alpha + C_D sin\alpha) \cdot cos\gamma - g \tag{37}$$

$$\ddot{z} = \frac{\rho A}{2m}(\dot{x}^2 + \dot{y}^2 + \dot{z}^2) C_S \cdot sin\gamma \tag{38}$$

and the vector velocity argument:

$$\alpha = arctg\frac{\dot{y}}{\dot{x}} \tag{39}$$

but

$$\gamma = arctg\frac{\dot{z}}{\sqrt{\dot{x}^2+\dot{y}^2}} \tag{40}$$

The instantaneous velocity is:

$$v = \sqrt{\dot{x}^2 + \dot{y}^2 + \dot{z}^2}, \tag{41}$$

where C_D is coefficient of Drag, which depends on Reynolds number. The coefficient of Lift C_L in the case of sphere with revolutions describes the influence of the spin number. Coefficient of Side force C_S besides of influence of Reynolds number can be connected with the effect of side wind v_w and can also describe the influence of interaction of the component of velocity $v_{x'}$ and spin s in the case of deflection of axis of revolutions.

Boundary and initial conditions:

$$x(0) = 0 \tag{42}$$

$$y(0) = y_0 \tag{43}$$

value of velocity:

$$v(0) = \sqrt{\dot{x}^2(0) + \dot{y}^2(0) + \dot{z}^2(0)} = v_0 \tag{44}$$

$$\alpha(0) = arctg\,\frac{\dot{y}(0)}{\dot{x}(0)} = \alpha_0 \tag{45}$$

but

$$\gamma(0) = arctg\,\frac{\dot{z}(0)}{\sqrt{\dot{x}^2(0)+\dot{y}^2(0)}} = \gamma_0 \tag{46}$$

By conversion of Eqs. (36 – 41) to ordinary first order differential equations and $C_D = f(Re)$, $C_L = g(s)$ and $C_s = h(Re, s, v_{x'})$ system can be solved numerically as with initial conditions, for example by Runge-Kutta method.

5.4.1 Example of ballistic calculation

The results of experiment (presented in Chapter 4 and in publications: [D3], [D6], [D1] and [D7]) can be summarized as a solution of coefficient dependences, as mentioned in description of 3D ballistics: $C_D = f(Re)$, $C_L = g(s)$ and $C_s = h(Re, s, v_{x'})$. The purpose is to use the values (C_D, C_L, C_S) in numerical calculation, therefore interpolation of the data is needed. Based on the system of ballistic equations the program, which would calculate trajectories, can be simply prepared. The program for numerical calculation of the system of 3D ballistic equations can in

each step (iteration) update the values of aerodynamic coefficients: C_D, C_L *and* C_s according to new conditions described by Reynolds number *Re,* revolutions *n* and side angle of attack β. A simplified version of the calculation was used to show the example of flight in the area of a volleyball field, as visible in the Figure 5-10.

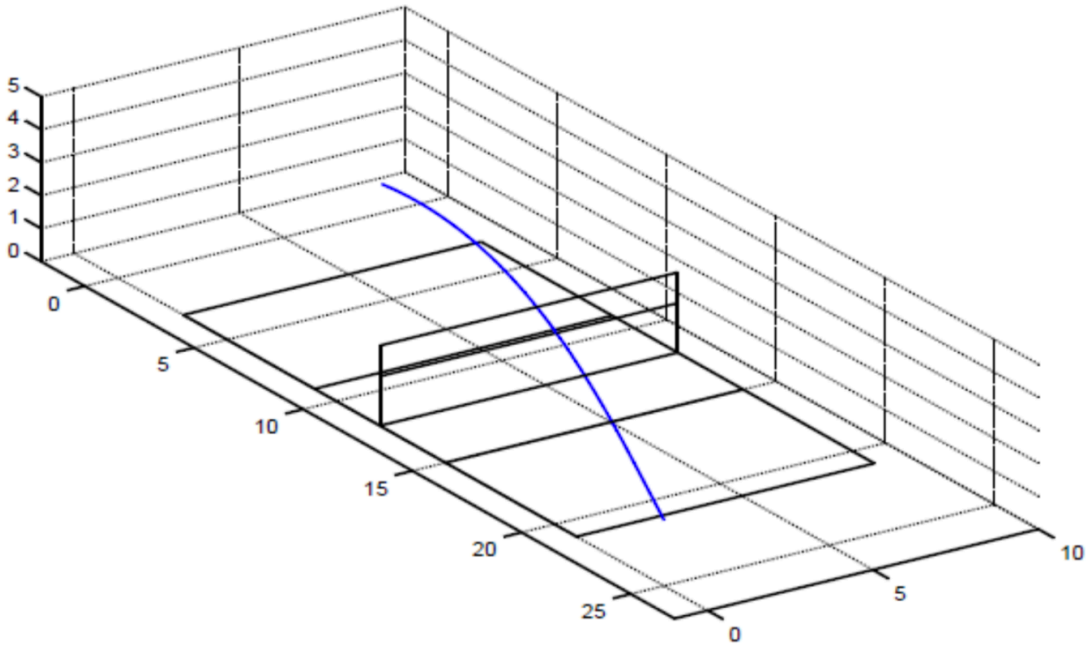

Figure 5-10: Example of flight of volleyball in volleyball field

The instrument of ballistics together with the set of values from the experiment (aerodynamic characteristics) can be used for calculation of each case of the flight of a ball, including the following special cases: flight without rotation, flight with side wind, flight with deflection of axis of rotation.

5.4.2 Influence of side wind on the flight

As mentioned in the description of 3D ballistic equations, the system of equations can also deal with influence of side wind on the trajectory of the ball. The side wind would have to be brought to the system of equations by the aerodynamic coefficients. Here is the recommended procedure:

First: let's assume principle of superposition can be used in this case. With simplification of the superposition the values of aerodynamic coefficients measured for side angle of attack $\beta \neq 0$ can be used.

For the purpose of calculating the influence of the side wind the values of aerodynamic coefficients gained in the experiment can be seen according to Figure 5-11, where v_∞ is general velocity of airstream, β is side angle of attack, v_W is side wind velocity and v_C is parallel airstream velocity.
Actual values of velocities v_W and v_C are counted according to sinus and cosinus functions acting on angle β. Thanks to maximum value of β is around $\beta = 45°$ and maximum value of measured air stream velocities $v_\infty = 25\ m/s$, it is possible to describe case of flight: $v_C = 17.6\ m/s$ and $v_W = 17.6\ m/s$. It is important to mention again that the simplification of applying principal of superposition is large.

The effect of side wind can be applied independently on revolutions n.

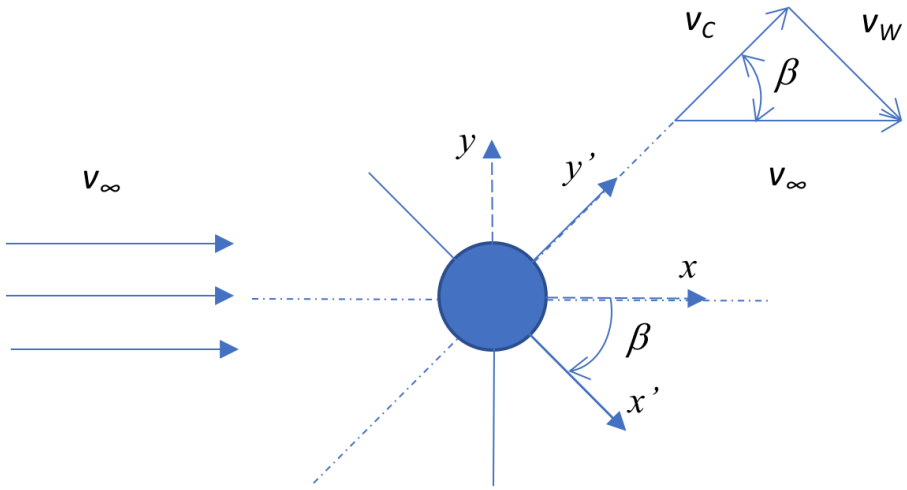

Figure 5-11: Description of side wind superposition

The practical influence of side wind can be used in calculation of the flight of a ball in beach volleyball, which is played in open space and wind often interacts with the ball.

5.5 FLIGHT OF THE BALL WITHOUT ROTATION (*n = 0 rps*)

The phenomena of acting Lift and Side force on a sphere without rotation are observed in many sports, such as football, volleyball, etc. – cases are recorded and also described in the point of view of aerodynamics. In the case of a volleyball it is well described by Wei Qing-Ding [13], even though the conclusion of [13] is:
["*The experimental results suggest that under the action of an unstable tail vortex system the separation region is changeable, and that the fluctuation of drag and lateral forces is the same order of magnitude as the mean drag, no matter whether the seam of the Volleyball is symmetric or asymmetric, with regard to the flow.*"] Theoretical description is not provided in the source [13].

Brief description of the phenomena of knuckling effect:
The flight of a volleyball in normal conditions is in range of velocities $v_\infty = 15 – 35\ m/s$. In the case of beach volleyball (ball, which was observed in tests) $v_\infty = 12 – 28\ m/s$, which corresponds to $Re = (196\ 143 – 457\ 669)$. As mentioned in Chapter 1 Introduction: according to Hoerner, [4]: $Re_{CRIT.} = 300\ 000,\ C_D = 0.3$). So, the common flight conditions of a volleyball are in the area of critical Reynolds number. Mathematically critical velocity corresponding to $Re_{CRIT.} = 300\ 000$ is $v_{CRIT.} = 18.35\ m/s$. In realistic conditions the whole area of critical conditions must be considered. The transition from laminar to turbulent flow is the cause of knuckling effect, but only the effect of transition would not cause the "unpredictable" flight path. Knuckling effect occurs due to unsymmetrical transition. The unequal transition arises due to unsymmetrical pressure distribution on the surface. This is caused by geometrical shape, inhomogeneities in the stream and stream structures in the separation area.

Pressure distribution was not measured (only computed by CFD in Section 5.7), but Lift force and side force (together with drag all the forces are providing us with information about the pressure distribution on the surface) were detected in most of the measured cases of a ball without revolutions, as it is shown in Figure 5-12 and Figure 5-13. In the case of a ball without any rotation, $n = 0\ rps$, it is possible to neglect the turn of angle β and compare all the cases as independent results of measurements. As spherical object is measured, geometry is not changed by arising of side angle of attack β. As revolutions n = 0 rps, there is not any division of vector

of angular velocity. And the effect of turn of frame including spindle is deducted by method of measurement.

5.5.1 Investigations of flight of ball without rotation – statistical approach

The results of coefficient of Lift C_L and side force C_S are presented in Figure 5-12 and Figure 5-13 respectively. It is easily visible, that the dependences are disorganized even values of C_L, C_S are appearing randomly. Therefore statistical approach is performed as follows: out of six different values for the angles of attack β is median counted. Results of medians are depicted in Figure 5-14. In the case of coefficient of Drag values looks to follow expected trends and likewise trend of C_D for smooth sphere, as presented in Figure 1-2.
The values of medians of coefficient of C_L and C_S are very low and therefore close to expectations of $C_L = C_S = 0$ for flight of a ball without rotation.
If it is assumed, that $C_L = C_S = 0$, then values of C_L and C_S which are not equal to zero can be evaluated as ***uncertainty*** and further statistical approach can be performed:

Standard deviation was calculated for medians of coefficients as follows:

$$Var(X) = \frac{1}{N}\sum_{i=1}^{N}(x_i - \bar{x})^2 \tag{47}$$

$$\sigma = \sqrt{Var(X)} \tag{48}$$

where *Var (X)* is dispersion and σ is standard deviation. Standard deviation of median of coefficient of Lift is:

$$\sigma_{C_L} = 0.032$$

and standard deviation of median of coefficient of Side force is:

$$\sigma_{C_S} = 0.013.$$

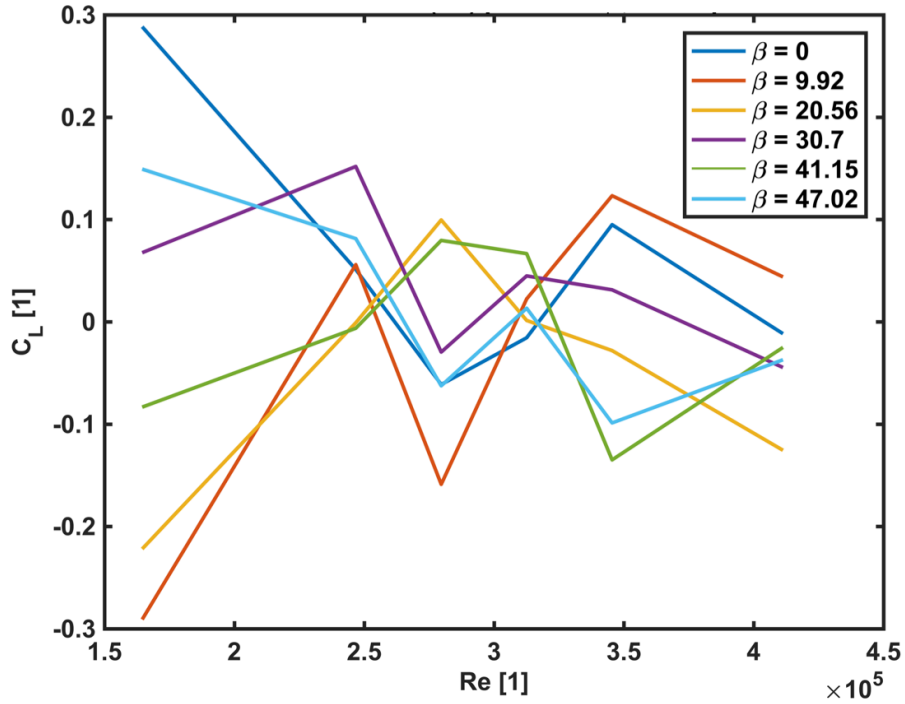

Figure 5-12: The effect of Reynolds number *Re* on coefficient of Lift C_L for $n = 0$ *rps* and various β

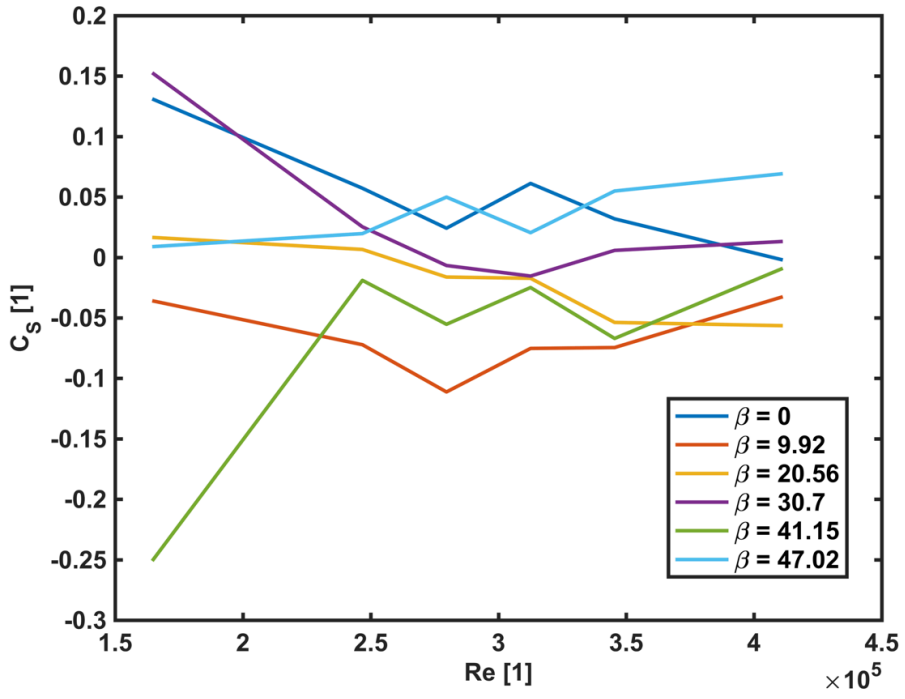

Figure 5-13: The effect of Reynolds number *Re* on coefficient of Side force C_S for revolutions $n = 0$ *rps* and various β

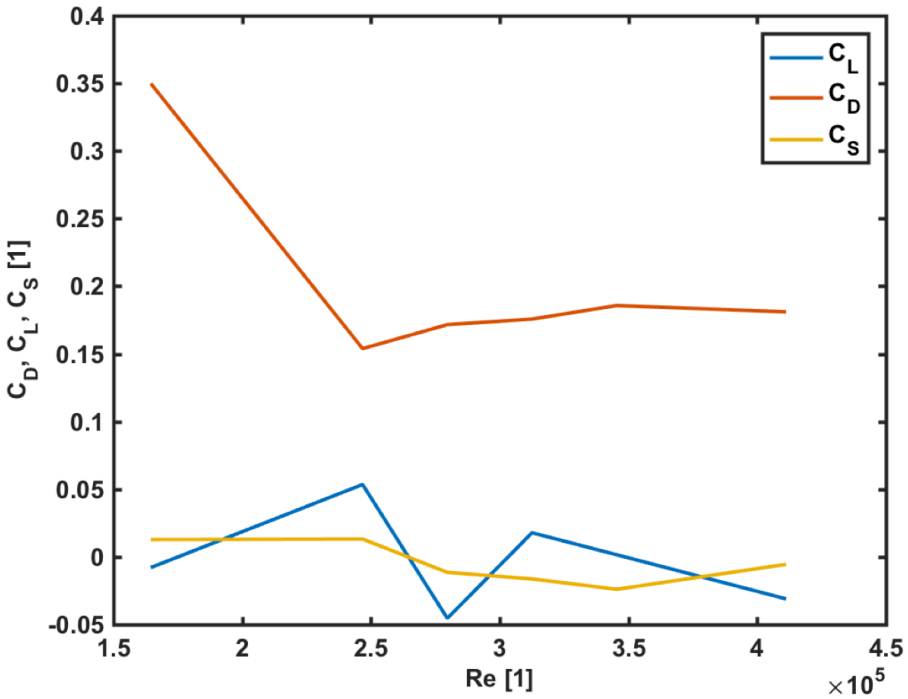

Figure 5-14: The effect of Reynolds number acting on median values of coefficients of aerodynamic forces, *n = 0 rps*

5.5.2 Comparison of results of C_D with results in references

The results of coefficient of Drag achieved in a statistical approach are compared in this Section to a similar case, which was studied from references, Asai 2010 [12]. Comparison of two different volleyballs and a smooth sphere is shown in the Figure 5-15, measurements were performed in comparable conditions, intensity of turbulence < 1%. It is visible, that transition of sphere is around *Re = 300 000*, while transition (C_D *= 0.3,* [4]) of the volleyballs is $Re_{C\ MVA200}$ = 214 000 and $Re_{C\ VLS300}$ = 186 000, as presented in [D6].

Based on Hoerner 1974 [18] and according to discussion in [D6] it is very likely, that surface roughness is an important factor in shifting transition to lower Reynolds numbers, as it is in the case of volleyballs. The influence of roughness of surface of the volleyball is discussed more thoroughly in Section 5.6.

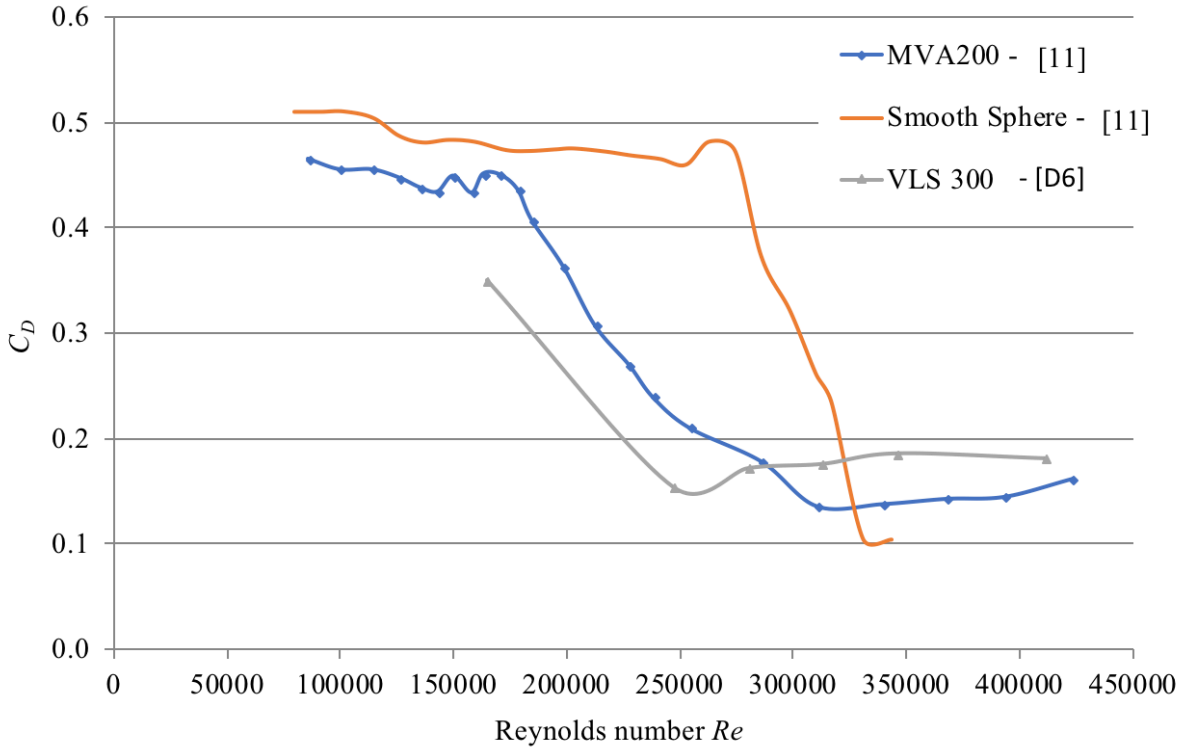

Figure 5-15: The comparison of the effect of *Re* on different volleyballs and sphere

Summary:

The resulting values of coefficient of Lift C_L and coefficient of Side force C_S are for individual cases significantly unequal to zero and are even unpredictable. In some cases, where C_L and C_S are of the higher magnitude than C_D, there are confirmed measured evidences of the phenomena of knuckling effect, sometimes also called "floating". By statistical approach it was shown, that with growing amount of results (amount of measured cases) the values of the coefficients are close to zero (statistical quantities, such as dispersion and standard deviation were stated). The observed phenomena shows characteristics of randomness and unpredictability. Individual cases, where $C_L >> 0$ or $C_S >> 0$ are important evidence of knuckling effect, even was recorded one case, where $C_S > C_D > C_L$.

The description and explanation of the phenomena was stated based on evidence.

5.6 INFLUENCE OF ROUGHNESS OF SURFACE

The influence of surface roughness as mentioned in 5.5.2 is described thoroughly in this Section. Measurement of surface roughness was performed and published in [D6], example of

the measurement by device: Machine: MarTalk, sliding unit: DriveUnit. PGK 20, probe: MFW-250:2 (#1855) - 2.0% is shown in the Figure 5-16.

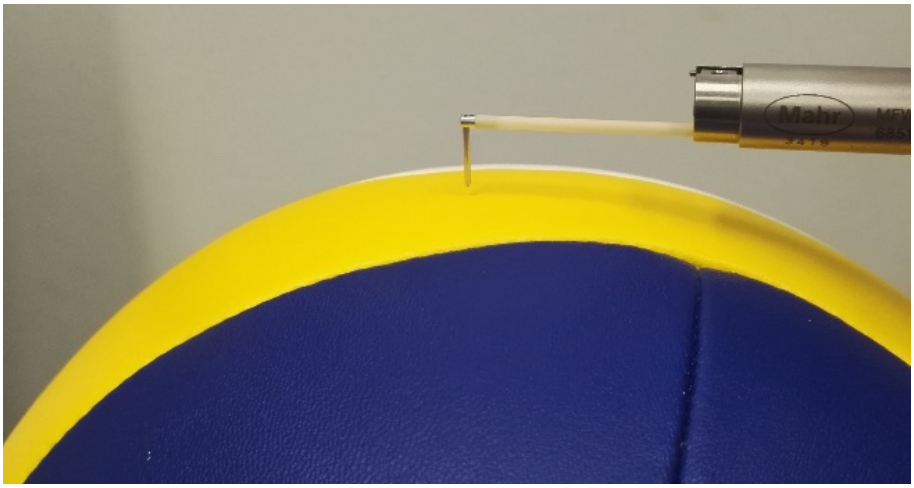

Figure 5-16: Example of measurement of surface roughness

Values of roughness ratio *k/d* were in [D6] stated:

$k/d_{MVA200} = 22.34 \times 10^{-5}$, $k/d_{VLS300} = 28.58 \times 10^{-5}$.

The measurement of surface roughness explained the earlier transition of a volleyball in comparison to a smooth sphere and also earlier transition of ball VLS 300 in comparison to ball MVA200.

Analysis of surface roughness, which was made is cited from [D6]:

Table 5-6: Values of transition, defined by critical Reynolds number ($C_D = 0.3$) according to surface roughness. Values of $Re_{CRIT.}$ are stated according to Asai [12], Achenbach [18] and Figure 5-15.

	Smooth sphere $k/d = 0$	Sphere $k/d = 25 \times 10^{-5}$	MVA200 $k/d = 22.34 \times 10^{-5}$	VLS300 $k/d = 28.58 \times 10^{-5}$	Sphere $k/d = 150 \times 10^{-5}$
$Re_{CRIT.}$	300 000	260 000	214 000	186 000	170 000

Based on the values of $Re_{CRIT.}$ of measured volleyballs, it was expected that surface roughness (defined by ratio k/d) of measured volleyballs is higher than $k/d = 25 \times 10^{-5}$ and lower than $k/d = 150 \times 10^{-5}$. This expectation was not accomplished in the case of MVA200, this could be caused by dimples on the surface of MVA200. Results of $Re_{CRIT.}$ of both investigated volleyballs is lower than expected according to Achenbach [18], rough surface sphere. Seams on the surface of a volleyball is explanation of speeding up transition on the surface of volleyballs.

The influence of surface roughness on the aerodynamic characteristics of a volleyball is even more intensive than in the case of smooth sphere, compared to Achenbach [18]. This phenomena could be explained by rough surface profile – presence of seams. Because available studies, such as [29] concluded: [*"...It appears that the force on a curveball does not depend on the orientation of the seams as suggested..."*] influence of seams was not observed thoroughly. The influence of seams is difficult to quantify, CFD calculation could be the first step in the investigation.
Next recommendation on this particular topic would be to study the influence of roughness on the coefficient of Lift and Side force. Without particular tests or comparison with references it can be only presumed: the influence of surface roughness is the same on the Lift and Side force as it was shown on the Drag coefficient.

5.7 COMPARISON WITH CFD – ONE DEFINED CASE

In fluid dynamics is important to combine experimental and CFD methods, economic reasons often decide the method used. If possible the best way of investigation of realistic cases in fluid dynamics is combinations of CFD and experimental approaches. Often experiment is used to prove results of CFD, but sometimes it can be also useful to use CFD for verifying the results of experiments. The case was presented at conference, Hlaváček [30]. Author of the dissertation thesis formulated the assignment of the case and was a consultant of the project.

5.7.1 Assignment of CFD case

Computational fluid dynamic approach was used to calculate results of coefficient of Drag and of Lift of two defined conditions of flight of a beach volleyball.

Conditions of computation:

- Mass of the ball: $m = 0.262\ kg$
- Airstream velocity: $v_\infty = 21\ m/s$
- Side angle of attack: $\beta = 0°$
- Revolutions *n*, 1. case: $n = 0\ rps$
- Revolutions *n*, 2. case: $n = \pm 8.75\ rps$

Geometry is visible in the Figure 5-17, additionally it is important to note:

- Diameter of the ball: $d = 0.24\ m$
- Diameter of the spindle: $\delta = 0.008\ m$
- Proportional roughness: $k/d = 28.58 \times 10^{-5}$

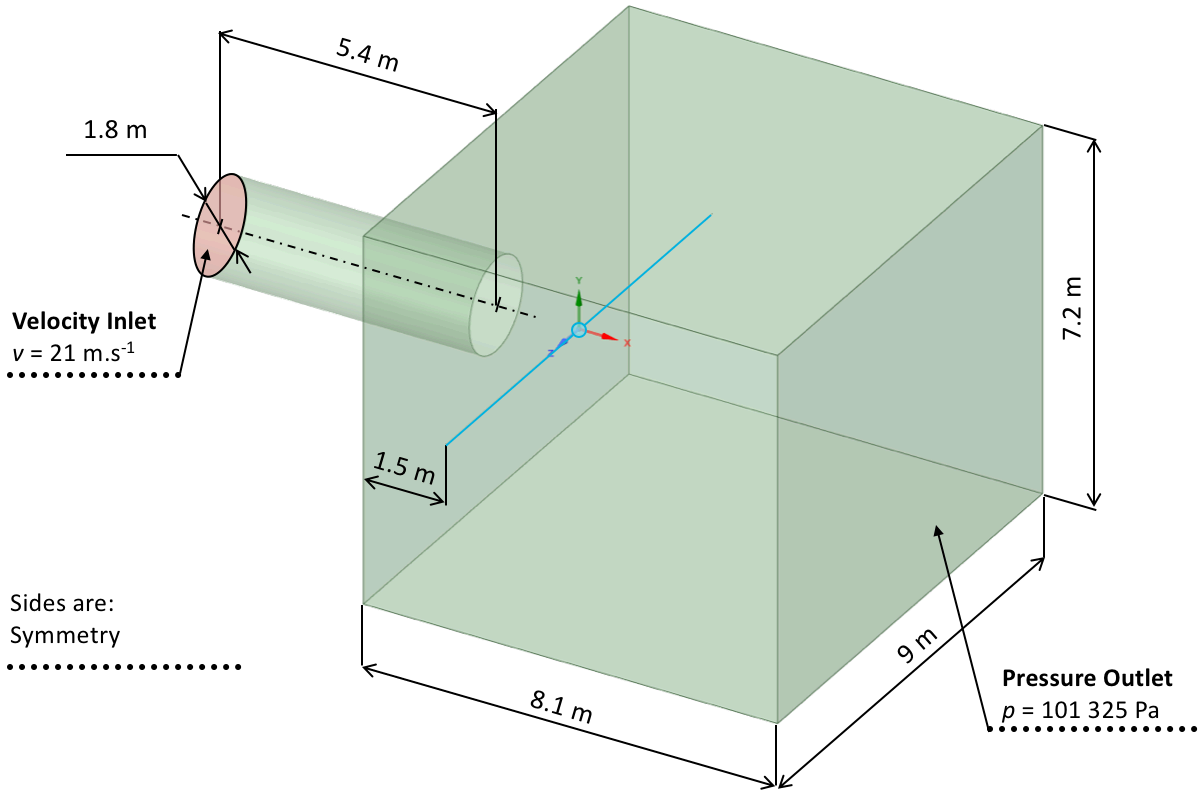

Figure 5-17: The description of geometry of the computed example

5.7.2 Mesh and properties of the calculation

Mesh is visible in the Figure 5-18. Detailed description of the mesh is in Table 5-7. Further properties of the computational cases are in Table 5-8 and Table 5-9.

Table 5-7:Mesh properties

Software	**Amount**	**Type of cells**	**Min. Ortho. Quality**	**Max. Aspect Ratio**	**Max. y^+**
ANSYS ICEM CFD 19.0	10.64 mil.	Hexagonal	0.021	10 024	0.92 / 5.22 *

* y^+ = 0.92 the case of smooth sphere,
y^+ = 5.22 the case of roughness of the surface.

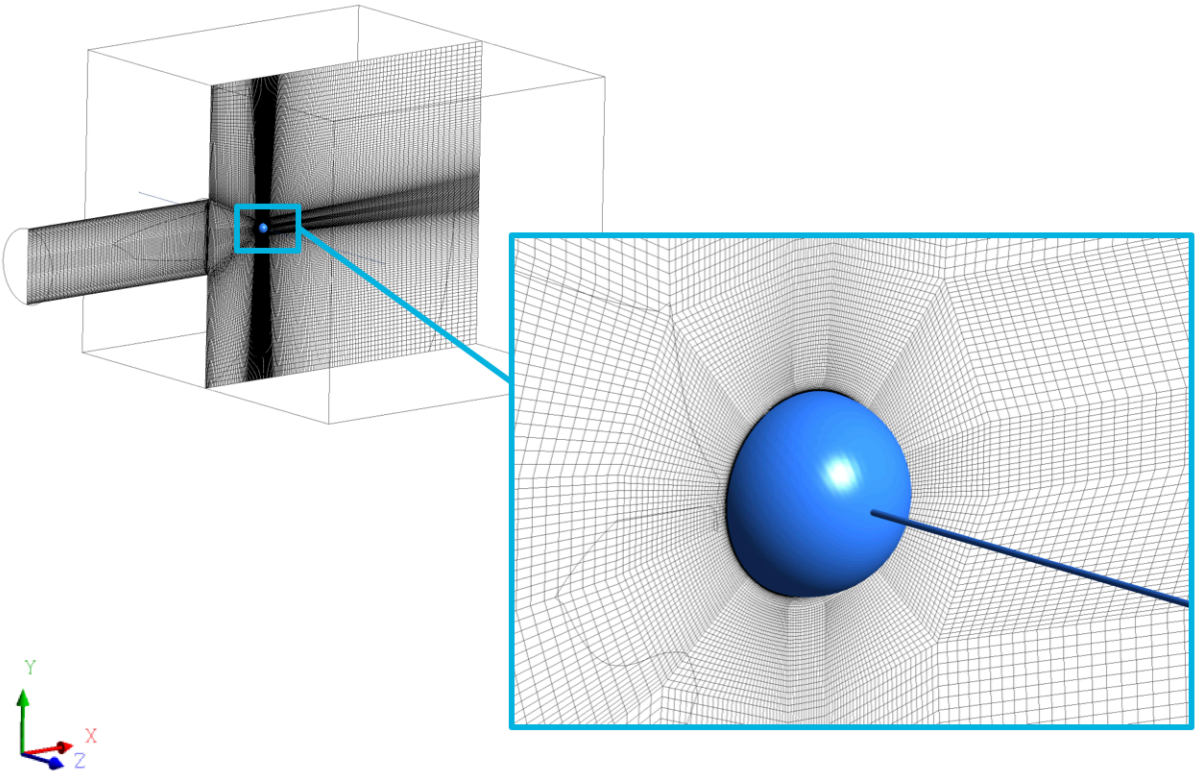

Figure 5-18: Mesh detail

Table 5-8: Characteristics of the computation I

Precision	**flowing**	**Models**	**Time of calculation**
Double	Stationary	Turbulence: k-ω SST	8 hours
	Compressible fluid	Ideal gas	12 processors

Table 5-9: Characteristics of the computation II

Software	**Type of solver**	**Pressure-Velocity Coupling**	**Discretization in space**	**Discretization of pressure**
ANSYS Fluent 19.0	Pressure Based	Simple	Second Order Upwind	Least Squares Cell Based

5.7.3 Results of the CFD

The velocity distribution and pressure distribution are two visualizations, which results in CFD. In the Figure 5-19 is compared case of flow around the ball a) $n = 0$ *rps* and b) $n = 8.75$ *rps*. In the Figure 5-20 pressure distribution is depicted in the same way. In both figures it is easily visible, that velocity and also pressure distribution in the case of n = 8.75 rps is intensively affected by the revolutions. This influence of revolutions was expected and already discussed in Chapter 4.

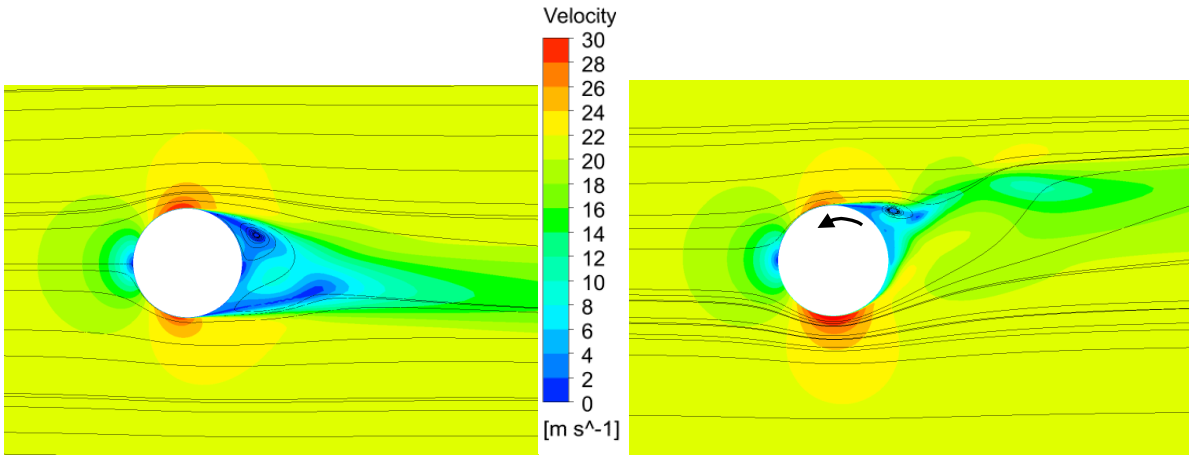

Figure 5-19: The velocity distribution in the plane of symmetry:

a) $n = 0$ *rps* b) $n = -8.75$ *rps*

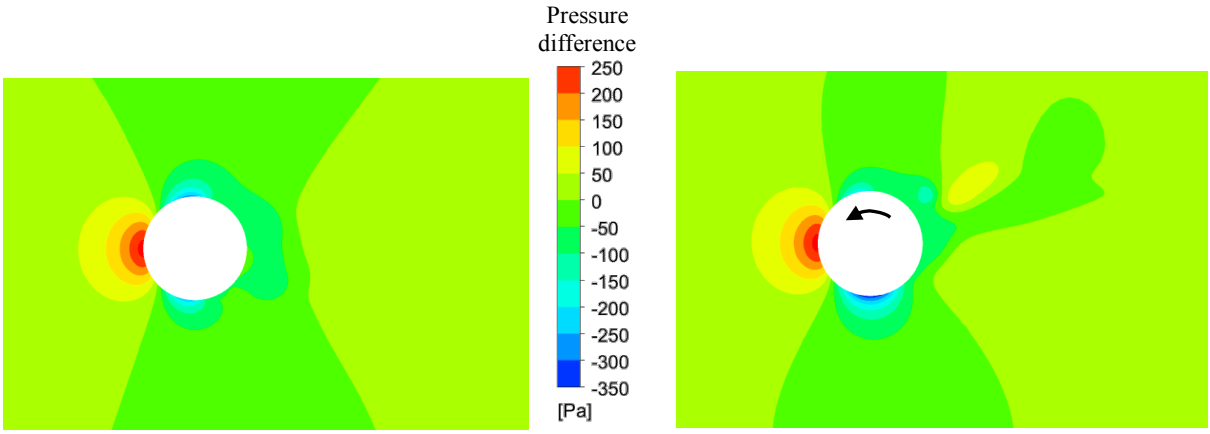

Figure 5-20: The pressure distribution in the plane of symmetry:

a) *n = 0 rps* b) *n = - 8.75 rps*

5.7.4 Influence of the spindle and other visualizations

The volleyball was in the experiment supported by the spindle (as described in 3.1), the same set up was used for CFD case. The influence of the spindle to aerodynamic characteristics was in the case of experiment deducted by two independent measurements (with and without ball). CFD is able to visualize the influence of spindle on vorticity, results are visible in Figure 5-21 and Figure 5-22. In Figure 5-22 the influence of the revolutions of the ball is easily visible: pair of vortexes of the same size and opposite direction are created in the wake behind the ball. The complete structure behind the ball is very interesting and deserves to be studied thoroughly, experimentally PIV methods can be used. The vorticity is defined by Eq. (49):

$$\vec{\Omega} = \nabla \times \vec{v} = \left(\frac{\partial}{\partial x}, \frac{\partial}{\partial y}, \frac{\partial}{\partial z}\right) \times \left(v_x, v_y, v_z\right). \tag{49}$$

Furthermore the pressure and the wall shear distribution on the surface of the sphere can be depicted, as is visible in the Figure 5-23 and Figure 5-24. The pressure distribution is presented as a basic quantity, which defines aerodynamic forces acting on the ball. The wall shear is depicted to illustrate how moments are created on the surface of the volleyball.

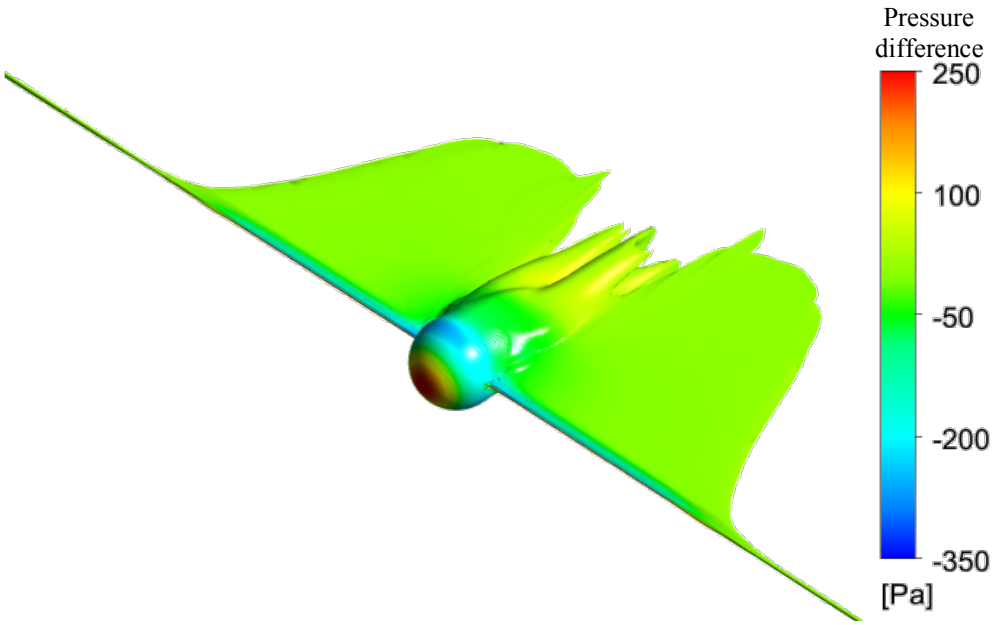

Figure 5-21: The influence of spindle on vorticity, *n = 0 rps*

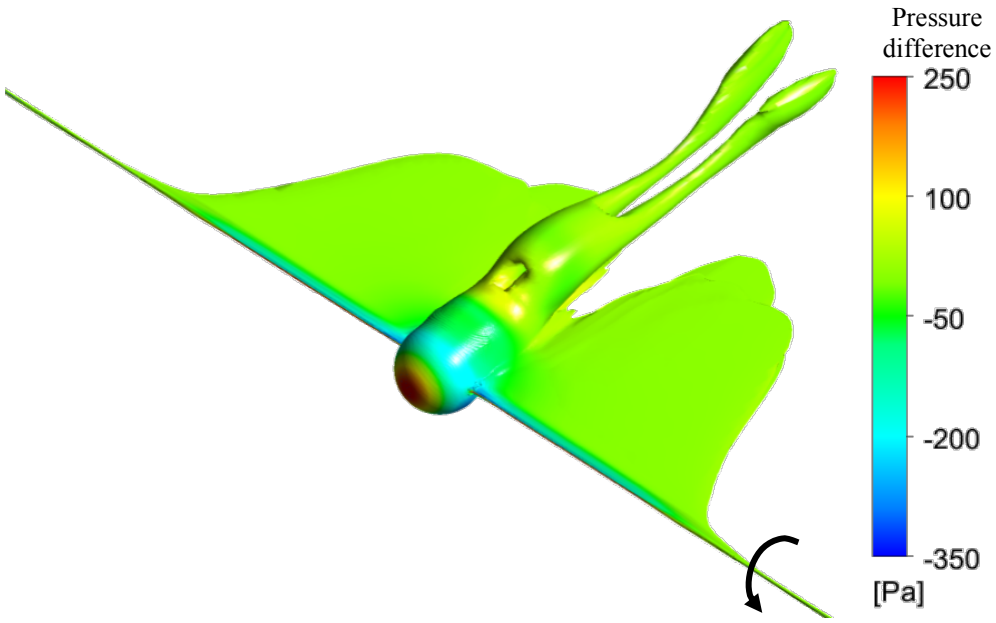

Figure 5-22: The influence of the spindle on vorticity, *n = 8.75 rps*

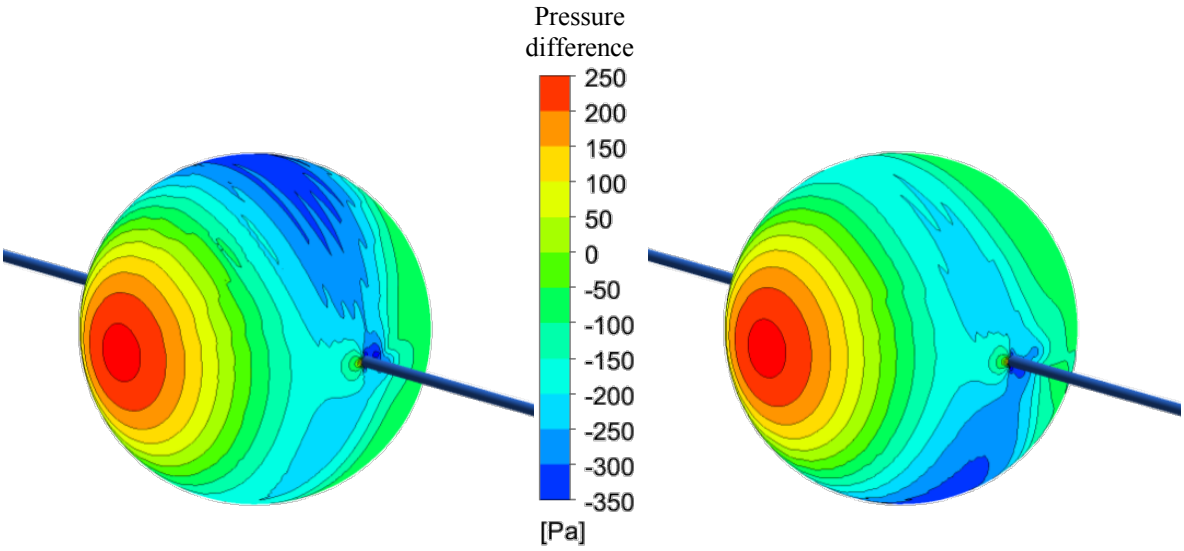

Figure 5-23: Pressure distribution on the surface of the volleyball:

a) $n = 0\ rps$ b) $n = 8.75\ rps$

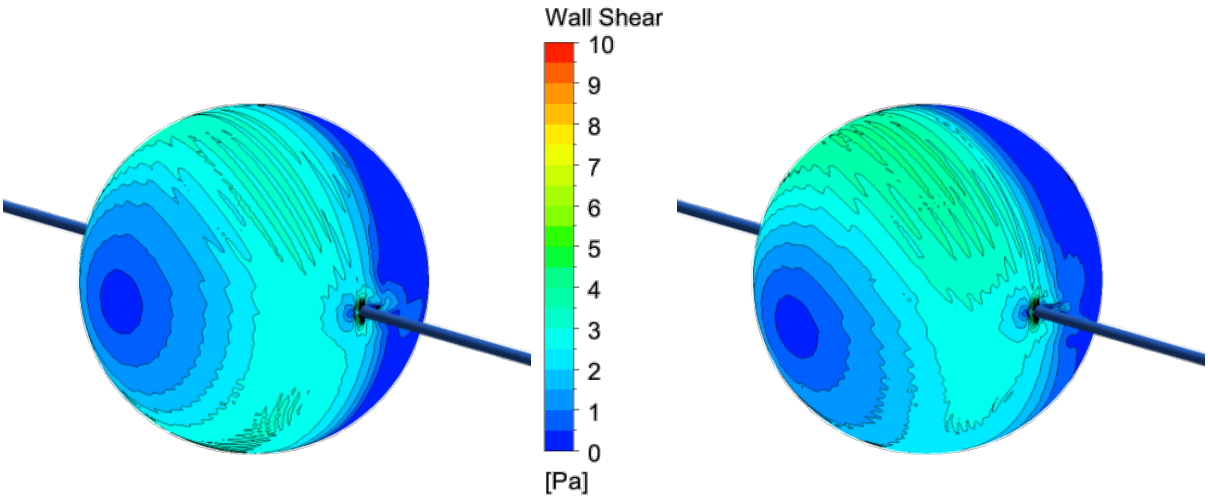

Figure 5-24: Wall shear distribution on the surface of volleyball:

a) $n = 0\ rps$ b) $n = 8.75\ rps$

5.7.5 The comparison of quantitative results

The quantitative results of aerodynamical characteristics are compared in following tables: Table 5-10 and Table 5-11.

Table 5-10: The results of CFD

$n\ [s^{-1}]$	F_L [N]	F_D [N]	C_L [1]	C_D [1]
0	1.03	3.04	0.088	0.259
+ 8.75	3.34	3.96	0.285	0.337
− 8.75	− 3.64	4.36	− 0.310	0.371

Table 5-11: The results of experiment

$n\ [s^{-1}]$	F_L [N]	F_D [N]	C_L [1]	C_D [1]
0	0.93	3.77	0.090	0.380
+ 8.75	2.50	3.46	0.250	0.350

As it is visible from values in Table 5-10 and Table 5-11, especially in the case of coefficient of Lift C_L, results of CFD and experiment in the defined conditions are in agreement.

Summary:

The CFD calculation results and experimental results are in agreement. The CFD also confirmed expectations very well and imaginations of velocity distribution on the surface of the sphere and influence of spindle was shown in the figures. Verification of all results (288 different conditions) would be very time consuming.

Note: The CFD calculation was used for verifying one case (defined by conditions) out of 288 measured cases. One CFD calculations was computed on 12 processors for 8 hours. If all results were calculated computation would take 96 days and nights on 12 processors.

6 CONCLUSIONS

The investigation of the aerodynamic characteristics of a volleyball in flight was performed. The set of data of aerodynamical characteristics, which forms the fundamentals of ballistics for complete description of the flight was found by experimental tests. This is evaluated as a main individual contribution to the aerodynamical study of flight of a volleyball. The meaning of the results of the experimental investigation is described in separate Chapters of the Doctoral thesis. The application of the gained data and knowledge is considered in Chapter 5 Discussion and analyses.

The experimental set up was designed based on requirements: the ball is in the test section of wind tunnel, the ball is able to rotate by controlled revolutions, the axis of revolutions is adjustable according to the side angle of attack β, six forces are measured. Brief description of the technical solutions, used devices including methodology is in Chapter 3 Experiment. The complete description is published in [D6]. The experiment was performed.

The results of the experiment are performed in the dimensionless numbers, aerodynamical characteristics are displayed in coefficients of Drag C_D, coefficient of Lift C_L and coefficient of Side force C_S and coefficients of moments. The effect of the aerodynamical coefficients observed acting on Reynolds number Re and revolutions n is shown in practical three-dimensional plots for constant side angle of attack β.

First are presented and discussed results of coefficient of Drag in the case of side angle of attack $\beta = 0°$. The low value of coefficient of Drag without revolutions $C_{D(n = 0)}$ was detected in the interval of Reynolds numbers: $240\,000 < Re < 340\,000$, the area was called as a transition area. This area corresponds to critical Reynolds number for a smooth sphere, which is $Re_{C\_sphere} = 3 \times 10^5$. Further more area of low C_D was found for $Re = (160\,000 – 280\,000)$ in the interval of revolutions $n = (5 – 8.75)$ *rps*. This effect is considered as an evidence that revolutions have impact on the transition. This is important individual contribution to aerodynamic study of the flight of a volleyball. The effect should be studied in more detail in the future.

The results of coefficient of Lift C_L, $\beta = 0°$ confirm the presence of the Magnus effect. There was also detected Lift at $n = 0$ *rps* despite the theory expectations. This low Lift is described as a unsymmetrical transition on the surface of the ball. Idealistic simplification of the symmetry is broken by the observed data. The effect is evidence of flight of "knuckle ball" – the

unpredictable flight of a ball. In the results of coefficient of Lift, it was found also the effect of area of critical Reynolds number (decrease of the coefficient of Lift) and hypothesis, which was already published in [D2] was confirmed. The hypothesis was formed based on separate experimental results: in the course of $C_L = f(n)$ *(Re = const.)* is "breaking point" at $n = 8.75$ *rps*, after which the Magnus effect is not that intensive anymore.
The results of coefficient of Side force C_S show: the higher Reynolds number the lower coefficient of Side force – the revolutions do not influence the C_S course.

All coefficients of moments Roll, Pitch and Yaw were calculated based on measurements of six forces. The results are depicted in three dimensional plots. The basic meaning of the coefficients of moments is explained as partial information about the pressure distribution on the surface. The coefficient of moment compares pressure distributions on two hemispheres of the ball, therefore it is method of evaluation of symmetry of pressure distribution on the surface. The practical examples of the effect explanation are figured.

The effects of side angle of attack on coefficients of forces are described in the next part of the Doctoral thesis. All results are shown and discussed. The highest attention is paid to evaluation of effect of β on coefficient of Lift C_L. The vector of velocity v_∞ was transformed to rotated coordinate system according to angle β. The results are statistically evaluated. The direct dependence of coefficient of Lift C_L on spin n was found and defined by Eq. (35):

$$C_L = 0.127 \cdot s^3 - 0.4824 \cdot s^2 + 0.585 \cdot \mathrm{s}, \tag{35}$$

with reliability $R^2 = 0.4799$. The dispersion and standard deviation of the population of coefficient of Lift were calculated, $Var(C_L) = 0.0094$ and $\sigma(C_L) = 0.0967$. This is the next important contribution to the aerodynamical study of flight of a volleyball.

The special case of flight of the ball without rotation was studied and explanation of the knuckling effect is stated. The fact that coefficients of forces follow the theoretical expectations with growing amount of measured cases was shown by statistical approach. It is well shown in Figure 5-14:

- C_D decreases rapidly from laminar flow to transition and then increases slightly lead to turbulent flow.

- C_L and C_S tend to zero, but in individual cases the values of C_L and C_S can be even higher than values of C_D. By the language of statistics: in the dispersion (calculation of random errors) are described all the cases of knuckling effect.

The knuckling effect is explained by disruption of symmetry of pressure distribution on the surface of the ball. The symmetry is disrupted due to transition area in the meaning of interval of Reynolds numbers. Practically the transition from laminar to turbulent flow appears on one side of the ball earlier then on the other side, that causes the movement of the ball to perpendicular direction to the flying path – knuckling effect – unpredictably. This effect is evidenced by the values of coefficients of Lift and of Side force acting on the ball in flight without revolutions $n = 0\ rps$.

The influence of roughness of the surface of the volleyball is studied based on comparison of coefficient of Drag C_D of two different types of volleyballs. It is shown, that the roughness of the surface has an impact in the expected trend, the higher the roughness of surface the lower critical Reynolds number. This dependence corresponds to Achenbach 1974 [18], who described the effect of roughness on sphere. The results of investigation of roughness influence were published in [D6] and [D5].

The calculation of uncertainties of all data was shown in the separate Section 4.4, practical case of the calculation was performed and solution was depicted in the practical Figure 4-22. The conclusion is made, that uncertainties don't essentially influence the courses of the dependences of observed quantities.

The assignment of the case for comparison of results of experiment and CFD calculation was formulated. The results of the computation are shown and described according to source [30]. In the particular conditions, which were proposed to the CFD calculation the results are in good agreement with experiment. In the CFD was also described the influence of supporting spindle on the vorticity around the ball. The CFD calculation of all defined conditions, which were measured would be time consuming.

The set of aerodynamic characteristics acting on the volleyball in flight, that is the main individual contribution of the work, was in Chapter 5 used into equations of three-dimensional ballistics. The three-dimensional ballistic equations were published in [D1]. The set of

equations together with the set of aerodynamic characteristics can be used for calculation of all types of flight of volleyball including special cases: 1. flight without revolution – flight with knuckling effect, 2. the effect of side wind acting on the volleyball in the flight, 3. flight of a ball with deflection of axis of rotation.

Even though the description of forces acting on the volleyball is with three dimensional ballistics and with a set of aerodynamic characteristics completed, there are still many areas, which needs to be studied more thoroughly:

1. the effect of revolutions on transition, the effect on separation of the boundary layer,
2. the breaking point in the course of coefficient of Lift,
3. the experimental observation of the pressure distribution on the surface,
4. the effect of seams on the separation of boundary layer,
5. and others.

Practically the results and the experimental device, which was designed and constructed can be used in the evaluation of volleyball qualities. The aerodynamical characteristics of different volleyballs (and also other sports balls) can be compared using the device.
The conclusions and knowledge gained in the Doctoral thesis can be used in development of new sports balls and in the theory of sports training.

REFERENCES

[1] Jacob, E. N.: Sphere Drag tests in variable density wind tunnel, *NACA Technical Note No. 312,* Langley Memorial Aeronautical Laboratory, Washington, 1929

[2] Bacon, D. L., Reid, E. G.: The resistance of sphere in the wind tunnel and in air, *NACA Report No. 185*, Government Printing Office, Washington, 1924, at: https://ntrs.nasa.gov/archive/nasa/casi.ntrs.nasa.gov/19930091250.pdf

[3] The effect of Reynolds number on the Drag coefficient C_D of a smooth sphere of diameter d, at: https://i.stack.imgur.com/axAi7.png

[4] Hörner, S.: Tests of spheres with reference to Reynolds number, turbulence and surface roughness, *NACA Report No. 777*, Washington, 1935, at: https://ntrs.nasa.gov/archive/nasa/casi.ntrs.nasa.gov/19930094640.pdf

[5] Van Dyke, M.: An album of fluid motion, The Parabolic Press, Stanford, 1982

[6] Terra, W, Sciacchitano, A, Scarano, F: Aerodynamic Drag of a transiting sphere by large-scale tomographic-PIV, Springer, published online: 7 June 2017, DOI 10.1007/s00348-017-2331-0

[7] Newton, I.: “Dispersion of light” In Philosophical Transactions, Abridged, vol. I, 1672. Reprinted in Moments of Discovery, vol. I, ed. George Schwartz and Philip W. Bishop. New York: Basic Books, 1958

[8] Mehta R.D.: Sports ball aerodynamics. In: Nørstrud H. (eds) Sport Aerodynamics. CISM International Centre for Mechanical Sciences, vol 506. Springer, Vienna, 2008

[9] Magnus, G.: (1852) "Über die Abweichung der Geschosse,"Abhandlungen der Königlichen Akademie der Wissenschaften zu Berlin, pages 1-23., *In German*

[10] Mehta, R.D.: Aerodynamics of sport balls, Annual Rewiew of Fluid Mechanics, page 151 – 189, In: M. van Dyke: Annual Reviews, Palo Alto, Vol. 17, 1985

[11] Mehta, R.D.: Sports balls aerodynamics: effects of velocity, spin and surface roughness, pages 1 – 13 In: Materials and Science in Sports, Conference, Coronado, 2001

[12] Asaia, T., Itob, S., Seoc, K., Hitotsubashi, A: Aerodynamics of a new volleyball, Procedia Engineering 2 (2010) 2493–2498, Elsevier, 2010,

[13] Wei, Q.-D., Lin, R.-S., Liu, Z.-J. : Vortex-induced dynamic loads on a non-spinning volleyball, Fluid Dynamics Research, Volume 3, Issue , pp. 231-237, Elsevier, 1988 DOI: 10.1016/0169-5983(88)90071-8

[14] FIVB: Volleyball history, at: http://www.fivb.org/en/volleyball/History.asp

[15] FIVB: Volleyball rules 2017 – 2020, at: http://www.fivb.org/EN/Refereeing-Rules/documents/FIVB-Volleyball_Rules_2017-2020-EN-v06.pdf

[16] Anderson, J. D. Jr.: Fundamentals of Aerodynamics, 2nd edition, New York, McGraw-Hill, 1991, ISBN 0-07-001679-8

[17] Figure of Roll, Pitch, Yaw, at: https://www.researchgate.net/profile/Suneeta_Godbole/publication/262055313/figure/fig2/AS:213872930758658@1428002688513/Average-roll-pitch-and-yaw-angles.png

[18] Achenbach, E.: The effects of surface roughness and tunnel blockage on the flow past spheres, Journal of Fluid Mechanics, vol. 65, part 1, pp 113 – 125, Great Britain,1974, https://doi.org/10.1017/S0022112074001285

[19] Fage, A.: Experiments on a sphere at critical Reynolds numbers, Aero. Res. Council, R&M no. 1766, 1936

[20] Suryanarayana, G. K., Meier, G. E. A.: Effect of ventilation on the flowfield around a sphere, Experiments in Fluids 19 (1995), pp. 78 - 88, Sringer – Verlag, 1995

[21] Muto, M., Tsubokura, M., Tsubokura, Oshima N.: Negative Magnus Lift on a rotating sphere at around the critical Reynolds number, published online: 2012, DOI 10.1063/1.367357, at: https://www.researchgate.net/profile/Makoto_Tsubokura/publication/261028356/figure/fig7/AS:317657531338766@1452746865570/Profiles-of-time-averaged-pressure-coefficient-on-sphere-surface-as-function-of-ph-in.png

[22] Figure of Magnus effect explanation, at: http://www.aircraftnerds.com/2017/12/what-is-magnus-effect.html

[23] Texier, B. D., Cohen, C., Quere, D., Clanet, C.: Physics of knuckleball, New Journal of Physics 18, Institute of Physics, 2016, doi:10.1088/1367-2630/18/7/073027

[24] Errors, theory of. Encyclopedia of Mathematics. URL: http://www.encyclopediaofmath.org/index.php?title=Errors,_theory_of&oldid=28547

[25] de Rocquigny, E., Devictor, N., Tarantola, S.: Uncertainty in Industrial Practice: A Guide to Quantitative Uncertainty Management, John Wiley & Sons, 2008, ISBN: 0470770740, 9780470770740, URL: https://books.google.cz/books?id=qg8bqw6ByskC&pg=PA305&lpg=PA305&dq=European+Prestandard+ENV+13005:+1999&source=bl&ots=5mDyo0cqgn&sig=nUGPbzqMNG-_hUtPbYAF2O6rWxs&hl=cs&sa=X&ved=0ahUKEwiDhcePr_3bAhXoDsAKHfzYC7IQ6AEIMDAB#v=onepage&q=European%20Prestandard%20ENV%2013005%3A%201999&f=false

[26] Guide to the expression of uncertainty in measurement (G.U.M), CEN standard ENV 13005:1999, URL: https://infostore.saiglobal.com/en-gb/standards/env-13005-1999-298568/

[27] Terms and conditions for FIVB homologation (APPROVAL) balls to be used in official volleyball competitions, FIVB, URL: http://www.fivb.org/EN/Technical/Homologation/FIVB_Volleyball_Homologation_Procedures.pdf

[28] Sareen, A., Zhao, J., Lo Jacono, D., Sheridan, J., Hourigan, K., Thompson, M. (2018). Vortex-induced vibration of a rotating sphere. Journal of Fluid Mechanics, 837, pages: 258-292.
doi:10.1017/jfm.2017.847

[29] Kothmann, B.D.: Aerodynamics of Sports Balls, January 2007 – on-line presentation: http://www.scielo.br/scielo.php?pid=S0102-47442004000400003&script=sci_arttext&tlng=en

[30] Hlaváček, D.: Simulation of flow around volleyball In Proceedings of Conference Techsoft and Meeting of Users of Ansys, 23. – 25. 5. 2018, Harrachov, Techsoft Engineering, spol. s r.o., - *In Czech,*
available: https://www.techsoft-eng.cz/sluzby-seminare-a-konference-detail-seminare-a-konference/setkani-uzivatelu-a-konference-2018

[31] Fox, R.W., McDonald, A.T.: Introduction to fluid mechanics, John Wiley & Sons, New York 1994

[32] Watts, R.G., Ferrer, R. (1987) The lateral force on a spinning sphere: Aerodynamics of a Curvebal. Am. J. Phys., 55, 40-44,
http://dx.doi.org/10.1119/1.14969

[33] Chattot J.-J., Hafez, M.: Theoretical and Applied Aerodynamics and Related Numerical

Methods, Springer, 2015:
http://www.springer.com/978-94-017-9824-2

[34] Linhart, J.: Fluid mechanics I, Plzen, 2009 – *In Czech*, ISBN: 9788070437667, http://home.zcu.cz/~bebrl/mechtekutin_linhart.pdf

Authors references:

[D1] Šafařík, P., Dumek, J.: Modelling of flight of volleyball In: Proceedings Conference Techsoft and meeting of users of Ansys, 23. – 25. 5. 2018, Harrachov, Techsoft Engineering, spol. s r.o. - *In Czech*

[D2] Dumek, J., Pátek, Z., Karásek L., Šafařík, P.: Aerodynamic experimental data on rotating lifted volleyballs In Jonáš, P., Uruba, V.: Proceedings Colloquium Fluid Dynamics 2014, Institute of Thermomechanics AS CR, v.v.i., Prague, 2014

[D3] Dumek, J., Šafařík, P.: Aerodynamic experimental tests of forces and torques acting on the volleyball In Proceedings Topical Problems of Fluid Mechanics 2017, Prague, 2017 Edited by David Šimurda and Tomáš Bodnár, Institute of Thermomechanics AS CR, v.v.i., pp. 113-116
DOI: https://doi.org/10.14311/TPFM.2017.015

[D4] Dumek, J., Šafařík, P., Pátek, Z.: Description of experimental setting: volleyball in the wind tunnel, In: Ježek, J., Nožička, J., Adamec, J., Šafařík, P.: Proceedings of Student's Work in the Year 2017/2018, CTU in Prague, Prague, 2018,
Available at: http://stc.fs.cvut.cz/pdf18/8505.pdf?_=1523224602

[D5] Dumek, J., Urban, J.: Measurement of surface roughness of volleyball, Acta Mechanica Slovaca ISSN 1335-2393, Slovakia, 2018– *in the editorial office: 22.18.ams.0014*

[D6] Dumek, J., Šafařík, P., Pátek, Z., Asai, T.: On the flight of volleyball, In Proceedings Topical Problems of Fluid Mechanics 2018, Prague, 2018 Edited by David Šimurda and Tomáš Bodnár, Institute of Thermomechanics AS CR, v.v.i., pp. 65-72
https://doi.org/10.14311/TPFM.2018.009

[D7] Dumek, J., Šafařík, P.: Complete description of forces acting on a flying beach volleyball, EPJ Web of Conferences 180, 02021 (2018), DOI: https://doi.org/10.1051/epjconf/201818002021

Other publications of the author:

[D8] Dumek, J., Reismuller, R.: Flight of volleyball at service from the perspective of aerodynamics I, in: Martínková, I.P.: TVSM, 83, 2017, nr. 3, ISSN 1210-7689, UK FTVS Prague, 2017 – *in Czech*

[D9] Dumek, J., Reismuller, R.: Flight of volleyball at service from the perspective of aerodynamics II, in: Martínková, I.P.: TVSM, 83, 2017, nr. 4, ISSN 1210-7689, UK FTVS Prague, 2017 – *in Czech*